CHARACTERIZATION OF GAS-OIL-WATER IN A HORIZONTAL PIPELINE

BY

OKUNRINJEJE, LUKMAN TUNDE

A Thesis Presented to the
DEANSHIP OF GRADUATE STUDIES

KING FAHD UNIVERSITY OF PETROLEUM & MINERALS

DHAHRAN, SAUDI ARABIA

In Partial Fulfillment of the
Requirements for the Degree of

MASTER OF SCIENCE

In

MECHANICAL ENGINEERING

DECEMBER 2012

KING FAHD UNIVERSITY OF PETROLEUM & MINERALS

DHAHRAN 31261, SAUDI ARABIA

DEANSHIP OF GRADUATE STUDIES

This thesis, written by OKUNRINJEJE, LUKMAN TUNDE under the direction of his thesis advisor and approved by his thesis committee, has been presented to and accepted by the Dean of Graduate Studies, in partial fulfillment of the requirements for the degree of **MASTER OF SCIENCE IN MECHANICAL ENGINEERING.**

Dr. Luai Al-Hadhrami
(Advisor)

Dr. Zuhair Gasem
Department Chairman

Dr. Abdelsalam Al-Sarkhi
(Co-Advisor)

Dr. Salam A. Zummo
Dean of Graduate Studies

Dr. Mohamed A. Habib
(Member)

8/4/13
Date

Dr. Meamer El Nakla
(Member)

Dr. Wael Ahmed
(Member)

Dedicated

to

Alh. Safiriyu Araba

(Aranse-Oluwa)

ACKNOWLEDGEMENTS

I would like to appreciate my advisor, **Dr Luai Al-Hadhrami** and co-advisor, **Dr Abdelsalam Al-Sarkhi** for their support and valuable suggestions during this study. Thanks are also due to the Center of Engineering Research and Deanship of scientific Research for the provision of the facilities for this study. I also acknowledge my other committee members, **Dr. M. El Nakla, Dr. Wael Ahmed and Dr. M. A. Habib** for their valuable advice, guidance and understanding during this work.

My gratefulness also knows no bound to King Fahd University of Petroleum & Minerals (KFUPM) for the opportunity to accomplish this work and for the financial support. I would also like to thank all the KFUPM community for the conducive learning environment they gave me during the time of this study. I would also like to appreciate Mr. Siddiqui for his time while orienting me with the initial process of the operating procedure of the experimental set up.

In conclusion, I will have to extend my gratitude to Alh. S.A Araba, my wife and my beloved parents back home for their prayers, love, patience and encouragement. In all, to God alone is the glory.

TABLE OF CONTENTS

LIST OF TABLES

LIST OF FIGURES

THESIS ABSTRACT (ENGLISH)

NAME: OKUNRINJEJE, LUKMAN TUNDE

TITLE: CHARACTERIZATION OF GAS-OIL-WATER IN A HORIZONTAL PIPELINE

MAJOR: MECHANICAL ENGINEERING

DATE: DECEMBER 2012

This experimental work was carried out using gas-oil-water three-phase flow loop set up in the Center for Engineering Research of the Research Institute, King Fahd University of Petroleum and Minerals. The objective of this work was to investigate the flow pattern and measure the pressure drop in a horizontal pipe with 2.25cm inner diameter and compare the experimental results with existing models.

The experiments were conducted at room temperature of 20℃ using oil with viscosity of 1.77 cp, tap water and air. Superficial water and oil velocities range from 0.3 m/s to 3 m/s and superficial gas velocity range from 0.29 m/s to 52.5 m/s in order to cover wide range of flow patterns. The experiments were performed for 10% to 90% water cuts in steps of 10%. The flow patterns were observed and recorded using high speed video camera while the pressure drop was measured using pressure transducers and U-tube manometers.

The flow patterns and pressure gradients have been investigated for the gas-oil-water three-phase flow at different flow conditions in a horizontal pipe. About 377 data points were acquired and studied. The experimental results were compared with the Unified Model of Zhang and Sarica (2006) and they showed good agreement at low gas flow

rates but was poorly predicted at high gas flow rates. This might be due to some of the shortcomings of the model which includes: the mixing status of oil and water, slippage between oil and water, the average velocities of oil and water used in the model and the interfacial tension between oil and water that was not considered in the model.

MASTER OF SCIENCE DEGREE
KING FAHD UNIVERSITY OF PETROLEUM & MINERALS
Dhahran, Saudi Arabia

THESIS ABSTRACT (ARABIC)

الاسم: لقمان توندي أوكنريجيجي

العنوان: **خصائص تدفق الزيوت والمياه والغازات معا في الأنابيب الأفقية**

التخصص: الهندسة الميكانيكية

التاريخ: ديسمبر 2012

تم تنفيذ تجارب عملية على تدفق ثلاث موائع معا هي غاز وزيت وماء في مختبر تابع لمركز البحوث الهندسية الموتاجد في معهد البحوث في جامعة الملك فهد للبترول والمعادن. والهدف من هذا العمل هو مراقبة شكل التدفق للثلاث موائع وقياس الضغط لهذه الموائع في أنبوب أفقي ذو قطر داخلي 2.25سم ومقارنة نتائج التجارب مع نماذج التعرف على شكل التدفق والضغط المتوفرة.

وقد أجريت هذه التجارب على درجة حرارة من 20^0، وكانت كثافة الزيت المستخدم 780 كغ/م^3 ولزوجته 1.77 سم.بويز. وكانت سرعة النفط والماء داخل الأنبوب تتراوح من 0.3 م / ث إلى 3 م / ث، بينما تراوحت سرعة الغاز من 0.29 م / ث إلى 52.5 م / ث وذلك لتغطية مجموعة واسعة من أشكال التدفق. وقد تم أخذ صور لأشكال التدفق باستخدام كاميرة عالية السرعة، وتم قياس فرق الضغط باستخدام جهاز المانوميتر.

وقد تم التحقق في أشكال التدفق والضغط الناتج عن التدفق لهذه الثلاث موائع في انبوب أفقي. وتمت مقارنة النتائج التجريبية مع النموذج الموحد من تشانغ و ساريكا 206 وأظهرت اتفاق جيد.

درجة الماجستير في العلوم
جامعة الملك فهد للبترول و المعادن
الظهران المملكة العربية السعودية

NOMENCLATURE

A	Cross-sectional area of the pipe $[m^2]$
A_a	Cross-sectional area of the pipe occupied by air $[m^2]$
A_o	Cross-sectional area of the pipe occupied by oil $[m^2]$
A_w	Cross-sectional area of the pipe occupied by water $[m^2]$
AN	Annular flow pattern
cp	centipoise
D	Diameter of the pipe [m]
DB	Dispersed bubble flow pattern
EB	Elongated bubble flow pattern
f	Friction factor
FP_{Expt}	Experimental flow pattern
$FP_{Unif\ Mod}$	Unified model flow pattern
gpm	gallon per minute
H_L	Liquid holdup
ID	Inner diameter [m]
INT	Intermittent flow pattern

L	Length of the pipe [m]
lpm	liter per minute
m_a	Mass flow rate of gas (air) [kg/s]
m_o	Mass flow rate of oil [kg/s]
m_w	Mass flow rate of water [kg/s]
m_L	is the mass flow rate of liquid mixture [kg/s]
M_{total}	Total Mass flow rates [kg/s]
Q_a	Volumetric flow rate of air [m^3/s]
Q_o	Volumetric flow rate of oil [m^3/s]
Q_w	Volumetric flow rate of water [m^3/s]
Q_{Liquid}	Volumetric flow rates of the liquid [m^3/s]
Q_{total}	Total volumetric flow rates [m^3/s]
Re	Reynold's number
$Re_{mixture}$	Liquid mixture Reynold's number
SL	Slug flow pattern
SS	Stratified smooth flow pattern
ST	Stratified flow pattern

SW	Stratified wavy flow pattern
V_a	Average in-situ velocity of air [m/s]
V_o	Average in-situ velocity of oil [m/s]
V_w	Average in-situ velocity of water [m/s]
V_{Smix}	Superficial mixture velocity [m/s]
VSG	Superficial velocity of gas (air) [m/s]
VSO	Superficial velocity of oil [m/s]
VSW	Superficial velocity of water [m/s]
VSL	Superficial velocity of liquid mixture [m/s]
WC	Water cut

Greek Symbols

ρ_a	Density of air [kg/m^3]
ρ_o	Density of oil [kg/m^3]
ρ_w	Density of water [kg/m^3]
ρ_L	Density of liquid mixture [kg/m^3]
μ_a	Viscosity of air [$Pa.s$]
μ_w	Viscosity of water [$Pa.s$]

μ_o	Viscosity of oil [$Pa.s$]
μ_L	Viscosity of liquid mixture [$Pa.s$]
ΔP	Pressure drop [Pa]
$\frac{\Delta P}{\Delta L}$	Pressure gradient [Pa/m]
$\left(\frac{\Delta P}{\Delta L}\right)_{TP}$	Pressure gradient of three-phase air-oil-water [Pa/m]
$\left(\frac{\Delta P}{\Delta L}\right)_{Water}$	Pressure gradient of single-phase water [Pa/m]
ε	Pipe roughness

CHAPTER 1

INTRODUCTION

1.1 Background

Multiphase flow can be referred to as the flow of more than one phase through a channel or pipe at the same time. The multiphase flow can either be gas-liquid-solid, solid-liquid, gas-solid or gas-liquid. The different phases are distributed in the pipe and they affect each other in different ways which makes it very difficult to accurately predict the flow behavior of multiphase flow. The most important characteristic of multiphase flow is its flow pattern, which is referred to as the physical distribution of the phases within the enclosure through which they flow and also the pressure gradient.

Gas-oil-water flow can be referred to as two phase, three component because it consists of two- phase (gas-liquid) and three components (gas-oil-water) flowing simultaneously in an enclosure. The gas-oil-water flow is a dominant occurrence in the oil and gas industry. The transportation of natural gas-oil-water mixtures through pipelines is the most relevant practice that relates to this area of research. The three-phase flow is not limited to the oil and gas industry alone but can also be encountered in chemical, civil and nuclear industries. In the oil and gas industry, some problems encountered frequently

are: calculation of the flow rates, liquid holdup and pressure drop in the pipeline. These problems need to be taken into consideration seriously, especially during the design of multiphase flow in tubing, the complexities in the analysis of three-phase flow experiments and separation system, sizing of gas lines, heat exchanger and condensate line [1].

The water cut (WC) is the water quantity at the pipe inlet as volume percentage of the total inlet volumetric flow rate. The water cut is always the basis for pipelines and equipment design. During the transportation of the multiphase flow, water in the system starts separation and thereby accumulates at the pipe bottom and that amount of water is being referred to as local water contents, local water or water holdup. The water holdup can be defined as the ratio of the volume of water to the total volume of liquid as a local content at the point of reference.

For different operating conditions, water concentrates at certain locations along the pipe which creates different water hold up profiles and pressure gradients [2]. The presence of water, salts and carbon dioxide gas in petroleum products are the main cause of carbon steel pipelines corrosion during oil transportation and storage. At low water cut, the corrosive water does not create problems when water is fully dispersed in oil.

Most oil wells operate at different water cuts, as high as 90%, which lead to different flow regimes. As water cut increases, water droplets start to coalesce and phase separation of oil and water occurs. In horizontal or near horizontal pipes, the three-phase flow along the pipe with air flowing at top of the pipe, oil flowing at the middle and water flowing at the bottom of the pipe due to difference in densities. As each phase wets

part of the pipe, therefore, the possibility of corrosion is high when water phase is in contact with the pipe wall. It is therefore important to understand the three-phase air-oil-water behavior in production pipelines and also predict the flow patterns, pressure gradient and consequently control the pipe corrosion. This study will also assist in energy savings by reducing the cost of operation of the three-phase flow loop once the flow pattern can be determined at a particular flow conditions thereby using a single phase pump as against the multiphase pump.

1.2 Literature Review

Experimental research was performed by Sobocinski [3] on the three-phase water-oil and air in a 7.62 cm internal diameter transparent horizontal plastic pipe. The test fluids used were diesel oil, water and air. He carried out 114 tests to observe flow pattern and measure pressure drop and holdup of the three-phase air-oil-water. This is one of the earliest researches on multiphase flow.

Experimental study was also carried out by Malinowsky [4] on three-phase air-oil-water flow in a horizontal pipe using the flow loop facilities of Tulsa University Fluid Flow Project (TUFFP). 34 tests were conducted in a 1.5 inch inner diameter transparent acrylic pipe to measure the pressure gradients. He compared his experimental results with that of Beggs and Brill [5] and with that of Duckler et al. [6]. He also back calculated the effective liquid viscosity from the measured pressure gradients which were different from the calculated effective liquid viscosities.

79 experiments were conducted by Laflin and Oglesby [7] on air-oil-water three-phase flow using the same facilities at TUFFP. Flow rates and pressure gradients were recorded while the flow patterns were plotted on the flow pattern maps of Beggs and Brill [5] and Mandhane et al. [8]. Their data were in the flow regime of intermittent flow and they also investigated flow rates near the inversion point.

Experimental study was carried out by Stapelberg et al. [9] on three-phase gas, water and mineral oil experiments in 23.8 mm and 59 mm internal diameter horizontal pipes. The viscosity of the oil was 31 centipoise (cp) and the flow regimes of stratified and slug flow were studied while also measuring the pressure gradients, slug lengths, slug frequency and other slug characteristics. New data were provided and inadequacy of methods that were used for calculating pressure gradient especially in stratified three-phase flows was also demonstrated.

Acikgoz et al. [10] performed experiments on the three-phase air-water-oil in a horizontal pipeline by observing the flow regimes and also constructing flow regime maps. The test fluids used were air-water and mineral oil with the oil properties of 864 kg/m^3 density and viscosity of 0.1164 Pa.s. The flow regime map was constructed by keeping the oil superficial velocity constant, increasing the water superficial velocity slowly and also keeping the air superficial velocity constant so as to determine the transition point from oil to water based flow. The same technique was used to acquire data for the flow regime transition points. The three-phase flow regime was classified into ten groups.

Experimental study was also carried out by Hall [11] on gas-oil-water three-phase flow in horizontal pipes. He also modeled the three-phase stratified flow by using the obtained

holdup to calculate the transition from stratified flow to slug flow. The model was compared with experimental data which showed that, the transition occurred at higher gas velocities than those predicted by the model. The oil layer was believed to be the reason, because it travels at a higher mean velocity since its lower interface was in contact with a moving water layer and not a fixed wall.

Lahey et al. [12] performed experiments in a 19 mm inner diameter pipe using three-phase fluids of air, water and mineral oil with viscosity of 116 cp. Flow patterns were observed while oil holdup and water holdup were measured. It was observed that, the region of the stratified flow for the small diameter was very restricted.

Donnelly et al. [13] performed two and three-phase air/water and air/oil/water experiments respectively in a 25.9 mm inner diameter pipe. Several flow patterns were observed while pressure drop and holdup were also measured for each system. Flow regime map was formulated and modifications to the momentum balance for the prediction of three-phase pressure gradient and phase slippage were also suggested.

Malhotra Ajay [14] also conducted two and three-phase flows in a water-oil-gas horizontal flow system. The experiments were performed in a 10.16 cm inner diameter, 10 m long plexi-glass pipeline with a 2 m long plexi-glass test section. Flow patterns were observed, pressure gradient were measured and compared with results from previous work and good agreement was reached. It was observed for the stratified oil-water-gas three phase flows that, the total liquid film height increases with increasing total liquid velocity but decreases with increasing gas velocity.

Holdups of stratified three-phase flow pattern of gas-oil-water was calculated by Taitel et al. [15]. Three steady state solutions for the upward inclined case were obtained. The only stable configuration was the one with the thinnest liquid layer. The major essential step for the calculation of the holdup, pressure drop and transition criteria of the flow pattern was found to be the information regarding the liquid and oil levels in the pipe.

Chen and Guo [16] investigated flow patterns and pressure drop of air-oil-water in two different helically coiled tubes with inner diameter of 39 mm and coil diameters of 265 mm and 522.5 mm respectively. Flow patterns were observed for both two-phase oil-water and three-phase air-oil-water. The flow patterns were classified into four different regimes in each case. Flow pattern transition criteria equations were also deduced from the experimental data. The transition criteria equations gave good agreement when compared with the experimental data. A modified Chisolm correlation was presented in order to predict the pressure drop of gas-oil-water three-phase flow in horizontal coiled tubes.

Baddie et al. [17] carried out experiments in an axial viewing system of a 37 m long, 78 mm inner diameter test section using oil, water and air. The effects of the entrained liquid flows on high gas velocities were studied. It was observed that, the entrained liquid phase in the gas core was mainly as a result of the intermittent bursting of waves at the bottom of the pipe.

Oddie et al. [18] also conducted two and three-phase flows experiment in a transparent 11 m long, 15 cm inner diameter pipe using kerosene, tap water and nitrogen. 444 tests were conducted for observing different flow patterns and measuring holdup. The flow pattern

and holdup were compared with the prediction of a mechanistic model of Petalas and Aziz [19] and the results gave good agreement.

Spedding et al. [20] carried out experiments on two different horizontal three-phase oil-water-air experimental setups. The inner diameter of the two set up were 25.9 mm and 50.1 mm in which measurements and observations were taken in a 2 m length set between the 1.7 m outlet section and 4 m inlet section for the first facility. For the second facility with the 50.1 mm internal diameter has a 4.52 m test section set between 2 m outlet and 6 m inlet. 22 flow regimes that is broadly classified into oil dominated and water dominated were described in the work. A new type of flow regime mapping scheme was also presented to successfully predict two and three phase systems.

Zhang and Sarica [21] developed a model called Unified model to predict the flow pattern and pressure gradient of three-phase gas-oil-water which was an improvement on the earlier unified model of Zhang et al. [22]. The Unified model was based on continuity equations and momentum equations. It considered different equations for all the flow patterns and also their transition criteria including the phase inversion. The Unified model inputs were pipe diameter, pipe roughness, angle of inclination, superficial velocities of gas, oil and water, densities of gas, oil and water, viscosities of gas, oil and water, the surface tensions between the gas and oil, gas and water and finally between the oil and water. The predicted outputs of the Unified model were always flow patterns, pressure gradient and liquid holdup. The model was compared with experimental measurements of three-phase gas/oil/water pipe flows. The three-phase unified model gave better predictions than that of the unified model of gas/liquid two-phase pipe flow when compared with the experimental measurements of Khorr [23] for stratified

gas/oil/water flow in horizontal and 1.5° downward pipes. Similar performance was noticed when the two models were also compared with the experimental measurements of Hall [11] on pressure gradients for three-phase slug flow in a horizontal pipe.

Adrian Wegmann et al. [24] carried out three-phase oil-water-air experiment using paraffin oil, deionized water and air for 5.6 mm and 7 mm inner diameters. Six flow patterns were observed and flow pattern maps were built for both 5.6 mm pipe and 7.0 mm pipe. The flow pattern maps were built with a constant air superficial velocity by varying both paraffin and water superficial velocity for each map. Different cases of flow pattern maps were built for the air superficial velocities range from 0.2 m/s to 6.77 m/s. There was no agreement when the experimental data were compared with existing three-phase flow maps which might be due to the geometrical configuration of the set up and physical properties of the fluids being used but there was a good match when compared with the theoretical transition boundary of Taitel et al. [15] in which the low viscosity ratio may be the reason.

Wang et al. [25] performed experiments on high viscosity oil/water/gas three-phase flows in a 2.067-inch inner diameter pipe. The test fluids used were oil within 150 cp and 570 cp viscosity, filtered tap water and natural gas. The flow patterns and slug characteristics were observed, pressure gradients and liquid holdup were measured. The experimental results were compared with the unified model predictions of Zhang and Sarica [21] and the differences were noted.

1.3 Research Motivation

The occurrence of gas-oil-water three-phase flow in the petroleum industry requires sound knowledge of the behavior of multiphase flow. Therefore, there is a need to fully understand and study the flow rates, flow regimes, pressure gradients and volume fractions of gas, oil and water going into the pipelines during transportation of petroleum products. There is need for further investigation in this area of research to better understand the flow characteristics during petroleum production at different flow conditions such as the geometrical configuration of the pipeline, the physical properties of the fluids and flow rates.

1.4 Thesis Objectives

The objective of this research work was to investigate the characteristics of gas-oil-water three-phase flow in horizontal pipe. Specifically, the flow patterns were investigated and the pressure drops at different flow conditions were also measured. Experimental data up to 90% water cut were acquired since most wells operate up to this water cut and the data were studied in details. The acquired experimental data were also compared with the Unified model of Zhang and Sarica [21].

1.5 Thesis Structure

The thesis is organized into four (4) chapters. Chapter 1 is introduction and literature review. It includes background information about multiphase flow, research motivation and thesis objectives. The literature review presents briefly some researches carried out in the field of air-oil-water three-phase flow as it relates to flow patterns and pressure drop. Chapter 2 is about the experimental setup and procedure and the uncertainty analysis as it relates to the design and construction of the flow loop and techniques used in carrying out the experiments. The uncertainty analysis and the errors in the instruments used in carrying out the experiments were also analyzed in details. Chapter 3 deals with the results and discussions. It considers the flow patterns and effects of different factors on the pressure gradients while chapter 4 presents the conclusions and recommendations. It discusses the outcome of the research and the recommendations resulting from the present work.

CHAPTER 2

EXPERMENTAL SETUP AND PROCEDURE

2.1 Description of the Gas-Oil-Water Three-Phase Flow Loop

The experiments were conducted under controlled room temperature of average of 20℃ in a horizontal gas-oil-water three-phase flow system. The schematic diagram is shown in Figure 2.1 while the photograph is shown in Figure 2.2. The single phase water was pumped first using a rotameter via a 2.2 KW, 3 hp centrifugal pump to the horizontal pipeline. Then, the oil is also pumped into the pipeline and they both combined at the Y-section of the PVC pipe as shown in Figure 2.3. The air is then mixed with the combined oil-water through a hose connected to the pipeline. The three-phase fluids (air-oil-water) then flow simultaneously to the acrylic pipe along the test section. The manometer was connected to the pressure taps along the test section to measure the pressure drop and also the flow patterns were observed. The three-phase fluids are then discharged into the slug catcher tank from the test section after which they are dumped into the separating tank. The separating tank and slug catcher have openings to allow the gas to escape to the atmosphere while the oil and water separates under gravity due to density differences in the separating tank. The oil and water were then returned to their original tanks through another pump connected to the separating tank while the mixture of the oil and water that

could not be separated in the tank was dumped inside the drain. The loop process was repeated again till all the experiments were conducted.

The oil and water were stored in separate tanks. The tanks are four in number, one was used for oil, another one was used for water while the remaining two were used as slug catcher tank and separating tank respectively. The tanks were made of fiber-glass with volume capacity of 1200 liters each as shown in Figure 2.2. The air compressor is the Kaeser compressor air center SM-12 manufactured by Kaeser Compressor Inc. It has an integrated refrigerated air dryer to avoid moist air inside the system and it also has variable speed drive to regulate the air flow rate inside the pipeline. The controlled pressure capacity of the air storage tank is 7 bar. The oil and water have two alternative rotameters each made from King Instrument Company as shown in Figure 2.4. The first rotameter covers lower volumetric flow rate range from 1 gpm to 10 gpm with a full scale error of $\pm$ 3% while the second rotameter covers higher volumetric flow rate range from 4 gpm to 40 gpm with a full scale error of $\pm$ 6%. The maximum flow rate obtained for water was 23 gallon per minute (gpm) while that of oil was 21 gpm. The air flow meter was manufactured by Omega to measure the air flow rate that goes into the pipeline with capacity range from 0 gpm to 338 gpm. The multiphase flow loop has three 2.2 KW and 3 horse-power centrifugal pumps manufactured by Crompton Greaves Ltd. Two of the centrifugal pumps were used to pump the oil and water each from their respective tank while the third pump was used to pump the oil and water from the separating tank back to their original tank controlled through a control panel as shown in Figure 2.5. The flow loop has a mercury U-tube manometer and a pressure transducer made from Rosemount Company to measure the pressure drop along the pipeline.

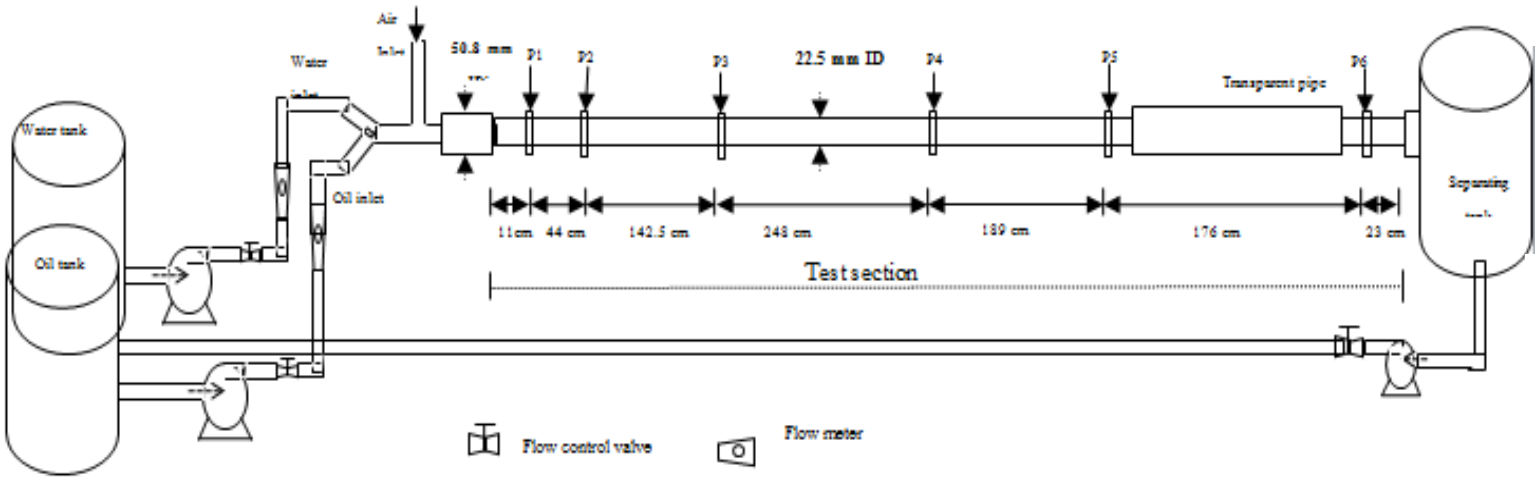

Figure 2.1 Schematic layout of the air-oil-water three-phase flow loop

Figure 2.2 Photograph of the air-oil-water three-phase flow loop

Figure 2.3 Photograph of the Y-section of oil-water

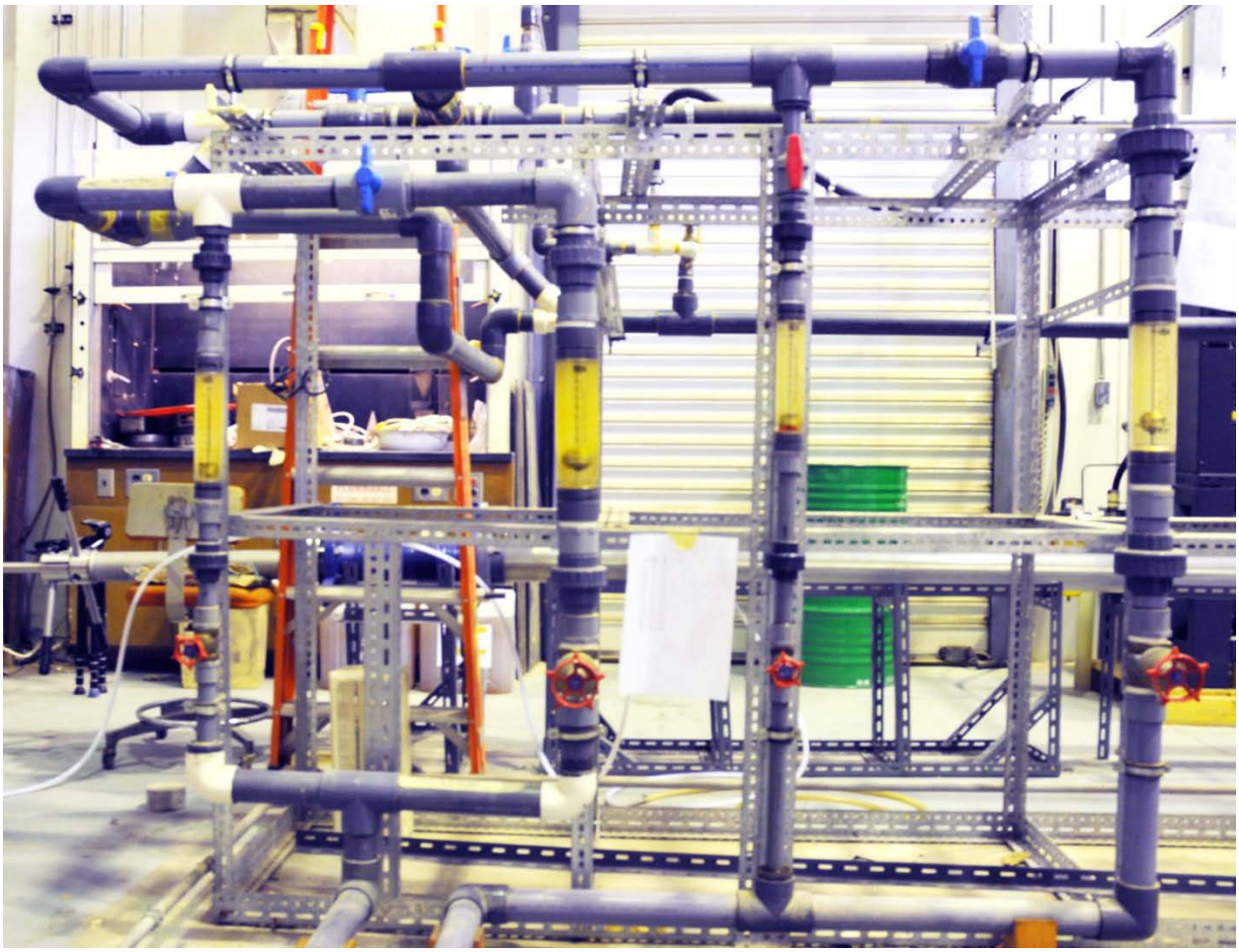

Figure 2.4 Photograph of the oil and water rotameter.

Figure 2.5 Photograph of the oil and water pumps and control panel.

2.2 Description of the Gas-Oil-Water Three Phase Test Section

The test section is 8.33 m long with internal diameter of 2.25 cm but with an entrance diameter of 5.08 cm. The three-phase air-oil-water enters the test section via the 5.08 cm entrance diameter which was then reduced to the 2.25 cm inner diameter in which the three-phase fluids flow till it discharges to the separating tank. A water insoluble dye was used to dye the oil in order to be able to distinguish it from the water. The test section has six pressure taps named P1 to P6 where the manometer and pressure transducer were connected. The test section also consists of a 2.75 cm inner diameter transparent pipe that is 136 cm long. The transparent pipe was used to visualize the flow pattern while the U-tube mercury manometer were connected at pressure tappings P3 and P6 in the pipeline by flexible tubing to measure the pressure drop while the pressure drop was also measured from the differential pressure transducer. The tappings were 6.13 m apart and the pressure drop was displayed in inches of mercury. A minimum pressure drop of 0.1 in. of Hg can be measured. The U-tube manometer is very sensitive and small changes in the pressure drop in the pipeline can easily be detected and also during phase inversion, much larger and sharp changes can be noted easily. The L/D of the test section when the pressure taps were placed at pressure taps P3 and P6 was 88. The length of each pressure tap from each other was as shown in the Figure 2.6. A high speed hp CW450t digital camera was also placed at 0.5 m perpendicular to the pipeline to record the flow patterns with shutter speed of 1/250. All observations and measurements were made in the test section.

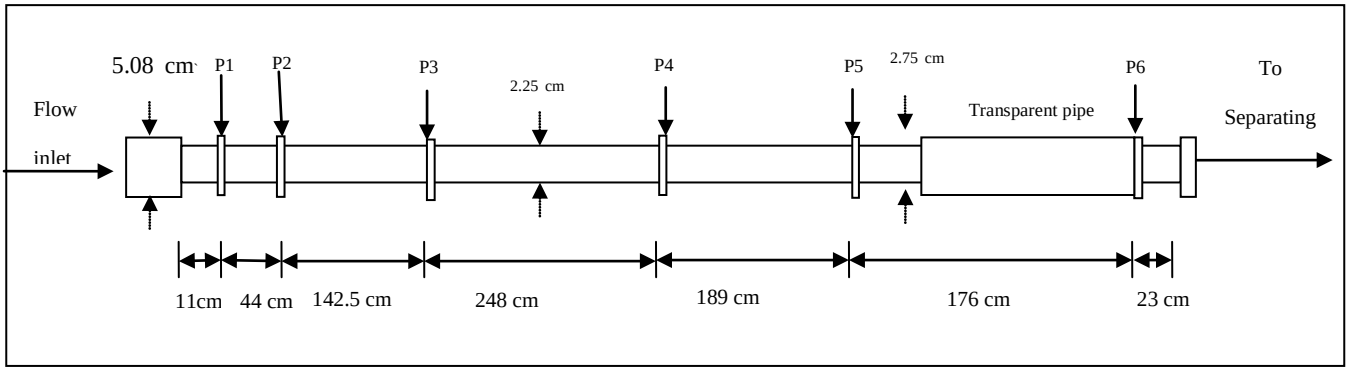

Figure 2.6 Schematic layout of the air-oil-water test section

2.3 Experimental Procedure of the Gas-Oil-Water Three Phase Flow Loop

The oil tank was filled with Safrasol D80 and its properties was shown in Table 2.1, the water tank was also filled directly from the main supply of tap water through a rubber hose while the air compressor was also switched on in order to fill it with air with pressure rating of 7 bar. Before switching on the power to commence the experiments, the following were checked accordingly:

1. No vacuum pressure exists in the PVC, the acrylic pipes connecting pumps with oil and water tanks and also the air compressor.
2. There was no liquid entrained inside the air compressor line.
3. All valves were closed and opened accordingly.
4. No air bubbles exist in all connection lines in the manometers and pressure transducer system, since the air bubbles will affect pressure drop measurements.

The main switch was then switched on after ensuring that everything was in order. The air compressor was switched on until pressure of 7 bar was attained, then the oil pump was turned on from the control panel until clear oil was seen in the pipe and then turned off. The water pump was also switched on and it allowed water alone to flow along the pipeline for some seconds so as to ensure that only water get into the manometers and transducers to avoid erratic measurements in the manometers. The oil was then switched on and the volumetric rates of both oil and water was controlled using the button in the control panel while the air flow meter and valves were also used to meter the desired flow

rates into the pipes. The three fluids (air-oil-water) flowed simultaneously after being mixed at the y-section of the PVC pipe were flowed up to the acrylic pipe. The viscosity of the oil at different temperatures was determined using a Viscometer as shown in Figure 2.7. The Safrasol D80 oil was poured in the viscometer cup and the temperature would be increased or decreased accordingly while the viscosity at that temperature would be displayed and recorded accordingly. The viscosity of the oil was also plotted against temperature to see its variation with temperature as shown in Figure 2.8. This was examined because the temperature of the room varies at times especially during winter and summer but mostly it is on the average of 20℃.

A fully developed flow was achieved before all the experimental data were recorded. Constant Machado et al [26] reported that a single phase fully developed flow could be reached at the distance of 50-100 pipe diameters at the low Reynolds number of 2500. For the multiphase flow, Jepson et al [27] proved that, a fully developed flow could be achieved at a pipe length less than 50 pipe diameters at a relatively high Reynolds number due to the interaction of the different phases. Therefore, for this particular test section with 0.0225 m inner diameter, L/D of 88 and for the velocity range of (0.2-3 m/s), a fully developed single phase water flow with Reynolds number between 11,777 and 100,000 with oil single phase and air single phase could be achieved at less than 1.8m from the inlet.

In addition, for air-oil-water flow, a fully developed turbulent flow can be achieved at less than 1.2m from the y mixing section. Since the distance between this y-section and the first pressure tap was around 1.87m, then a fully developed flow can be achieved

easily before taking measurements since L/D was 88 and the entrance length calculation was shown in appendix A.

The pressure drop was displayed in inches of water in the transducer while the difference in height of mercury in the U-tube manometer was also recorded. Once stabilized, pressure readings and flow are achieved in the manometers and transducers, pressure drop and flow patterns were then recorded for all experiments. The error in the manometer is 0.05 inch Hg. The experiments were performed under full pipe flow conditions. Videos of the flow regime were taken and the air-oil-water flow rates were varied for all the experiments. As soon as the oil or water in the initial tanks were exhausted, all pumps were switched off and oil and water were left in the settling tank while the air escapes from the top openings of the tanks in order to allow enough time for the oil and water to separate. Finally, the separating tank valves will be opened in order to allow the water to be recycled first to its tank since it would be at the bottom due to its higher density, followed by the oil. The mixed oil and water will be dumped in the drain. The process was repeated all over again till all the experiments were completed. Several experiments were performed in order to observe all flow patterns. The effect of water cut, liquid velocity, gas velocity, pressure drop and flow patterns were studied systematically.

Table 2.1 Properties of SAFRASOL D80

Product Name	**SAFRASOL D80**
Flash point	88℃
Density	800 kg/m^3
Viscosity	1.77cp at 20℃
Solubility in water	Insoluble

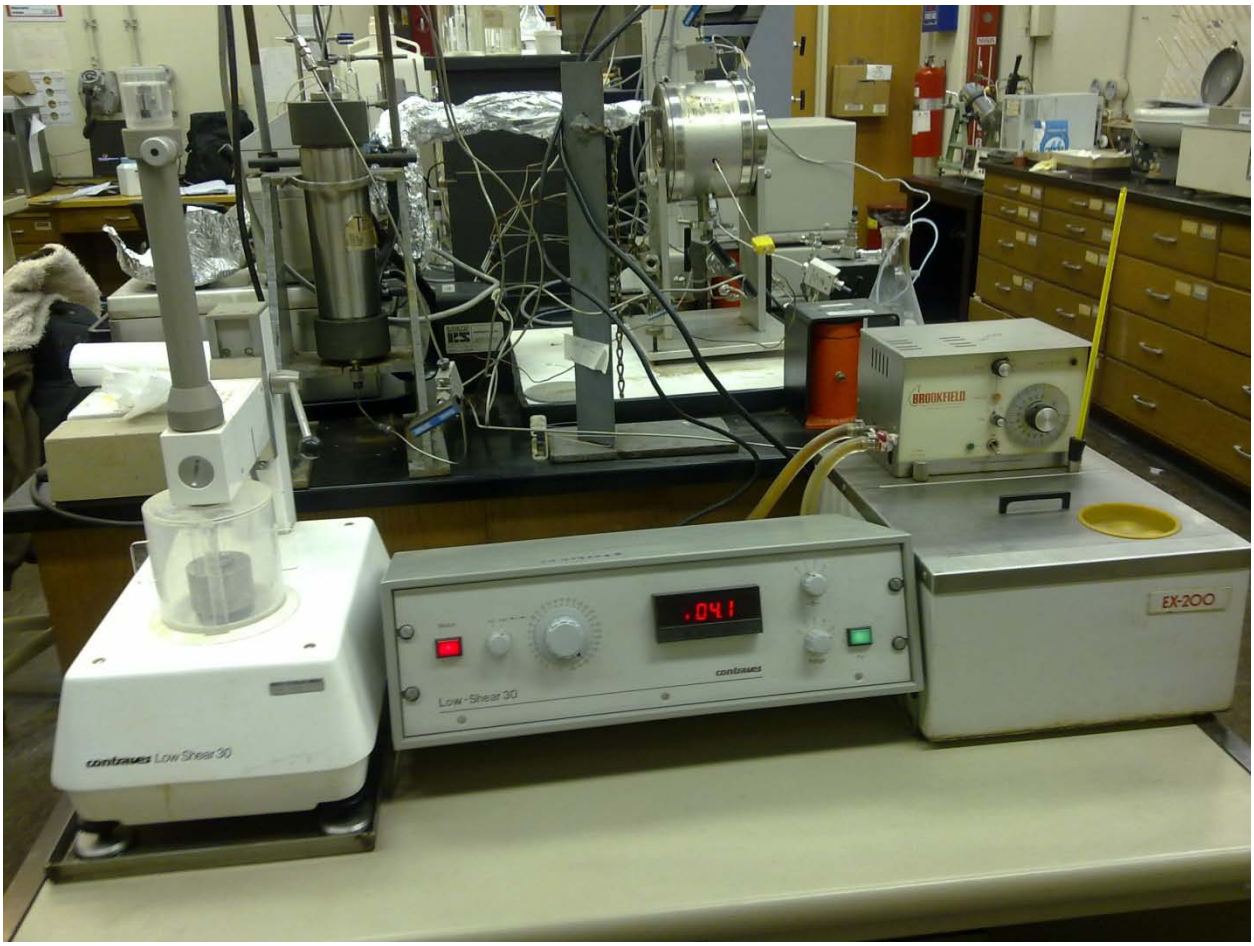

Figure 2.7 The Viscometer used to measure the viscosity of the Safrasol D80 at varying temperatures.

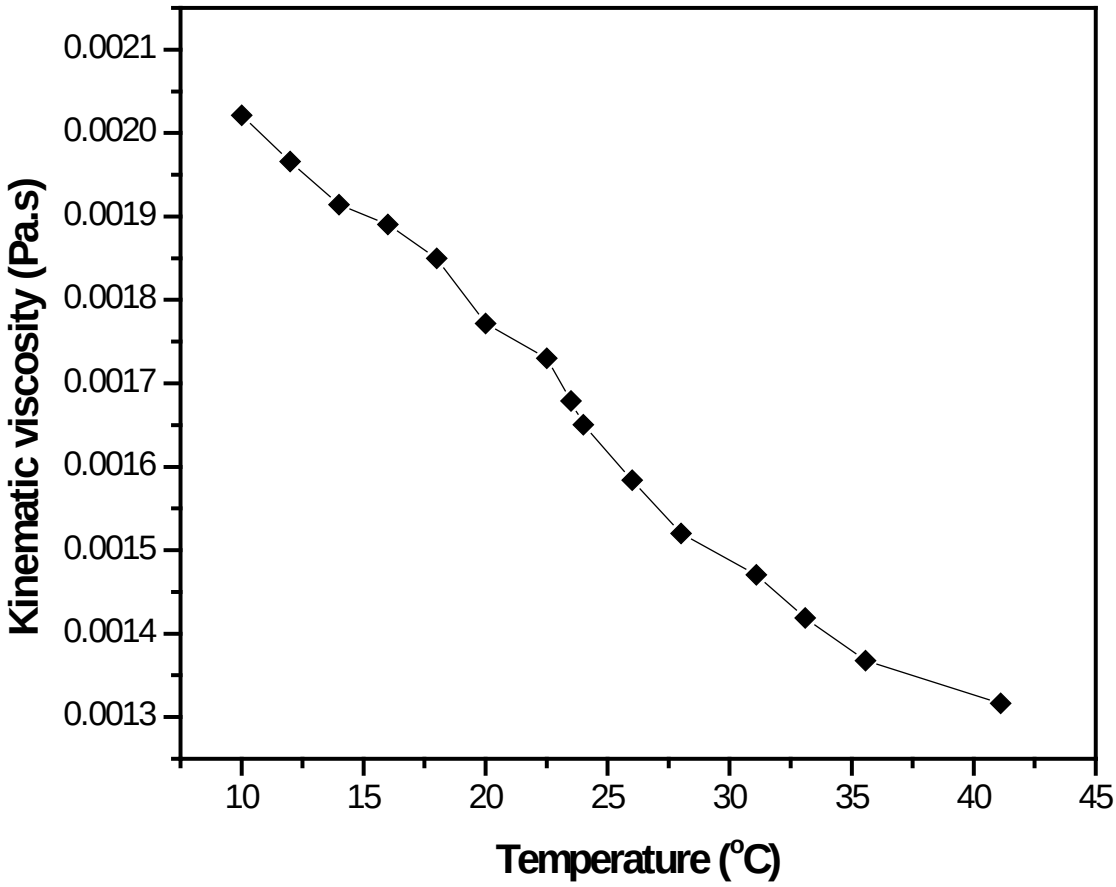

Figure 2.8 The variation of Safrasol D80 oil viscosity against temperature.

CHAPTER 3

UNCERTAINTY ANALYSIS

3.1 Definitions of Key Terms

In this section, some parameters used in air-oil-water flow are defined. When air-oil-water flow in a pipe with a cross sectional area of A, the following parameters can be defined:

1. Superficial velocity of a phase can be defined as the velocity which will result if only that phase flows alone in the pipe. It is the actual volumetric flow rate per unit area.

   The superficial velocities of air, oil and water are defined as follows:

$$V_{SO} = \frac{Q_o}{A} \tag{3-1}$$

$$V_{SW} = \frac{Q_w}{A} \tag{3-2}$$

$$V_{SL} = V_{SO} + V_{SW} \tag{3-3}$$

$$V_{SG} = \frac{Q_a}{A} \tag{3-4}$$

where $V_{SL}, V_{SO}, V_{SW}, V_{SG}$ and A are the superficial velocities of the liquid, oil, water, air and the pipe cross sectional area respectively (m/s)

Q_a, Q_o and Q_w are the input volumetric flow rates of air, oil and water respectively in m^3/s.

2. Water cut (WC) can be defined as water quantity at the pipeline inlet as volume percentages of the total inlet volumetric flow rate of the liquid.

$$WC = \frac{Q_w}{Q_{Liquid}} \tag{3-5}$$

Where Q_{Liquid} is the input volumetric flow rate of liquid

3. The liquid mixture density (ρ_{mix}) can be defined as follows:

$$\rho_{mix} = \frac{M_{total}}{Q_{total}} = \frac{m_o}{Q_{Liquid}} + \frac{m_w}{Q_{Liquid}} = \rho_o \frac{Q_o}{Q_{Liquid}} + \rho_w \frac{Q_w}{Q_{Liquid}} \tag{3-6}$$

$$\rho_{mix} = \rho_o(1 - WC) + \rho_w(WC) \tag{3-7}$$

where:

M_{total} ,m_o and m_w are total, oil and water mass flow rates respectively (Kg/s).

Q_{total} , Q_o and Q_w are total, oil and water volumetric flow rates respectively (m^3/s).

ρ_o and ρ_w are oil and water densities respectively (Kg/m^3).

4. Reynolds Number (Re) for the single phase water was calculated using

$$Re = \frac{\rho_w V_w D}{\mu_w} \tag{3-8}$$

While for the liquid mixture Reynolds number was

$$Re_{mixture} = \frac{\rho_L V_{SL} D}{\mu_L} \quad (3\text{-}9)$$

5. The friction factor (f) is a function of the Reynolds number of the flow and the relative roughness of the pipe (ε/D). For a horizontal pipe flow, it can be calculated from the following relation:

$$f = \frac{\Delta P}{L}\frac{2D}{\rho v^2} \quad (3\text{-}10)$$

where:

ΔP is the Pressure drop (Pa).

L is the distance between the two pressure taps (m).

D is the inner diameter of the pipe (m).

ρ is the fluid density (Kg/m^3).

v is the in-situ average velocity of the fluid (m/s).

ε is the pipe roughness (m).

In addition, for turbulent flow (Reynolds number up to 10^5) in smooth pipes, a very widely used empirical equation that gives very good approximation of the friction factor is a correlation that was proposed by Blasius for single phase:

$$f = 0.316Re^{-0.25} \quad (3\text{-}11)$$

The turbulent friction factor can also be determined using other correlations, such as the Zigrang & Sylvester 1985 correlation [28] defined in equation (3-12) below.

$$\frac{1}{\sqrt{f}} = -2log\left[\frac{\varepsilon/D}{3.7} - \frac{5.02}{Re}log\left[\left(\frac{\varepsilon/D}{3.7}\right) + \frac{13}{Re}\right]\right] \quad (3\text{-}12)$$

3.2 Calibration

At the completion of the multiphase flow loop, the manometers were calibrated and then tested by comparing the experimental single phase data with those from Blasius correlation. The results showed a close agreement between experimental data and Blasius data which means that the pipe is smooth. For the roughness of the pipe, it was estimated by comparing experimental data with Zigrang and Sylvester correlation. The roughness of the pipe was $1 \times 10^{-6}\ m$ which can be considered as a smooth pipe. This was done in order to ensure reliability of the experimental instruments and set up.

The roughness of the acrylic test section was estimated using water single phase pressure drop measurements for an average water velocity range of 0.95m/s to 2.86m/s. In order to avoid the wettability effect of the pipe on pressure drop measurements, oil was not used to achieve this objective. Pressure drops were measured and friction factor was calculated using equation (3-10). The measured friction factor was then compared with the friction factor calculated from Blasius equation (3-11) used for smooth pipe and also the Zigrang & Sylvester correlation (3-12) for different roughness. A figure of Reynolds number against the measured and calculated friction factor was plotted as shown in Figure 3.1. The roughness of the acrylic pipe used at the test section was estimated from this Figure 3.1. The Blasius and Zigrang & Sylvester correlation of $k = 1 \times 10^{-6}\ m$ gave a good approximation to the friction factor of the measured values. We can therefore say

that, the roughness of the pipe was $1 \times 10^{-6}\, m$ which can be considered as a smooth pipe. The calculation of the friction factor has been included in Appendix A.

Finally, the oil flow meters were calibrated for oil with the same specific gravity of Safrasol D80 while the air flow meter was also calibrated accordingly.

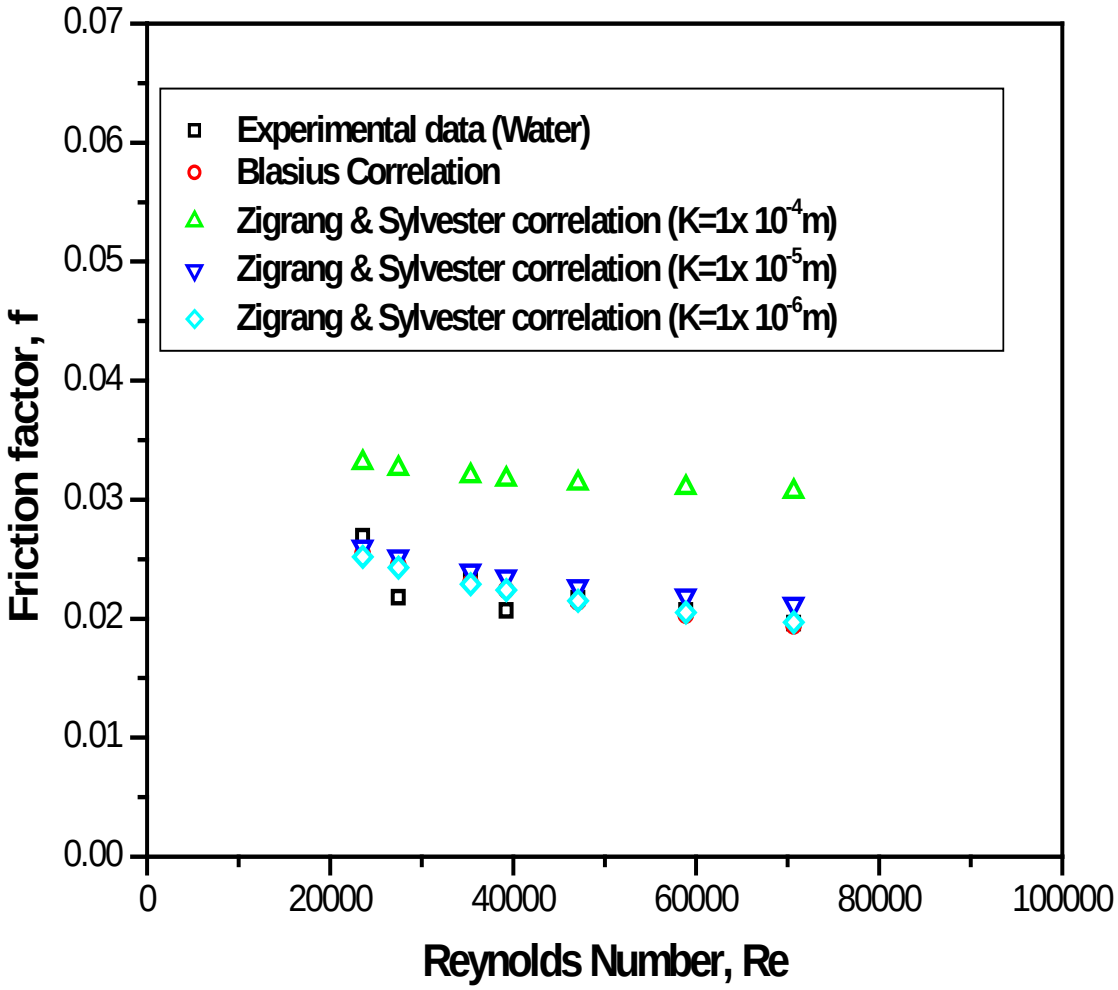

Figure 3.1 Friction factors for single phase water.

3.3 Data Reduction Equation

The pressure drop (ΔP) along the pipe was calculated after measuring the height difference in the U-tube manometer when steady and fully developed flow has been achieved in the pipe. The height difference in the U-tube manometer was recorded when it was steady and converted to pressure using the equation below:

$$\Delta P = \left(\rho_{Hg} - \rho_{H_2O}\right).\Delta L.\, g \qquad (3\text{-}13)$$

where:

ΔP is the Pressure drop (Pa).

ρ_{Hg} is the density of mercury (Kg/m^3).

ρ_{H_2O} is the density of mercury (Kg/m^3).

ΔL is the height difference in the U-tube manometer (m)

g is the acceleration due to gravity (m/s^2)

3.4 Uncertainty Analysis

There is possibility of uncertainty/error in every measurement. Error can be defined as the difference between the measured values and the true values. Since the true value is difficult to know, the error associated with that value will be difficult to know as well.

Uncertainty analysis is the method used to estimate the limits of the unknown error and also describe the credibility of the experimental data.

During the experimental measurements, various forms of uncertainty are liable to be included in the measured values. These uncertainties range from the precision and accuracy of the liquid and gas flow meters, uncertainty in the U-tube manometer readings and that from human. The uncertainties associated with the present experimental study are classified into the following groups.

3.4.1 Type A Uncertainty

Type A uncertainty are derived from the statistical analysis of experimental results. They are estimates that affect the precision of a measurement [29]. These are two sided uncertaintities which can be corrected by carrying out repeatability / reproducibility of a single measurement over a number of times. These uncertainties results mainly from human factors. In the absence of other types of uncertainties, repeated measurements yield results that fluctuate above and below the true or accepted value. Measurements subject to random errors differ from each other due to random, unpredictable variations in the measurement process. The precision of measurements subject to random errors can be

improved by repeating those measurements. The human errors accounted for in the cause of the study are;

- Parallax errors during reading of the U-tube manometers.
- Parallax error while measuring the length of the pressure taps.
- Parallax error while adjusting the flow meter readings.

Type A uncertainty are easily analyzed by statistical analysis. Owing to the sensitivity of the measurements in the study and the uncertainties mentioned above, a single reading in the study was ensured taken at three or more numbers of times. Statistical analyses were carried out on each of the measured values. The results are reported in the form of the mean reading and the overall uncertainty as shown in equation (3-14).

$$x = \bar{x} \mp H \tag{3-14}$$

Where x is the measured quantity (for example: manometer reading),

$\bar{x}$ is the mean of all values for a measurement,

H is the overall uncertainty

$$\bar{x} = \frac{1}{N}\sum_{i=1}^{N} x_i \tag{3-15}$$

$$H = \sqrt{H_o^2 + H_1^2 + H_2^2 + \cdots \ldots \ldots \ldots H_i^2} \tag{3-16}$$

H_o is the standard deviation of the set of value which connotes the human errors; the other uncertainties are the errors in measurements stated by the manufacturers of the measuring instruments used in taking the sets of values.

$S_{\bar{x}}$ is the Type A uncertainty with a 68% confidence level while for 95% confidence level, the student's t-distribution is used. The Type A uncertainty at 95% confidence level is $\bar{\bar{x}} - t_{95}S_{\bar{x}} \leq x \leq \bar{\bar{x}} + t_{95}S_{\bar{x}}$.

Type A can also be estimated as:

$$Type\ A = \frac{Standard\ deviation}{\sqrt{No\ of\ measurements}} \tag{3-17}$$

3.4.2 Type B Uncertainty

Type B uncertainties are those that affect the accuracy of a measurement. Type B uncertainties are one sided estimates and are difficult to trace. These kinds of estimates result from faulty setups and wrong calibration of the measuring instruments; thus, it cannot be corrected by repeating the experiments. In the absence of other types of uncertainty, repeated measurements yield results that differ from the true or accepted value by the same amount. To avoid this kind of uncertainty, all the measuring instrument used for the experiments were calibrated. This was the reason the single phase friction factor was measured and then compared with Blasius and Zigrang & Sylvester correlations to confirm the accuracy of these instruments. They were checked for consistency at various times during the period of the research.

Every Type B uncertainty source is well accounted for and each one of it is denoted as b_i and they are all combined to obtain the total Type B uncertainty, B_R using equation 3-18.

$$B_R = \left[\sum_{i=1}^{N}\left(b_i{}^2\right)\right]^2 \tag{3-18}$$

3.4.3 The Combined Uncertainty

The combined uncertainty U_y is the square root-sum of the squares of Type A uncertainty and Type B uncertainty. The combined uncertainty can be calculated using equation (3-19).

$$U_y = \pm\sqrt{(Type\ A)^2 + (Type\ B)^2} \tag{3-19}$$

In addition, when a parameter is calculated from two or more directly measured parameters, the uncertainty in the derived parameter must also be calculated based on the uncertainties of the parameters from which it was calculated. For the present research work, the total uncertainty of the derived parameter for the pressure gradient was performed.

If y is a function of a,b,c……, the uncertainty in the y will be as a result of independent uncertainties of a,b,c….. and can be expressed using the partial derivative below:

$$U_y = \sqrt{\left(\frac{\partial y}{\partial a}\right)^2 (U_a)^2 + \left(\frac{\partial y}{\partial b}\right)^2 (U_b)^2 + + \left(\frac{\partial y}{\partial c}\right)^2 (U_c)^2 + \cdots} \tag{3-20}$$

3.4.4 The Expanded Uncertainty

The expanded uncertainty U can be obtained by multiplying the combined uncertainty with a coverage factor k.

$$U = kU_y \tag{3-21}$$

Where k =1 for 68% confidence level

k =2 for 95% confidence level

k =3 for 99% confidence level

3.4.5 The Expanded Uncertainty Analysis

The uncertainty analyses for all the parameters used in this research are stated in Table 3.1 while its calculation has been included in Appendix B.

Table 3.1 The Uncertainty Analysis Results

Parameter	**Instrument**	**Expanded Uncertainty**
Test section inner diameter	Vernier Caliper	U_D= 0.0127 mm
Liquid flow rate	King instrument flow meter	U_L= 0.00792 m/s Expanded uncertainty is 0.26%
Gas flow rate	Kaeser instrument flow meter	U_G= 0.021 m/s Expanded uncertainty is 0.04%
Pressure drop	U-tube manometer Maximum Pressure drop = 58.71kPa Expanded uncertainty of $\pm$0.15% (58.71kPa gives 88.065Pa)	$(U_P)_{max}$= 58.71 kPa Expanded uncertainty is 0.15%

CHAPTER 4

RESULTS AND DISCUSSIONS

There is a need to fully understand and study the flow rates, flow patterns, pressure gradients and volume fractions of three-phase air, oil and water going into the pipelines during transportation of petroleum products. This need led to the construction of a multiphase flow loop that was discussed in chapter two.

The experiments were carried out in an acrylic pipe so as to visualize the flow patterns. The test fluids used were Safrasol D80 oil of density $800\,kg/m^3$ and dynamic viscosity of 1.77centi-poise at 20^oC, tap water with dynamic viscosity of 1 centi-poise and 1000 kg/m^3 density at 20^oC and air with dynamic viscosity of 0.000018 Pa s and 1.3 kg/m^3 density at 20^oC. These three different fluids were passed into the horizontal pipeline and the flow patterns were observed while the pressure gradients were measured and recorded. 377 data points were acquired and studied.

The table for the matrix range was as shown in Table 4.1:

Table 4.1. The matrix range for three-phase flow of air-oil-water

$V_{SG}\ (m/s)$	$V_{SL} = V_{SO} + V_{SW}\ (m/s)$	Water Cut (WC)
0.20-52.5	0.2 – 3.0	10% - 90%

The steps of variation of the matrix range for V_{SL} was 0.2 m/s, 0.5 m/s, 0.8 m/s, 1.0 m/s and 2.0 m/s for the flow pattern matrix while that of the pressure gradient was 0.3 m/s, 0.75 m/s, 1.2 m/s, 1.49 m/s and 3.0 m/s for each step of water cut up to 90%. For a particular V_{SL} at a particular water cut, every parameter will be fixed except for the V_{SG} that was varied. The range of the V_{SG} was 0.29 m/s, 0.63 m/s, 1.51 m/s, 3.07 m/s, 4.62 m/s, 7.56 m/s, 12 m/s, 16.8 m/s, 30 m/s, 44.9 m/s and 52.5 m/s for the pressure gradient. Then, the V_{SL} would be increased to the next step and the whole process of V_{SG} would be repeated for all the experiments. A sample of the matrix table for 30% water cut has been included in Appendix C.

This chapter is divided into two sections. Flow pattern of the three phase flow and different parameters that affect the pressure gradient of the three phase flow.

4.1 Flow Pattern

This is the geometric configuration of the gas and liquid phases in the pipe. The flow configurations differ from each other in the spatial distribution of the interface. In order to achieve a more accurate model of the flow and also to have a better understanding of the phenomena occurring during the gas-liquid phase flow, it is very paramount to recognize the boundaries between flow patterns. In addition, while there are research studies presented on flow pattern maps of air-oil-water, no one has presented on the flow pattern map of air-oil-water in a horizontal pipe with 0.0275 m ID using the same fluids properties especially the low viscosity of 1.77 cp of Safrasol D80 oil. Therefore, to assess the effect of Water cuts on changing flow patterns, it is necessary to identify different flow patterns of the horizontal co-current flow of air-oil-water.

Six flow patterns were observed visually for a (0.2 m/s – 2m/s) range of superficial liquid velocity, a (0.20m/s – 35.14 m/s) range of superficial gas velocity and a (0.1- 0.9) input water cut for co-current air-oil-water flow in a horizontal acrylic of 0.0275 m ID pipe. These patterns were presented schematically in Figures 4.1 to 4.6. The flow patterns are classified below and defined according to Collier and Thome [30]:

1. **Stratified flow pattern (ST):** This occurs at relatively low air, oil and water flow rates. The three phases are separated by gravity, where the water flows at the bottom of the pipe, the oil flows at the middle of the pipe and the air on the top. The stratified flow pattern is subdivided into **Stratified-Smooth (SS),** where the

gas-liquid interface is smooth, and **Stratified –Wavy (SW)** occurring at relatively higher air flow rates and stable waves form on the surface.

2. **Elongated bubble flow pattern (EB):** This occurs at relatively lower air flow rates when the flow is calmer. This flow pattern is considered as the limiting case of slug flow, in which the liquid (oil and water) slug is free of entrained bubbles.

3. **Slug flow pattern (SL):** This occurs when the air bubbles are almost the diameter of the pipe. The bubble has a characteristic spherical cap and the air in the bubble is separated from the pipe wall by a slowly descending film of liquid. The oil and water flow is contained in liquid slugs which separate successive air bubbles. These slugs might contain smaller entrained air bubbles transported along with the wake of the large bubble.

4. **Annular flow pattern (AN):** This occurs at very high air flow rates. The air flows in a core of high velocity, which may contain entrained oil and water droplets. The oil and water flow as a thin film around the pipe wall. The film at the bottom is usually thicker than that at the top, depending upon the relative magnitude of the air, oil and water flow rates. At the lowest air flow rates, most of the water and oil flow at the bottom of the pipe, while aerated unstable waves are swept around the pipe periphery and wet the upper pipe wall occasionally.

5. **Dispersed Bubble flow pattern (DB):** This occurs at very high superficial liquid (oil and water) velocities, the liquid phase is the continuous phase, in which the gas phase (air) is dispersed as discrete bubbles. At higher oil and water flow rates, the air bubbles are dispersed more uniformly in the entire cross sectional area of the pipe. Under this flow conditions, due to high oil and water flow rates, the three phases (air, oil and water) are moving at the same velocity and the flow is considered homogenous no-slip.

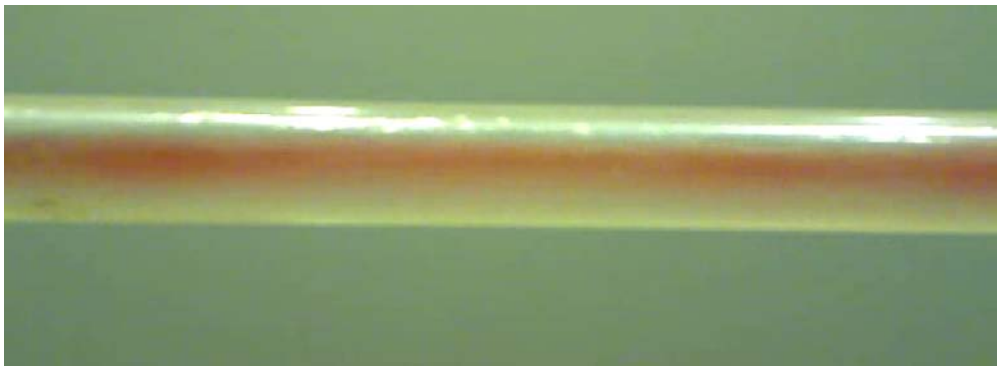

(VSO = 0.2 m/s, VSW= 0.8 m/s & VSG= 0.29 m/s)

Figure 4.1 Stratified smooth flow pattern

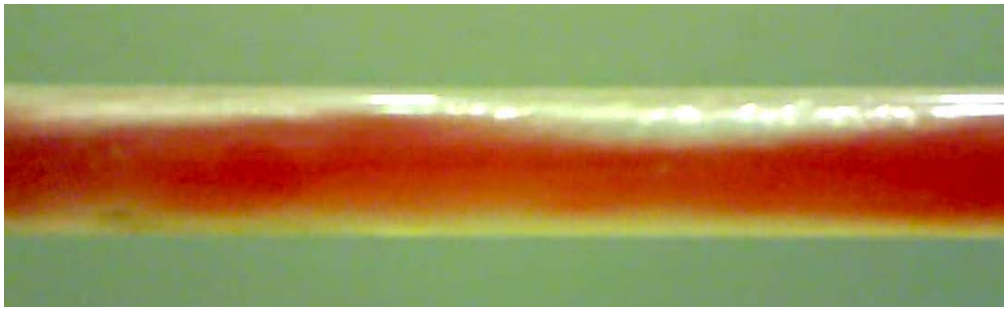

(VSO = 0.9 m/s, VSW= 0.1 m/s & VSG= 0.63 m/s)

Figure 4.2 Stratified wavy flow pattern

(VSO = 0.4 m/s, VSW= 0.1 m/s & VSG= 3.07 m/s)

Figure 4.3 Elongated bubble flow pattern

(VSO = 0.35 m/s, VSW= 0.15 m/s & VSG= 7.56 m/s)

Figure 4.4 Slug flow pattern

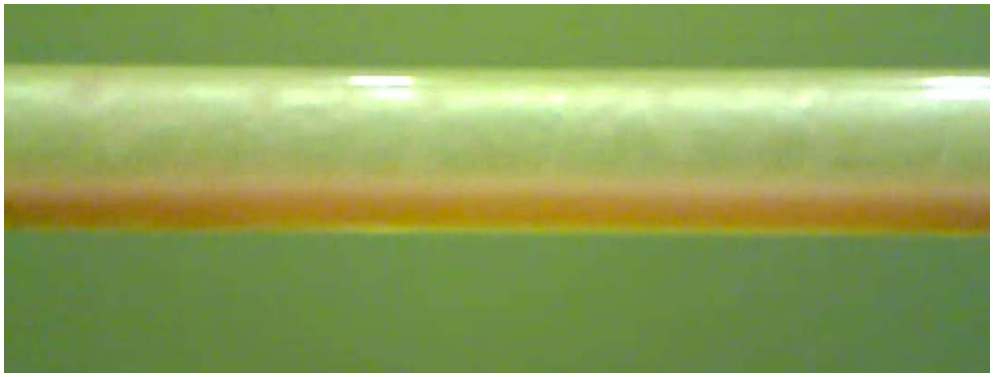

(VSO = 0.72 m/s, VSW= 0.48 m/s & VSG= 44.9 m/s)

Figure 4.5 Annular flow pattern

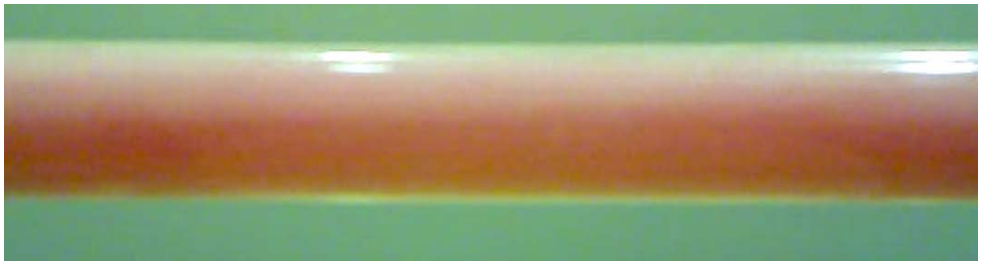

(VSO = 0.8 m/s, VSW= 1.2 m/s & VSG= 0.63 m/s)

Figure 4.6 Dispersed bubble flow pattern

The resultant flow pattern data for the air-oil-water flow are plotted in figures 4.7 to 4.15 for 10% to 90% water cut. As shown in the figures, the superficial liquid velocity ranges from 0.2m/s to 2m/s while the superficial gas velocity ranges from 0.20m/s to 35.14m/s. In all the water cut, we observed six different flow patterns with only five flow patterns present in each water cut.

The superficial liquid velocity V_{SL} is the sum of the superficial oil velocity V_{SO} and superficial water velocity V_{SW}. It can be represented mathematically as shown in equation (3-3),

$$V_{SL} = V_{SO} + V_{SW}$$

For the 10% water cut, it started with stratified wavy until we have the final transition to annular flow pattern. This was the case up to 1m/s superficial liquid velocity but for 1.5m/s superficial liquid velocity, we could not see the transition slug flow, while for high superficial liquid velocity of 2m/s, it started with dispersed bubble flow pattern till it transits to slug flow. This trend continues till it got to 40% water cut.

In addition, it was noticed that as the superficial liquid velocity increases, the flow pattern changes from elongated bubble to stratified wavy and finally to dispersed bubble for 50% water cut at lower superficial gas velocity but for higher superficial velocity, it was noticed that as the superficial liquid velocity increases, the flow pattern changes from slug flow to annular flow pattern. The 60% water cut is also similar to 50% water cut in flow pattern transition.

For 80% and 90% water cut, a new flow pattern was observed, which was stratified smooth flow pattern but dispersed bubble flow pattern was absent in both water cuts

unlike in the previous water cuts where we have stratified smooth absent with the presence of dispersed bubble.

Finally, at very high superficial gas velocity and high superficial liquid velocity, we noticed that the flow patterns were mostly annular flow pattern for all the water cuts.

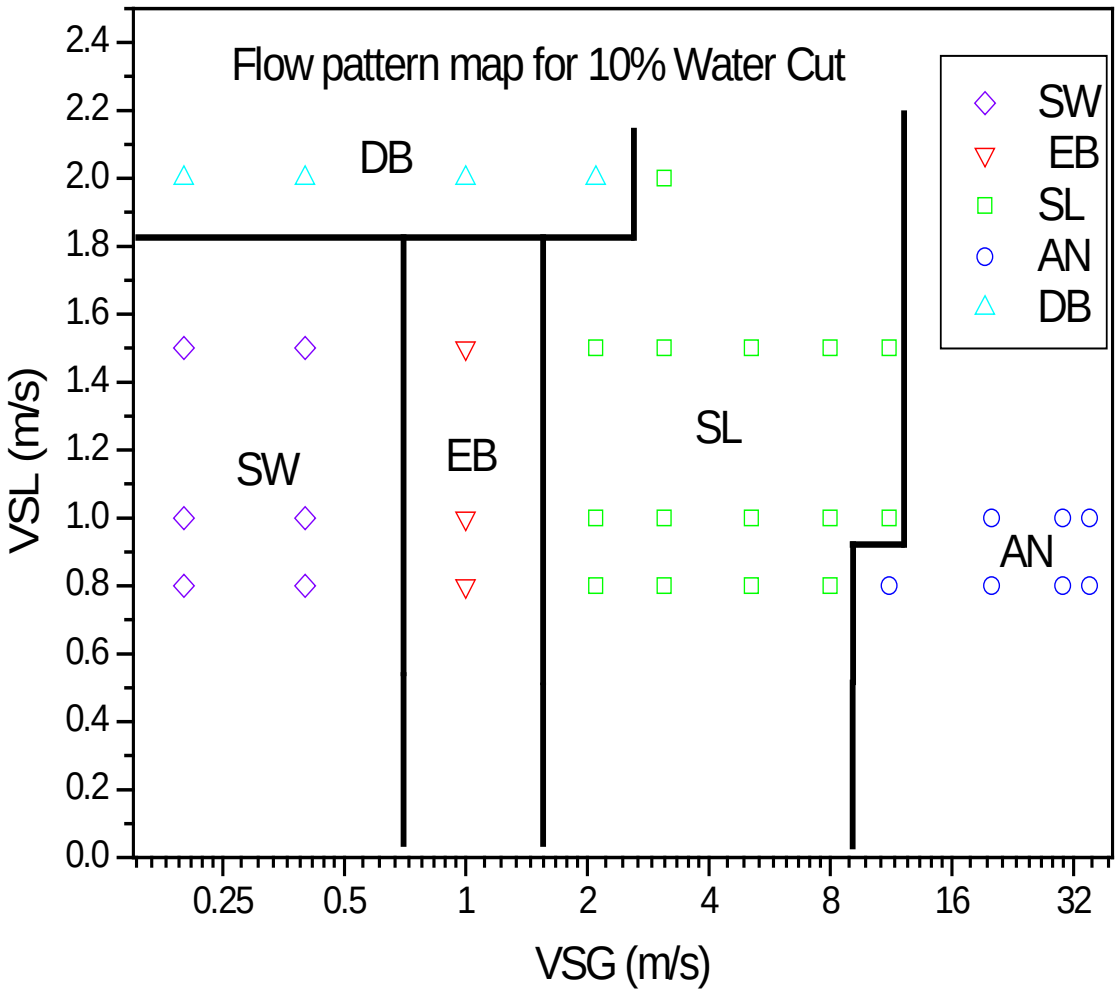

Figure 4.7 Flow Pattern map of Air-Oil-Water for 10% Water Cut.

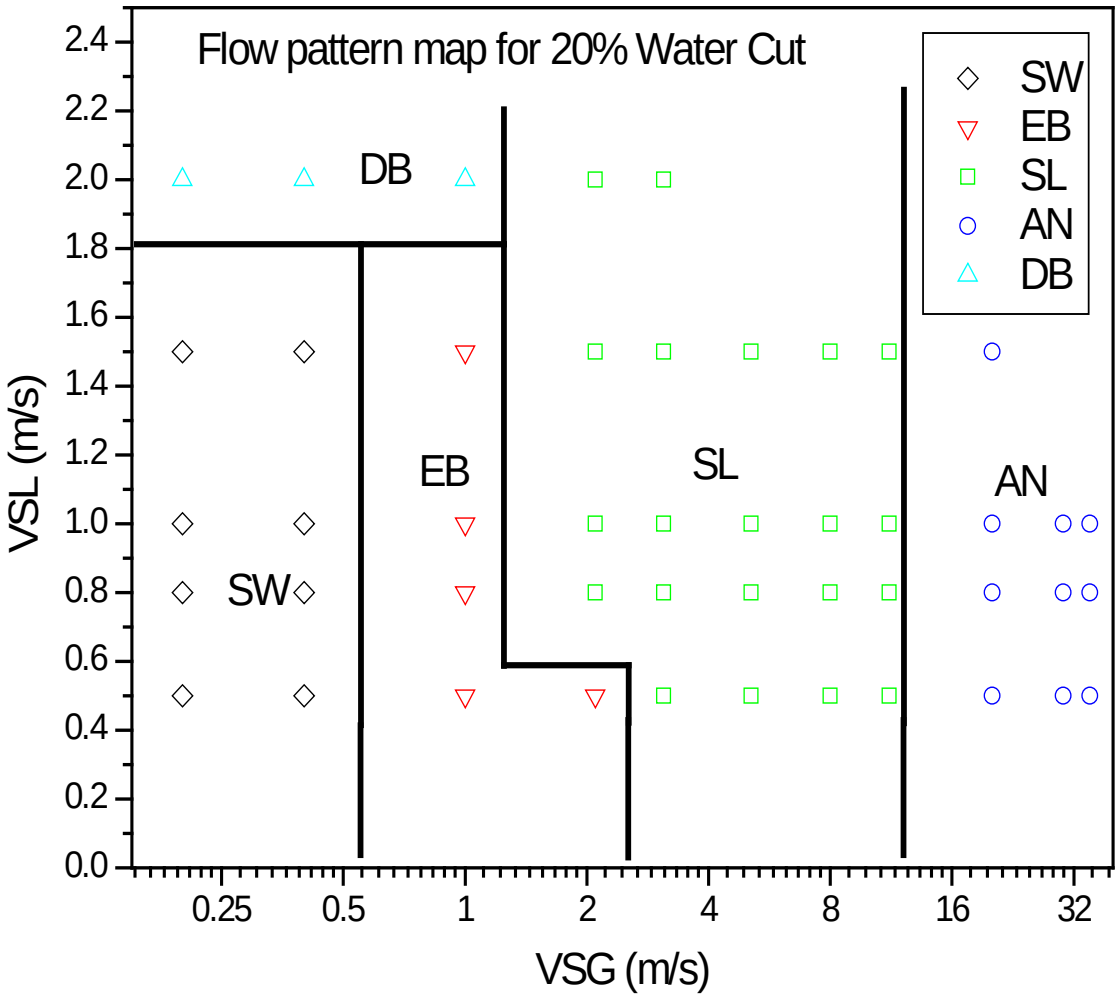

Figure 4.8 Flow Pattern map of Air-Oil-Water for 20% Water Cut.

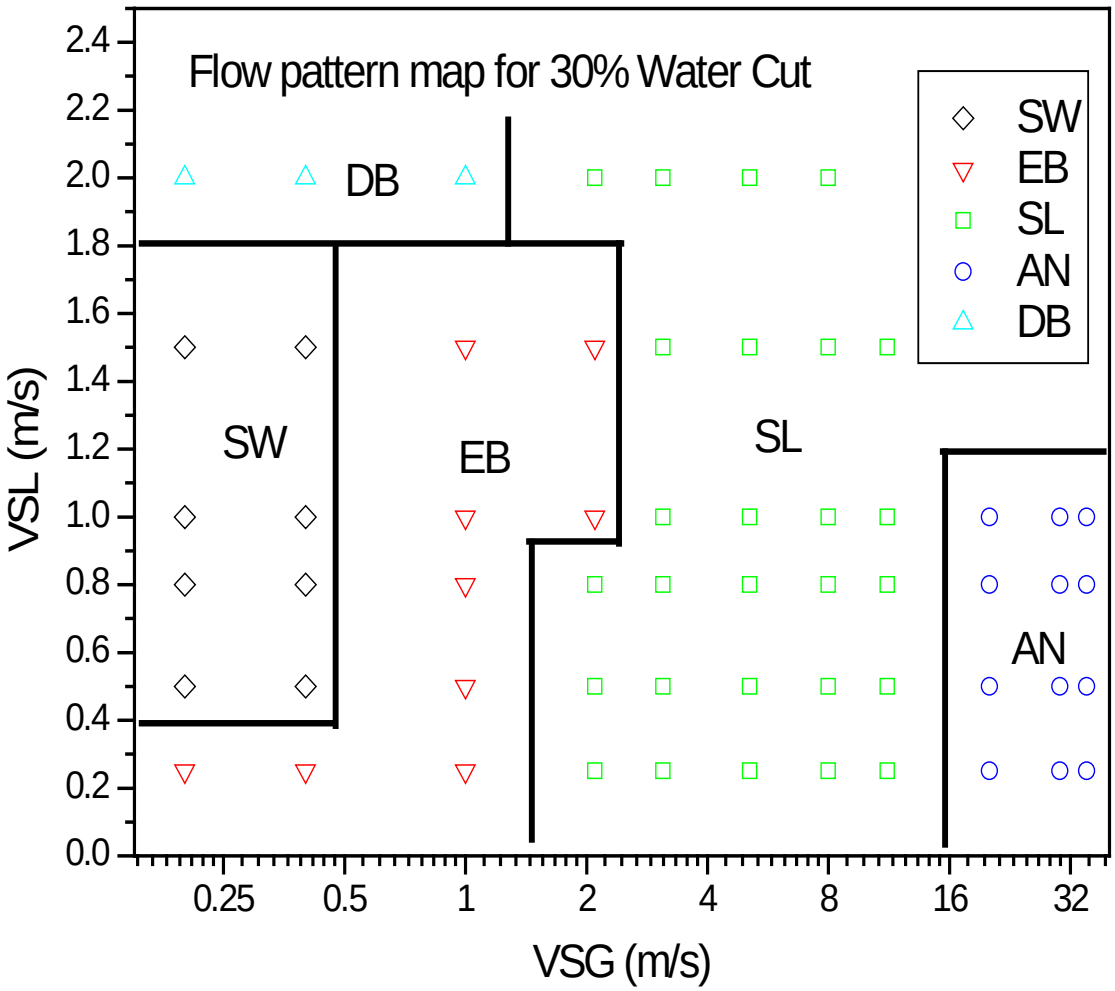

Figure 4.9 Flow Pattern map of Air-Oil-Water for 30% Water Cut.

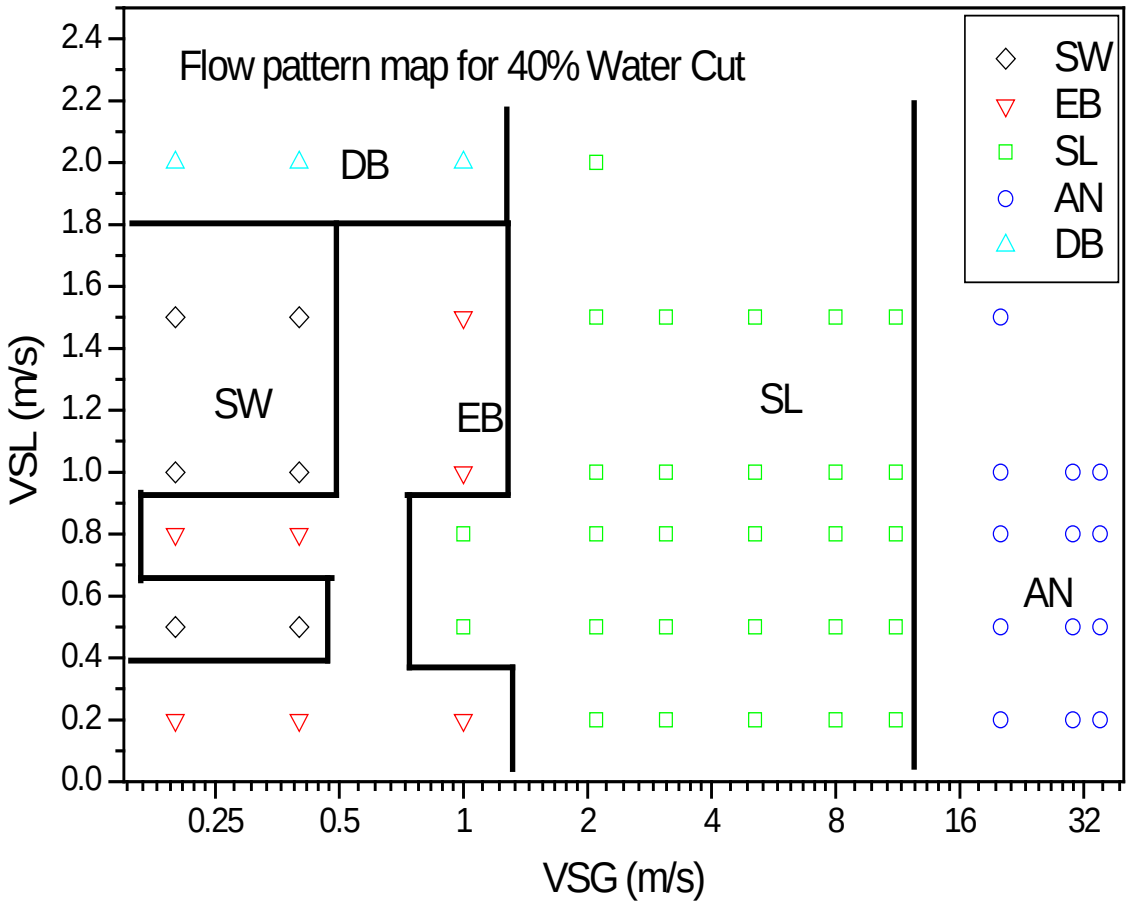

Figure 4.10 Flow Pattern map of Air-Oil-Water for 40% Water Cut.

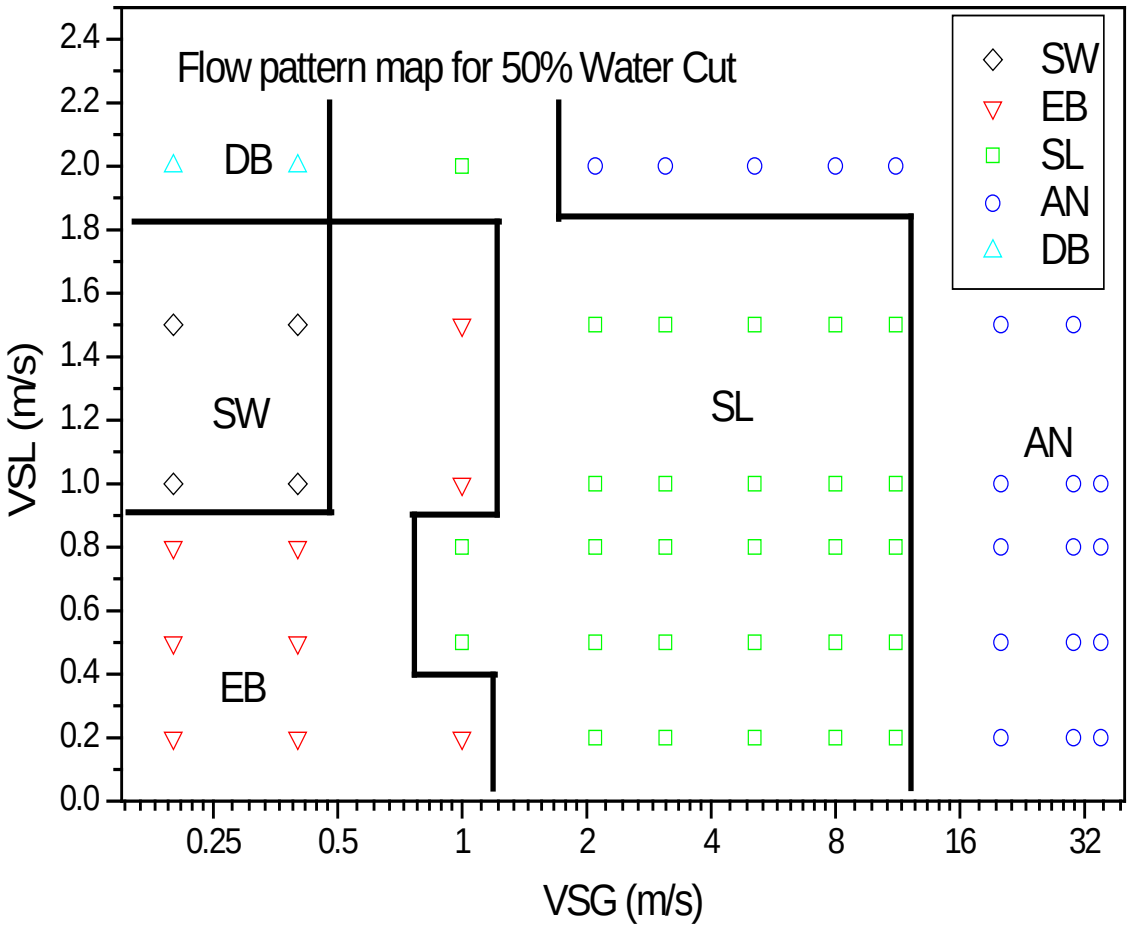

Figure 4.11 Flow Pattern map of Air-Oil-Water for 50% Water Cut.

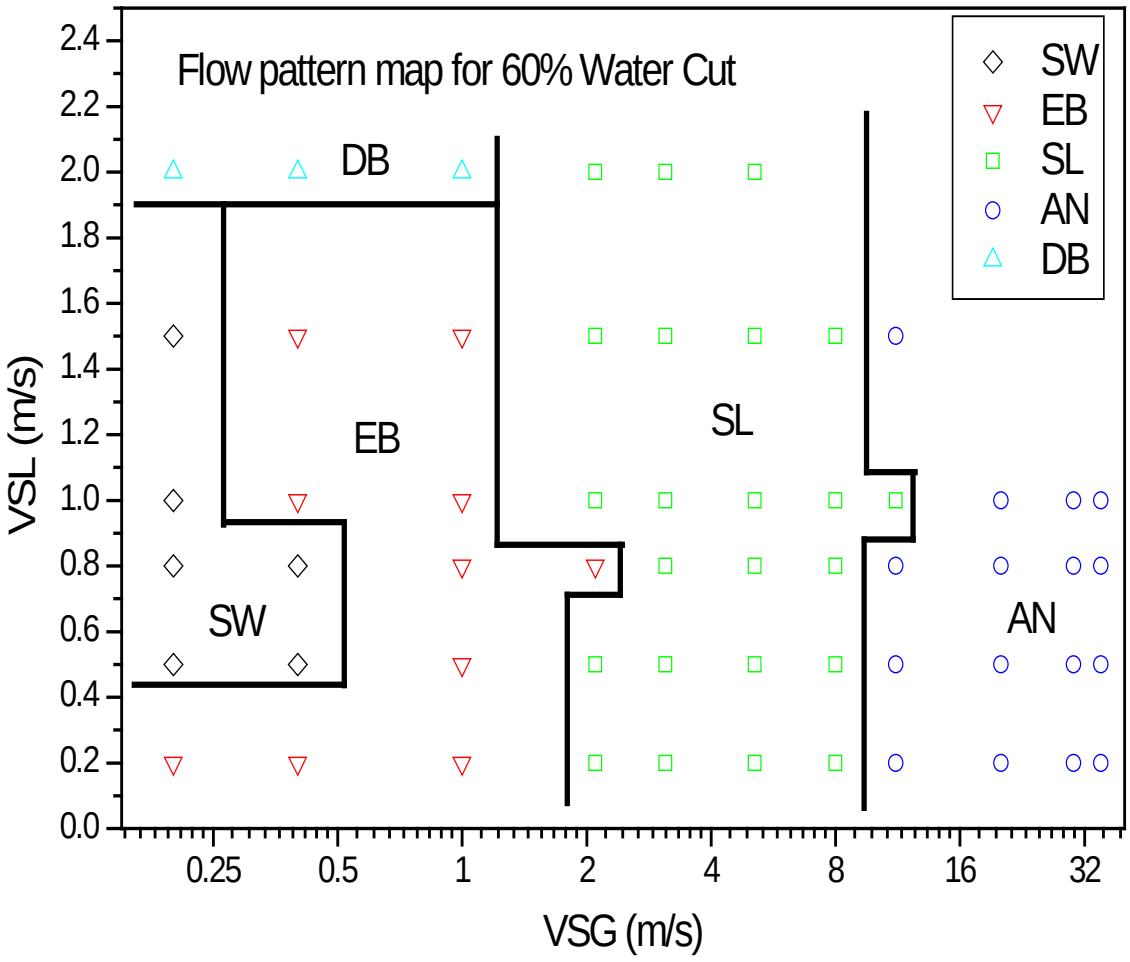

Figure 4.12 Flow Pattern map of Air-Oil-Water for 60% Water Cut.

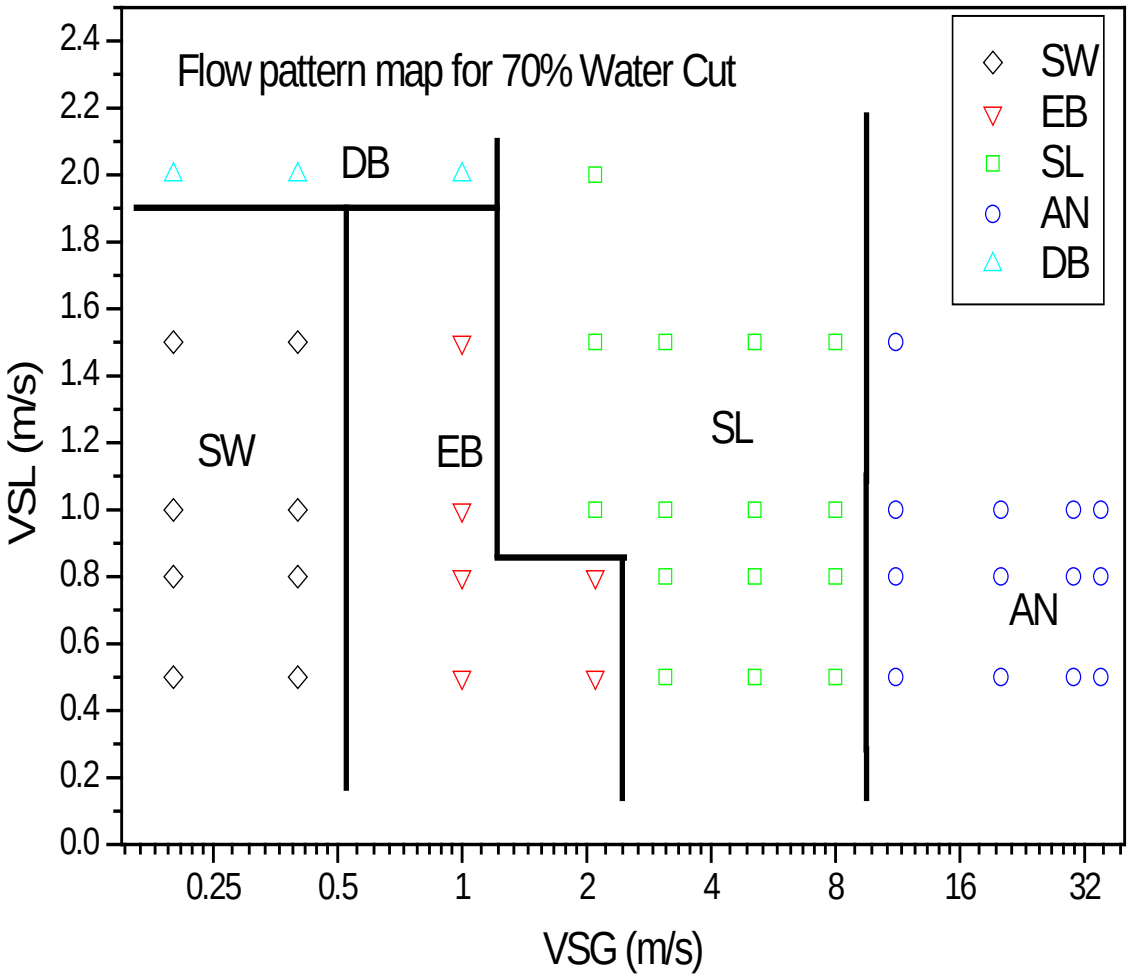

Figure 4.13 Flow Pattern map of Air-Oil-Water for 70% Water Cut.

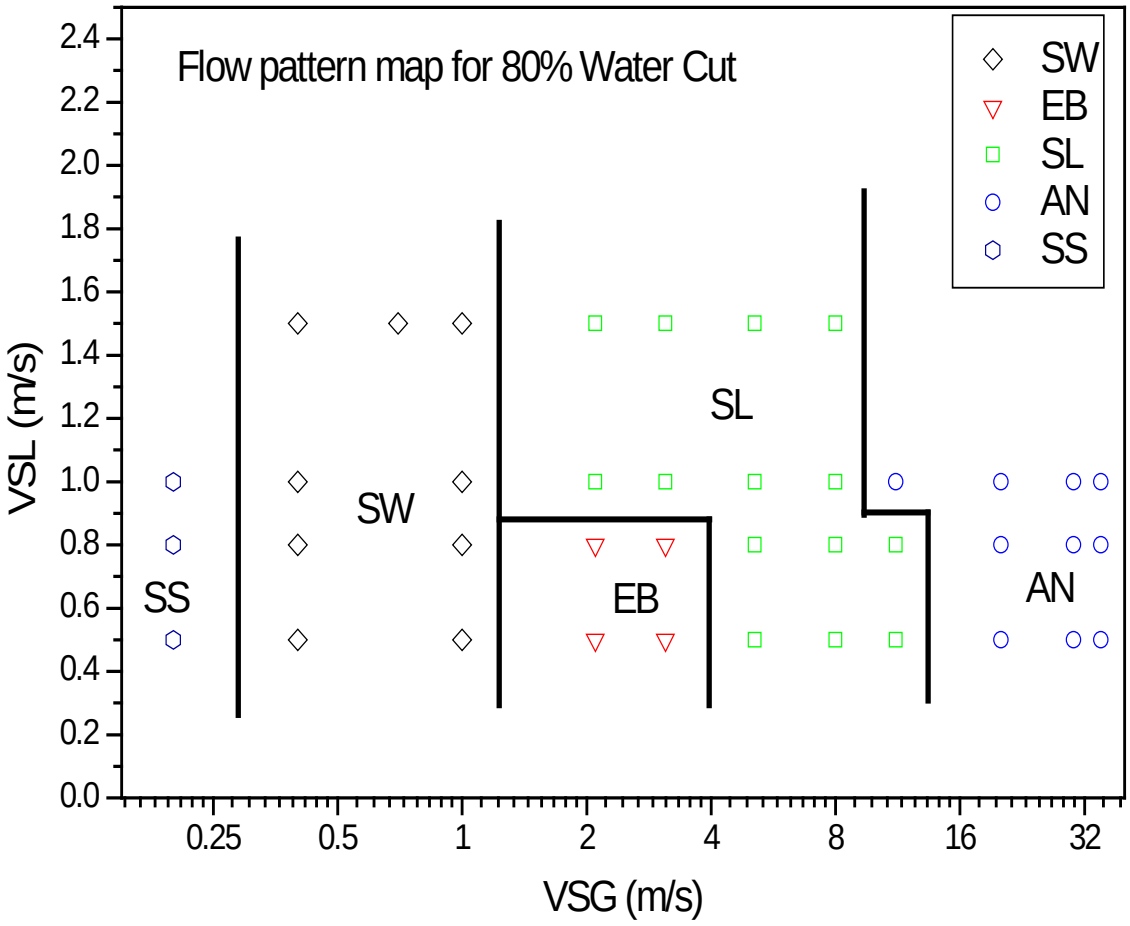

Figure 4.14 Flow Pattern map of Air-Oil-Water for 80% Water Cut.

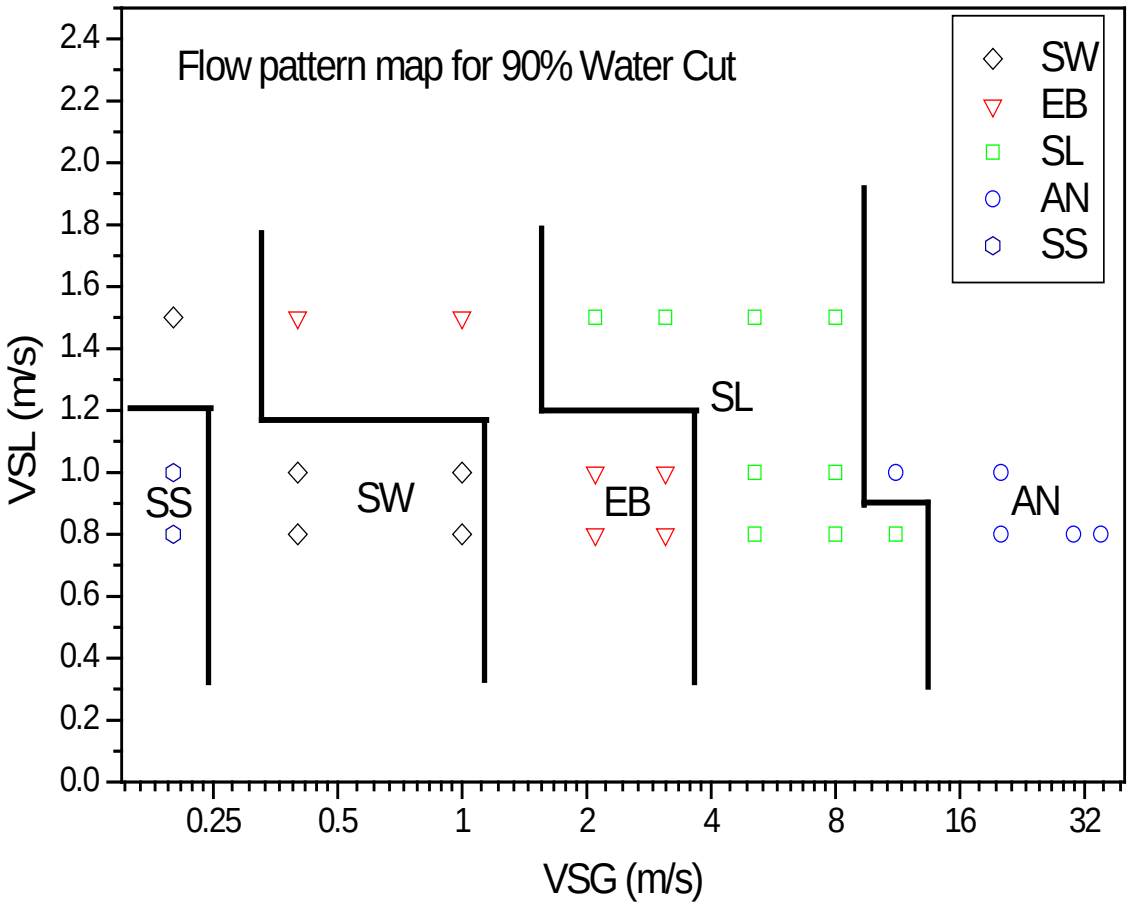

Figure 4.15 Flow Pattern map of Air-Oil-Water for 90% Water Cut.

4.2 Pressure Gradient

The pressure gradient of co-current air-oil-water flow in a horizontal acrylic pipe for superficial liquid velocities between 0.3m/s and 3m/s and superficial gas velocities between 0.29m/s and 52.5m/s and water cuts from 0.1 to 0.9 were presented in Figures 4.16 to 4.41. The first pressure tap was fixed at 1.87m from the pipe inlet in order to have accurate pressure measurement by allowing a complete reduction of turbulence created as a result of the pipe inlet and also to ensure that the flow is fully developed before recording any data since L/D was 88 and the entrance length calculation was shown in appendix A.

The pressure gradients increase with increasing gas and liquid flow rates. The effects of different factors were considered on the pressure gradients and these factors include the effect of superficial gas velocities VSG at different water cuts for varying superficial liquid velocities VSL, the effect of water cuts at different VSG for varying VSL, the effect of liquid mixture Reynold's number only and the effect of VSL at different water cuts.

4.2.1 Effect of Superficial Gas Velocities, VSG, on Pressure Gradients

It can be seen in Figure 4.16 to Figure 4.24 that, the pressure gradients increase with increasing gas and liquid flow rates. For 10% water cut, there were no large changes in pressure gradient for VSG between 0.29m/s and 0.63m/s, and the maximum difference

between VSL of 1.2m/s and 1.49m/s was 0.108 kPa/m and 0.180 kPa/m respectively. This was obvious since the flow patterns at these VSL were stratified.

At higher VSG, the situations were different and the pressure gradients were affected clearly by increasing VSG and the effect became clearer by increasing VSG and VSL. For instance, for VSG more than 16m/s, the pressure gradients were high for VSL of 1.2m/s and 1.49m/s which were 8.98 kPa/m and 10.92 kPa/m respectively at 52.5 m/s VSG. This is due to the fact that, the flow patterns were mainly annular flow pattern.

The trend for 20% water cut was also similar to that of 10% water cut except for the fact that, we were able to measure the pressure gradient for VSL of 0.75 m/s. It was noticed that, as the VSL increases for a particular VSG, the pressure gradient also increases. For instance, the pressure gradient at 52.5 m/s VSG for VSL of 0.75 m/s, 1.2 m/s and 1.49 m/s were 6.18 kPa/m, 9.63 kPa/m and 10.85 kPa/m respectively. We noticed that the pressure gradient at lower VSG below 12 m/s for 1.2 m/s and 1.49 m/s VSL were very close before we started to notice clearer difference at VSG of 16.8 m/s and above, while for 30% water cut, we were able to have additional VSL of 0.3m/s.

The 40% and 60% water cut were also similar in trends to that of 30% but for 50% water cut, we noticed inversion point for the VSL of 3.0 m/s at VSG of 12 m/s.

The 70% water cut was similar in trends to that of 20% water cut, while for 80%, we were able to introduce VSL of 2.24 m/s but the trend was still similar to that of 70% water cut. The 90% water cut was a little bit similar to that of 10% water cut with the exception of a maximum attained new VSL of 2.24 m/s in 90% water cut.

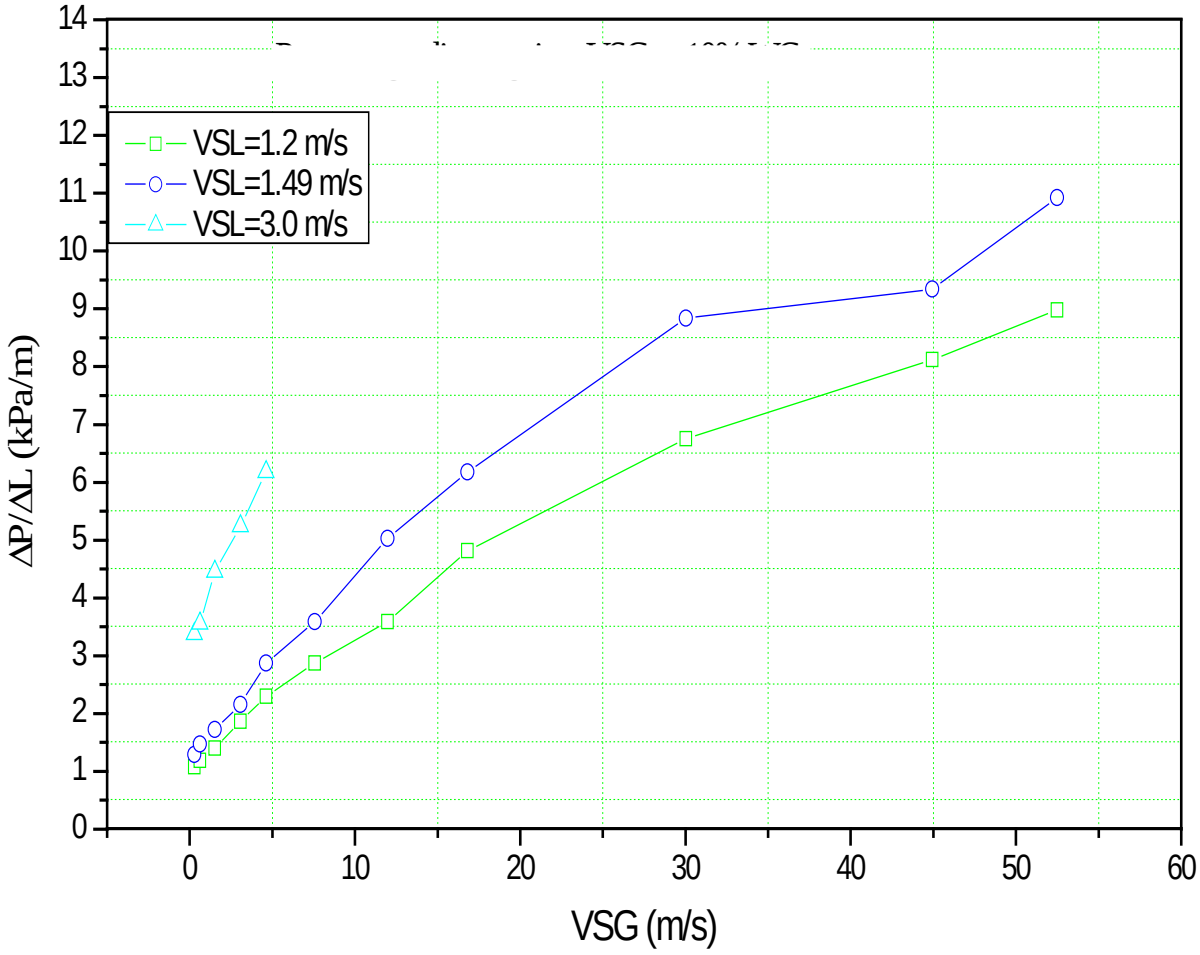

Figure 4.16 Effect of superficial gas velocities on pressure gradients for 10% Water Cut.

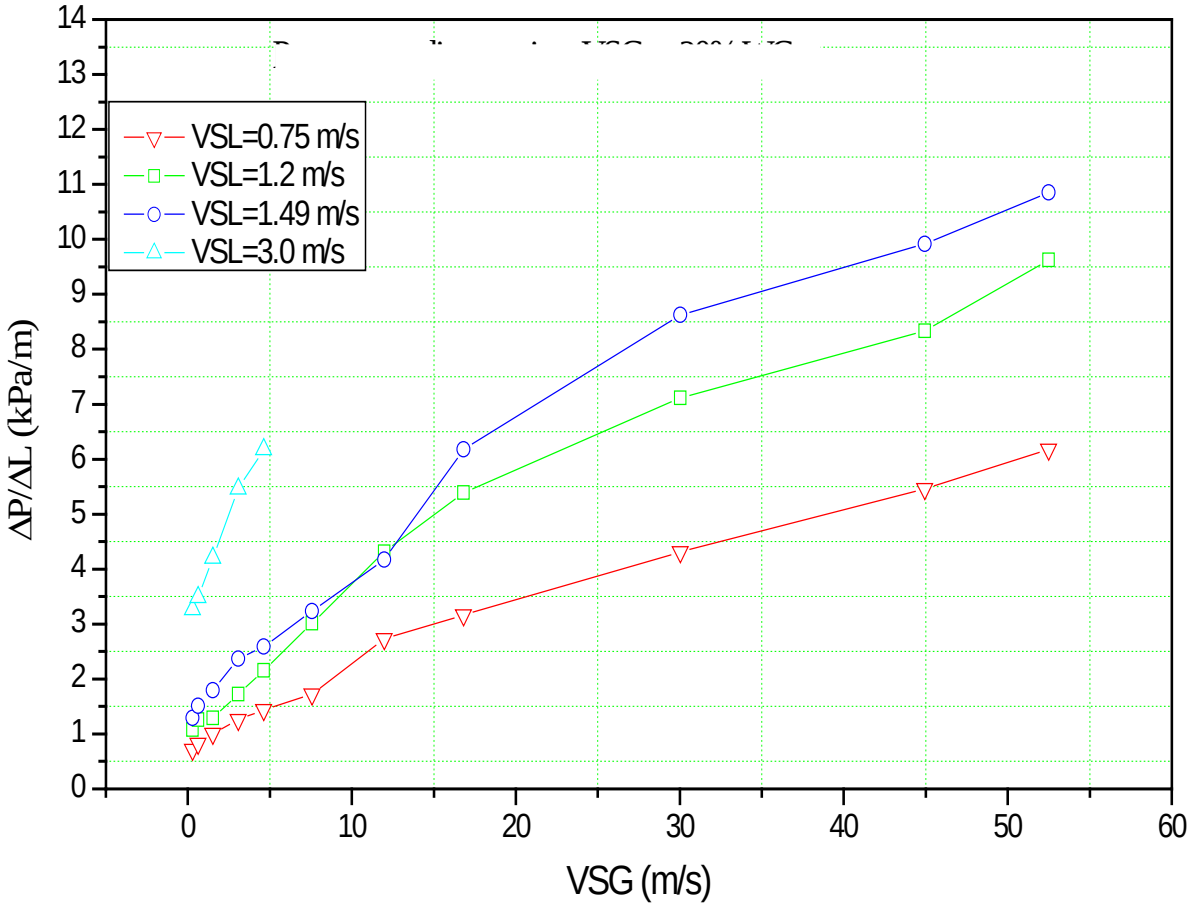

Figure 4.17 Effect of superficial gas velocities on pressure gradients for 20% Water Cut.

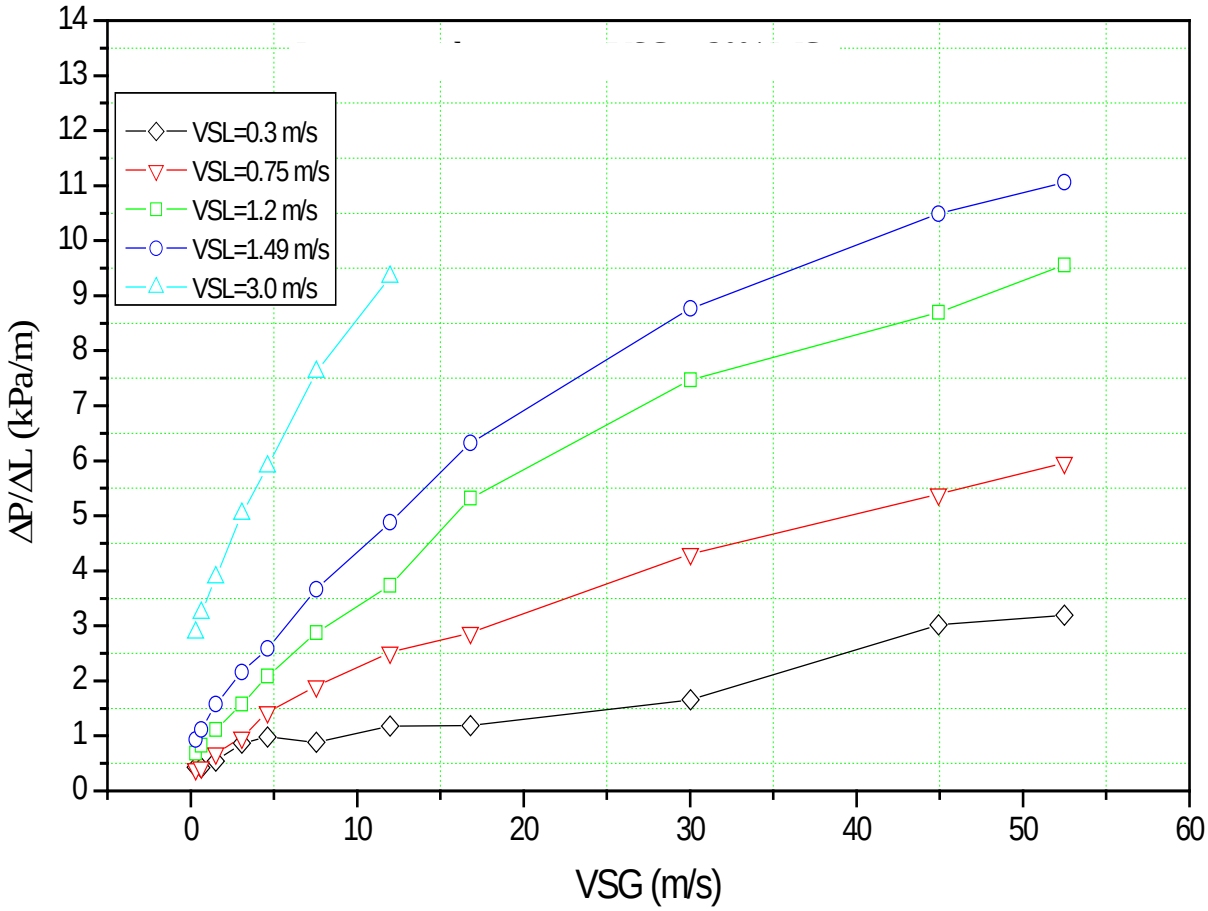

Figure 4.18 Effect of superficial gas velocities on pressure gradients for 30% Water Cut.

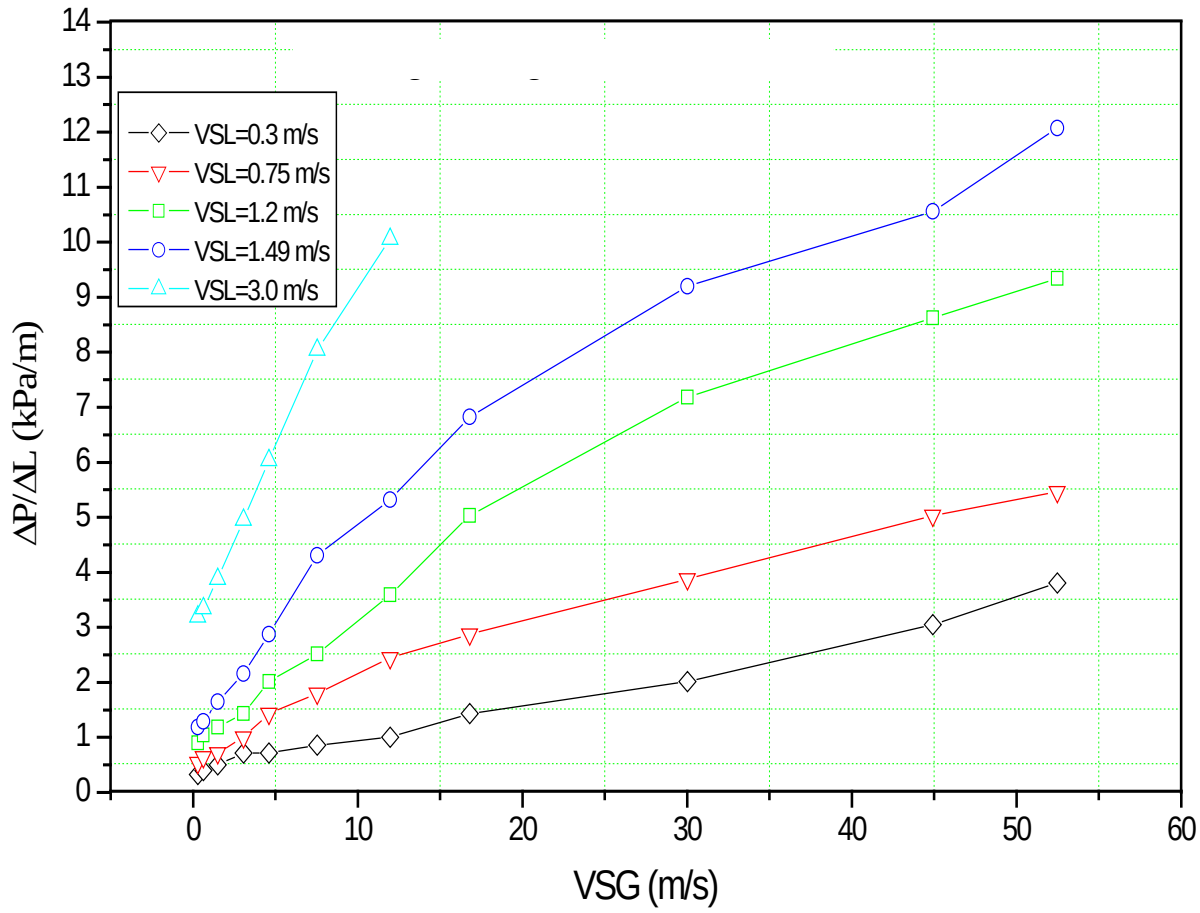

Figure 4.19 Effect of superficial gas velocities on pressure gradients for 40% Water Cut.

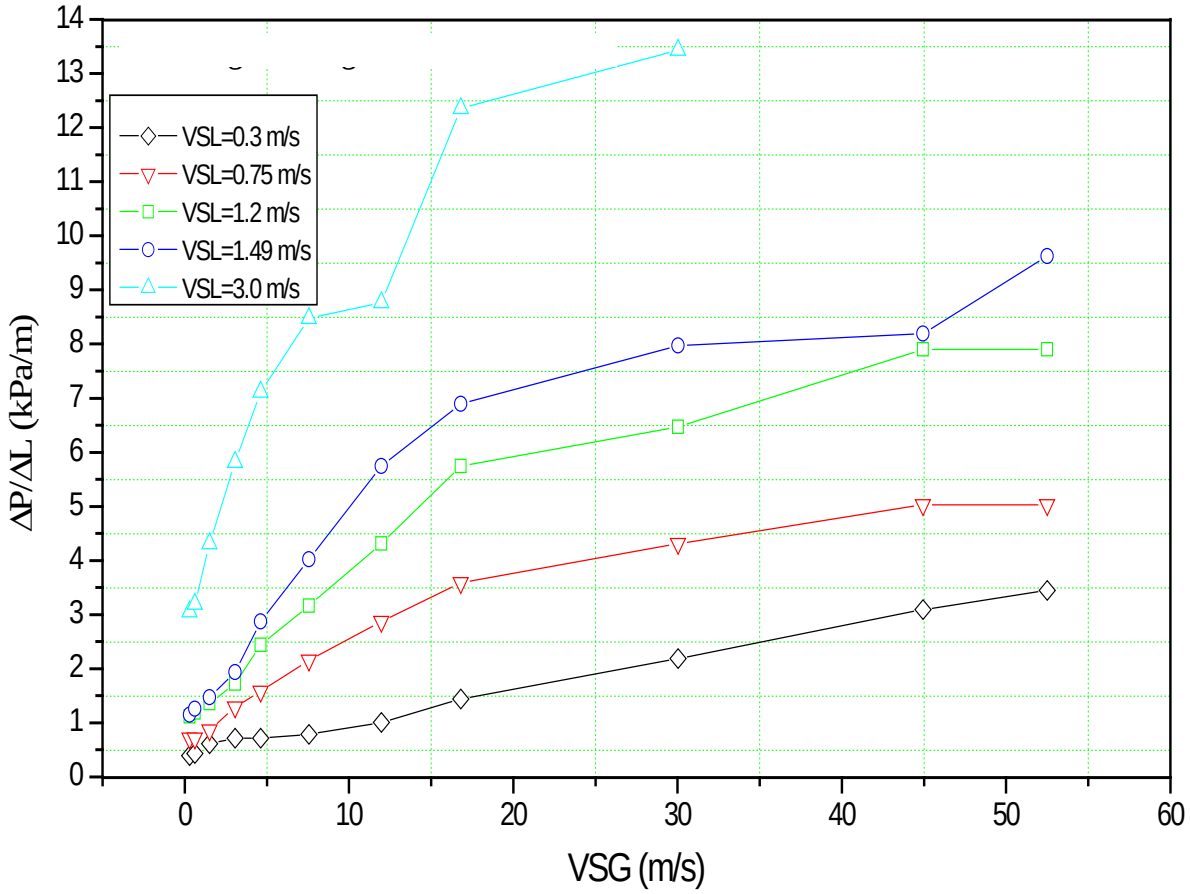

Figure 4.20 Effect of superficial gas velocities on pressure gradients for 50% Water Cut.

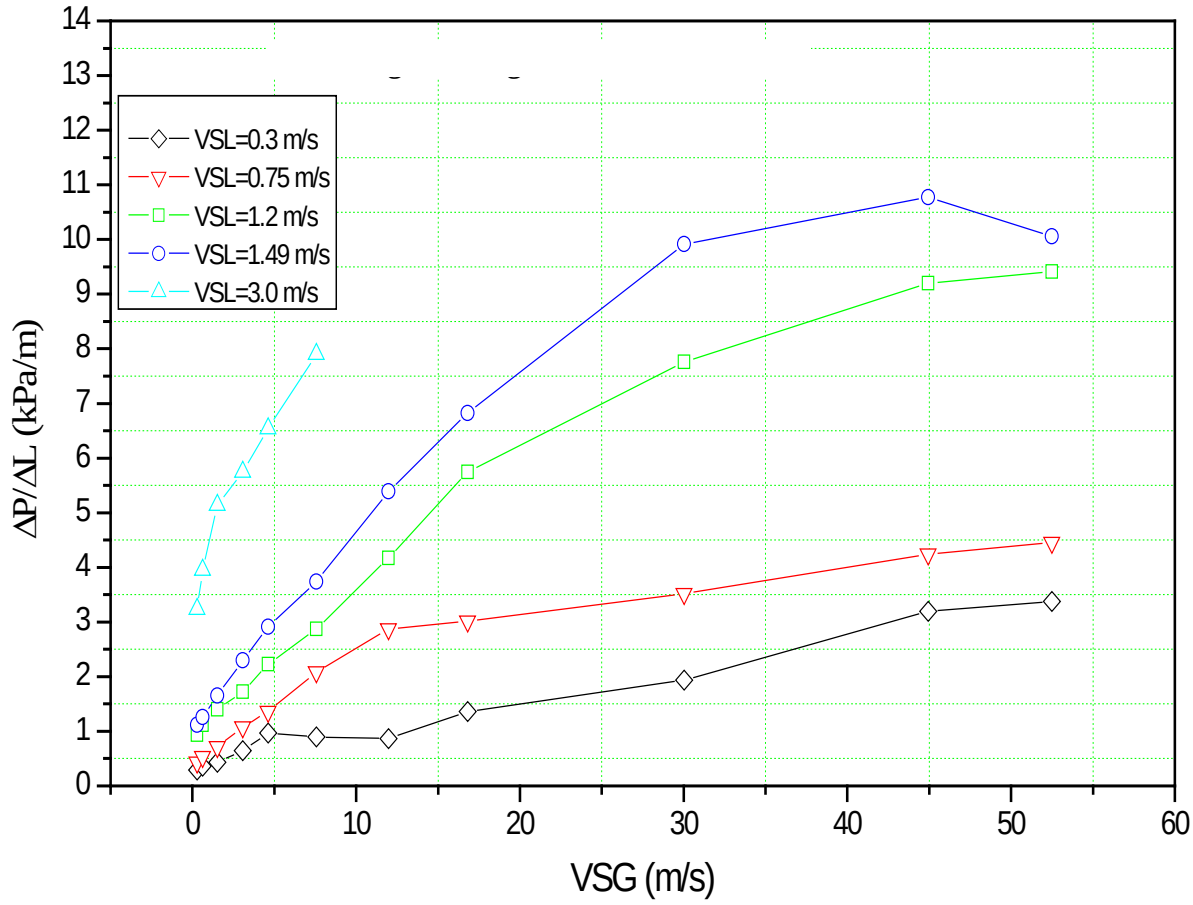

Figure 4.21 Effect of superficial gas velocities on pressure gradients for 60% Water Cut.

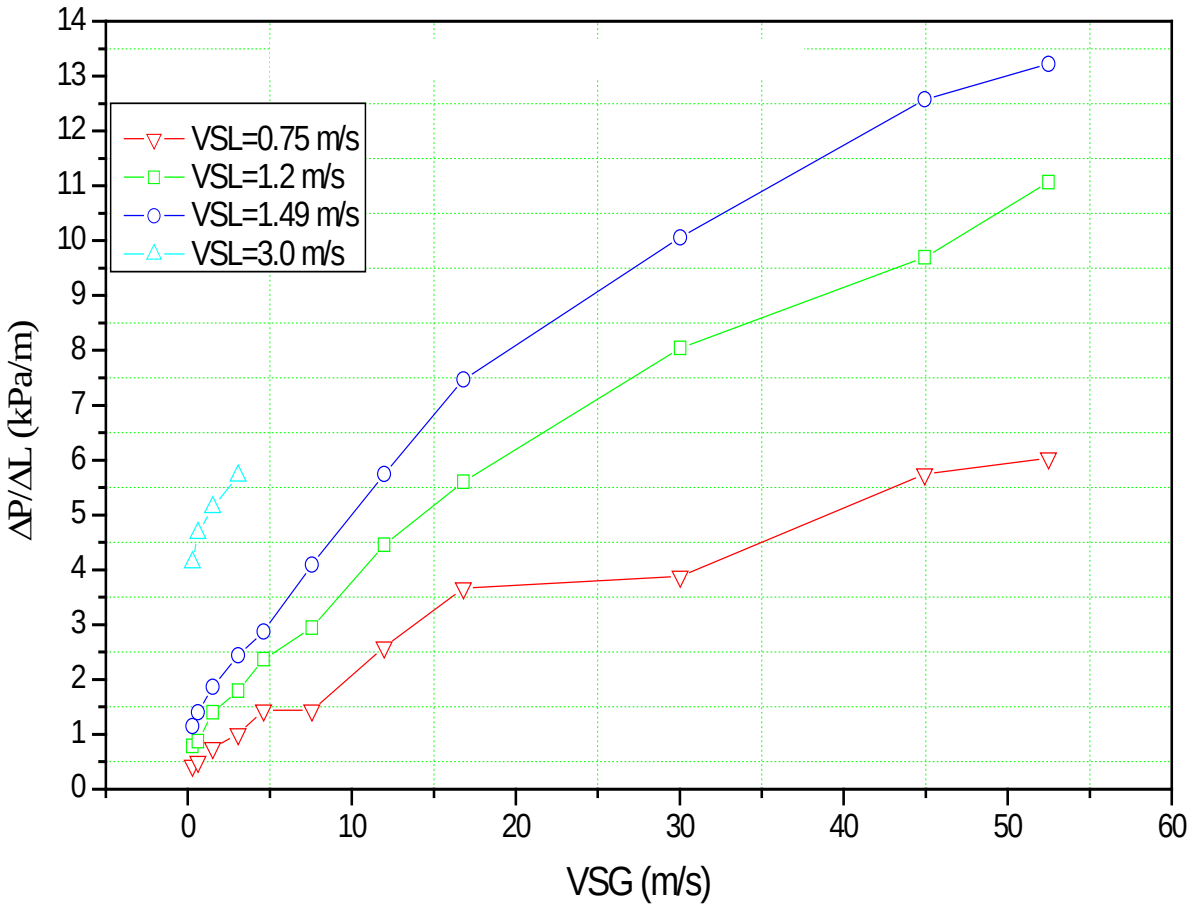

Figure 4.22 Effect of superficial gas velocities on pressure gradients for 70% Water Cut.

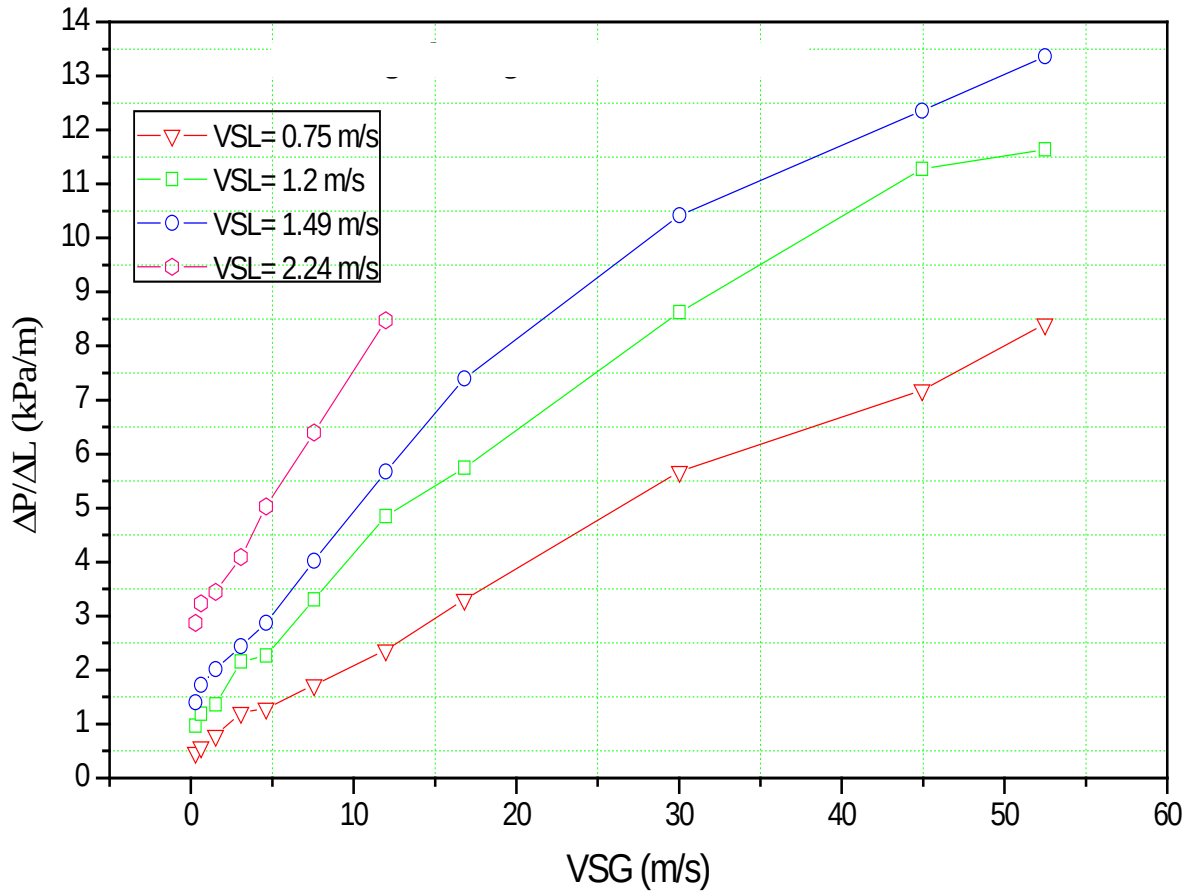

Figure 4.23 Effect of superficial gas velocities on pressure gradients for 80% Water Cut.

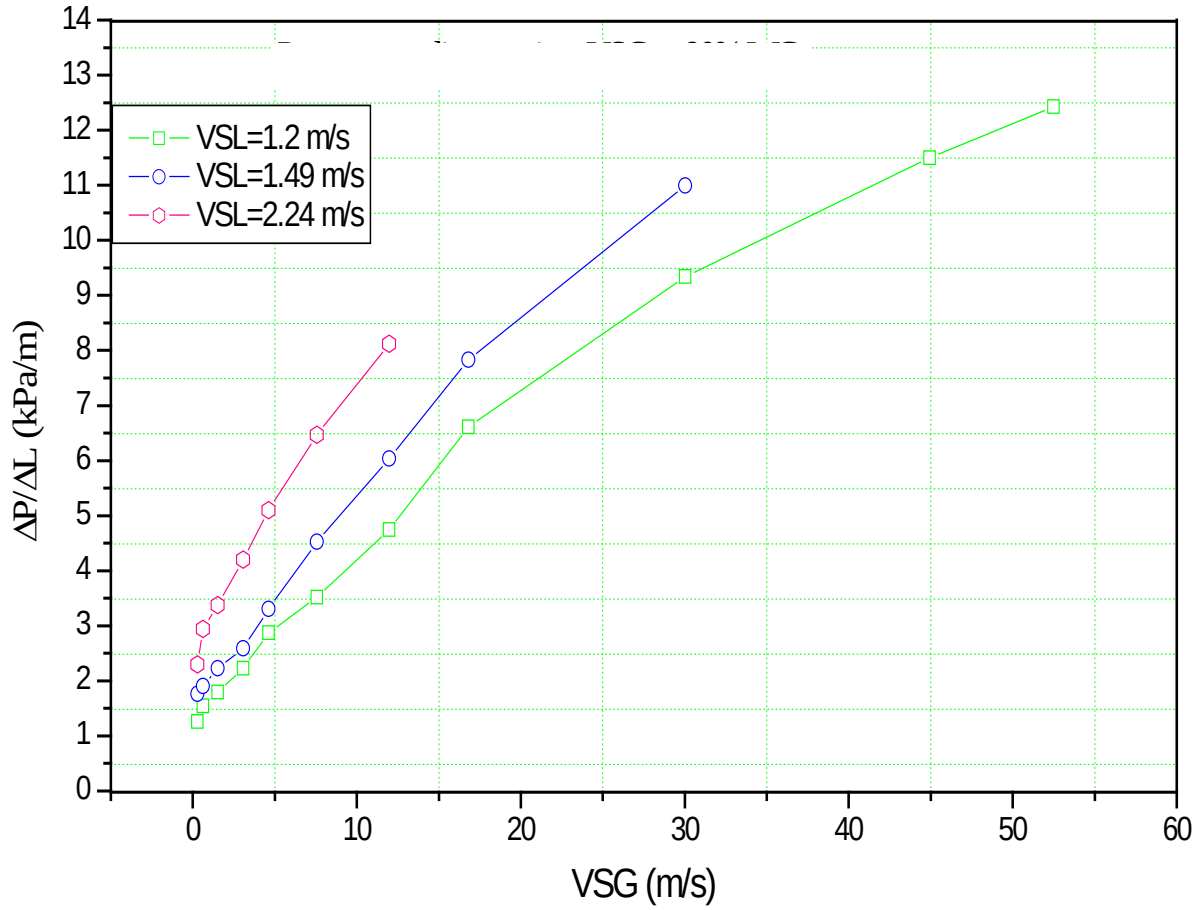

Figure 4.24 Effect of superficial gas velocities on pressure gradients for 90% Water Cut.

4.2.2 Effect of Water cut on Pressure Gradients

Figures 4.25 to 4.35 illustrate the effect of water cut on pressure gradients. The pressure gradient for VSG of 0.29 m/s at VSL of 0.3 m/s was at its maximum peak pressure gradient (phase inversion) at 30% water cut and then decreased at 40% water cut from 0.432 kPa/m to 0.323 kPa/m. As the water cut increased, the pressure gradient increased gradually to 0.395 kPa/m at water cut of 50% and then decreased sharply to its minimum to reach 0.287 kPa/m at 60% water cut. Also, for 0.75 m/s VSL, the pressure gradients started at 20% water cut with its maximum peak of 0.718 kPa/m and then decreased sharply to reach the minimum of 0.395 kPa/m at 30% water cut and then increased gradually to 0.539 kPa/m and later returned to the maximum peak pressure gradient of 0.718 kPa/m at 50% water cut and then decreased sharply to 0.431 kPa/m at 60% water cut and maintained this pressure gradient till 70% water cut and later increased a little bit to 0.474 kPa/m at 80% water cut. The VSL was increased to 1.2 m/s, the pressure gradient was found to be 1.08 kPa/m and it remained constant for 10% and 20% water cut and later decreased sharply to minimum of 0.683 kPa/m at 30% water cut and then increased gradually to 0.898 kPa/m at 40% water cut and later increased to 1.1 kPa/m at 50% water cut. It later decreased to 0.934 kPa/m at 60% water cut and decreased further to 0.790 kPa/m at 70% water cut and then increased to 0.967 kPa/m at 80% water cut and finally to the maximum peak of 1.26 kPa/m at 90% water cut.

For VSL of 1.49 m/s, the maximum peak of pressure gradient 1.76 kPa/m was also at 90% water cut while the minimum pressure of 0.934 kPa/m was at 30% water cut. The VSL was increased to 3 m/s and the maximum peak of pressure gradient was found to be

4.13 kPa/m at 70% water cut while the minimum pressure gradient of 2.87 kPa/m was at 30% water cut.

In order to study the consistency of the results, the VSG was varied by increasing it to 0.63 m/s and the whole process was repeated again. For VSL of 0.3 m/s, the maximum pressure gradient was 0.431 kPa/m at 50% water cut while the minimum pressure gradient of 0.359 kPa/m was at 60% water cut. As for 0.75 m/s VSL, the maximum pressure gradient was 0.826 kPa/m at 20% water cut and then decreased sharply to the minimum pressure gradient of 0.431 kPa/m at 30% water cut and then increased to 0.647 kPa/m at 40% water cut and then increased a little bit to 0.718 kPa/m at 50% water cut and then decreased to 0.539 kPa/m at 60% water cut and still decreased further to 0.503 kPa/m at 70% water cut and later increased to 0.575 kPa/m at 80% water cut.

The VSL was then increased to 1.2 m/s and maximum peak pressure gradient was 1.54 kPa/m at 90% water cut and the minimum pressure gradient was 0.826 kPa/m at 30% water cut, while for 1.49 m/s VSL, the maximum peak pressure gradient was 1.9 kPa/m at the same 90% water cut and minimum pressure gradient was 1.1 kPa/m at the same 30% water cut and finally for 3 m/s VSL, the maximum peak pressure gradient had increased to 4.67 kPa/m at 70% water cut and the minimum pressure gradient was 3.23 kPa/m at 30% water cut.

The VSG was increased to 1.51 m/s. For VSL of 0.3 m/s, the maximum peak pressure gradient was 0.611 kPa/m at 50% water cut and the minimum pressure gradient was 0.431 kPa/m at 60% water cut. As for VSL of 0.75 m/s, the maximum peak pressure gradient was 1.01 kPa/m at 20% water cut and then decreased sharply to the minimum

pressure gradient of 0.683 kPa/m at 30% water cut and then increased gradually to pressure gradient of 0.718 kPa/m at 40% water cut and there was further increase to 0.862 kPa/m at 50% water cut and then decreased to 0.718 kPa/m at 60% water cut and it then increased to 0.754 kPa/m at 70% water cut and finally increased to pressure gradient of 0.790 kPa/m at 80% water cut. For VSL of 1.2 m/s, the maximum peak pressure gradient was 1.8 kPa/m at 90% water cut and the minimum pressure gradient was 1.1 kPa/m at 40% water cut and the VSL was then increased to 1.49 m/s in which the maximum peak pressure gradient was 2.23 kPa/m at 90% water cut and the minimum pressure gradient was 1.47 kPa/m at 50% water cut. For the VSL of 3 m/s, the maximum peak pressure gradient was 5.14 kPa/m at 60% water cut and remained constant also for 70% water cut while the minimum pressure gradient was 3.88 kPa/m at 30% water cut which remained constant till 40% water cut.

The VSG was then increased to 3.07 m/s. For VSL of 0.3 m/s, the maximum peak pressure gradient was 0.868 kPa/m at 30% water cut and minimum pressure gradient was 0.647 kPa/m at 60% water cut, while for 0.75 m/s VSL, the maximum peak pressure gradient was 1.29 kPa/m at 50% water cut and the minimum pressure was 0.97 kPa/m at 30% water cut. For 1.2 m/s VSL, the maximum peak pressure gradient was 2.23 kPa/m at 90% water cut while the minimum pressure gradient was 1.44 kPa/m at 40% water cut. The VSL was increased to 1.49 m/s and the maximum peak pressure gradient was 2.59 kPa/m at 90% water cut while the minimum pressure gradient was 1.94 kPa/m at 50% water cut but for VSL of 3 m/s, the maximum peak pressure gradient was 5.82 kPa/m at 50% water cut and decreased sharply to the minimum pressure gradient of 4.96 kPa/m at 40% water cut.

For VSG of 4.62 m/s at 0.3 m/s VSL, the maximum peak pressure gradient was 0.983 kPa/m at 30% water cut and decreased sharply to 0.718 kPa/m at 40% water cut which remained constant till 50% water cut and later increased to 0.97 kPa/m at 60% water cut. The VSL was then increased to 0.75 m/s and had the maximum peak pressure gradient to be 1.58 kPa/m at 50% water cut while the minimum pressure gradient was 1.29 kPa/m at 80% water cut. For VSL of 1.2 m/s, the maximum peak pressure gradient was 2.87 kPa/m at 90% water cut while the minimum pressure gradient was 2.01 kPa/m at 40% water cut while for 1.49 m/s VSL, the maximum peak pressure gradient was 3.3 kPa/m at 90% water cut and the minimum pressure gradient was 2.58 kPa/m at 20% water cut which remained constant till 30% water cut. For VSL of 3 m/s, the maximum peak pressure gradient increased to 7.11 kPa/m at 50% water cut while the minimum pressure gradient was 5.89 kPa/m at 30% water cut. At this 50% water cut, the pressure gradient increases sharply due to a change of flow pattern from slug flow to annular flow and then drop suddenly because of change of flow pattern from the annular flow back to slug flow as shown in Figure 4.29.

The VSG was increased to 7.56 m/s. At VSL of 0.3 m/s, the maximum peak pressure gradient was 0.898 kPa/m at 60% water cut while the minimum pressure gradient was 0.790 kPa/m at 50% water cut. For VSL of 0.75 m/s, the maximum peak pressure gradient was 2.16 kPa/m at 50% water cut while the minimum pressure gradient was 1.44 kPa/m at 70% water cut. The VSL was then increased to 1.2 m/s and the peak maximum pressure gradient was found to be 3.52 kPa/m at 90% water cut while the minimum pressure gradient was 2.51 kPa/m at 40% water cut. For VSL of 1.49 m/s, the maximum peak pressure gradient was 4.52 kPa/m at 90% water cut while the minimum pressure

gradient was 3.23 kPa/m at 20% water cut but for 3 m/s VSL, the maximum peak pressure gradient increased to 8.48 kPa/m at 50% water cut while the minimum pressure gradient was 7.62 kPa/m at 30% water cut. At this 50% water cut, the pressure gradient increases sharply due to a change of flow pattern from slug flow to annular flow and then drop suddenly because of change of flow pattern from the annular flow back to slug flow as shown in Figure 4.30.

For VSG of 12 m/s and at 0.3 m/s VSL, the maximum pressure gradient was 1.18 kPa/m at 30% water cut while the minimum pressure gradient was 0.862 kPa/m at 60% water cut but for 0.75 m/s VSL, the maximum peak pressure gradient was 2.87 kPa/m at 50% water cut and it remained constant till 60% water cut while the minimum pressure gradient was 2.37 kPa/m at 80% water fraction. When the VSL was increased to 1.2 m/s, the maximum peak pressure gradient was 4.85 kPa/m at 80% water cut but the minimum pressure gradient occurred twice at 10% water cut and 40% water cut to be 3.59 kPa/m. For VSL of 1.49 m/s, the maximum peak pressure gradient was 6.03 kPa/m at 90% water cut while the minimum pressure gradient was 4.17 kPa/m at 20% water cut.

The VSG was then increased to 16.8 m/s. For VSL of 0.3 m/s, the maximum peak pressure gradient was 1.44 kPa/m at 40% water cut and remained constant till 50% water cut while the minimum pressure gradient was 1.19 kPa/m at 30% water cut. The VSL was then increased to 0.75 m/s and the maximum peak pressure gradient was 3.66 kPa/m at 70% water cut while the minimum pressure gradient was 2.87 kPa/m at 30% water cut and it remained constant to 40% water cut. For VSL of 1.2 m/s, the maximum peak pressure gradient was 6.61 kPa/m at 90% water cut while the minimum pressure gradient was 4.81 kPa/m at 10% water cut but for 1.49 m/s VSL, the maximum pressure gradient

was 7.83 kPa/m at 90% water cut while the minimum pressure gradient was 6.18 kPa/m at 10% water cut and remained constant till 20% water cut. The pressure gradient at higher values of VSL could not be measured due to high VSG being used and also the due to the device instrument limitation.

For VSG of 30 m/s and VSL of 0.3 m/s, the maximum peak pressure gradient was 2.19 kPa/m at 50% water cut while the minimum pressure gradient was 1.66 kPa/m at 30% water cut. The VSL was then increased to 0.75 m/s and the maximum peak pressure gradient was 5.68 kPa/m at 80% water cut while the minimum pressure gradient was 3.52 kPa/m at 60% water cut. For the VSL of 1.2 m/s, the maximum peak pressure gradient was 9.34 kPa/m at 90% water cut while the minimum pressure gradient was 6.46 kPa/m at 50% water cut but for 1.49 m/s VSL, the maximum peak pressure gradient was 10.99 kPa/m at 90% water cut while the minimum pressure gradient was 7.97 kPa/m at 50% water cut. In Figure 4.33, the circled region at 50% water cut for VSL of 0.75 m/s, 1.2 m/s and 1.49 m/s was as a result of phase inversion from oil continuous phase to water continuous phase.

The VSG was then increased further to 44.9 m/s. For VSL of 0.3 m/s, the maximum peak pressure gradient was 3.19 kPa/m at 60% water cut while the minimum pressure gradient was 3.02 kPa/m at 30% water cut but for 0.75 m/s VSL, the maximum peak pressure gradient was 7.18 kPa/m at 80% water cut while the minimum pressure gradient was 4.24 kPa/m at 60% water cut. For 1.2 m/s VSL, the maximum peak pressure gradient was 11.5 kPa/m at 90% water cut while the minimum pressure gradient was 7.9 kPa/m at 50% water cut but for 1.49 m/s VSL, the maximum peak pressure gradient increased to 12.57

kPa/m at 70% water cut while the minimum pressure gradient was 8.19 kPa/m at 50% water cut.

The VSG was finally increased to 52.5 m/s and the VSL was put at 0.3 m/s, the maximum peak pressure gradient was 3.81 kPa/m at 40% water cut while the minimum pressure gradient was 3.2 kPa/m at 30% water cut. The VSL was increased to 0.75 m/s, the maximum peak pressure gradient was 8.41 kPa/m at 80% water cut while the minimum pressure gradient was 4.45 kPa/m at 60% water cut but for 1.2 m/s VSL, the maximum peak pressure gradient was 12.43 kPa/m at 90% water cut while the minimum pressure gradient was 7.9 kPa/m at 50% water cut and finally the VSL was increased to 1.49 m/s, the maximum peak pressure gradient increased sharply to 13.36 kPa/m at 80% water cut while the minimum pressure gradient was 9.63 kPa/m at 50% water cut. It was noticed that, for a particular VSG, as the VSL increases, the maximum pressure gradient also increases.

It was observed that, as the water cut increases, the water becomes the continuous phase and therefore affects the flow dynamics in the pipeline and this can be observed in the variation of the pressure gradient. This change in the flow regime since water becomes the continuous phase is known as phase inversion. The possible explanation of the phase inversion phenomenon is that, the viscosity of the mixture (air, oil and water), which depends on the viscosity of the oil-water continuous phase and that of the air dispersed phase (air bubbles) in the oil-water, increases with increasing the water cut until reaching a maximum value where the phase inversion occurs (Arirachakaran et al [31]). Pal [32] argued that, the mixture viscosity in the dispersed flow increases as the droplet size of the dispersed phase decreases and the increase in the mixture viscosity with the smaller

droplet size could be due to the smaller distance between individual droplets. In addition, when the concentration of the small droplets dispersed phase is high, this will lead to a higher viscosity.

Finally, a dimensionless figure was also plotted in which the vertical axis was the ratio of the three-phase air-oil-water pressure gradient to single phase pressure gradient of water calculated from Blasius correlation while the horizontal axis represents the Water cut as shown in Figure 4.36 and 4.37 for VSG of 0.63 m/s and 16.8 m/s respectively. The VSG of 0.63 m/s and 16.8 m/s was chosen in order to see the effects at high and low superficial gas velocities. It was discovered that, for 0.63 m/s VSG, the ratio of the pressure gradient was maximum at VSL of 1.2 m/s and water fraction/ cut of 0.1 to be 84.5 while the minimum ratio of the pressure gradient was observed to be 1.99 at VSL of 1.49 m/s and water fraction/ cut of 0.9 for 0.63 m/s VSG. It was also observed that, the ratio of the pressure gradient decreases as water fraction/ cut increases from 0.1 to 0.9 while VSL increases from 0.3 m/s to 3.0 m/s. It was also discovered that, all the VSL follow similar pattern, that is, all the dimensionless pressure gradient approaches 1 as the water fraction/ cut increases towards 1.0. This showed that, the three-phase air-oil-water tends to single phase as the water fraction/ cut approaches 1.0 since the pressure gradient of the three-phase air-oil-water almost equals the single phase water pressure gradient as the water fraction/ cut tends to 1. Similar trend was observed for the VSG of 16.8 m/s. The VSL from 0.3 m/s to 1.49 m/s can only be achieved due to the high VSG and all the VSL follow similar pattern of approaching 1 as the water fraction/ cut also tends to 1.

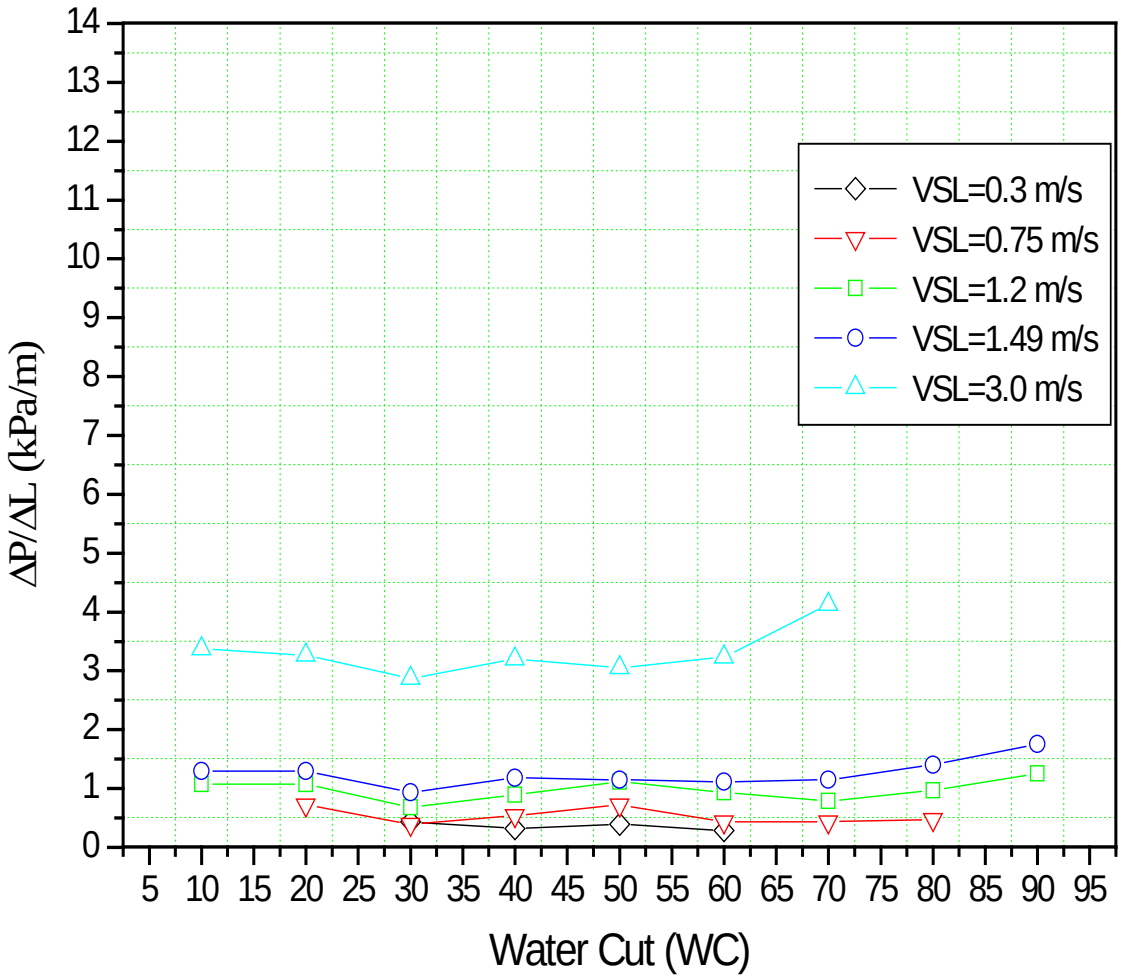

Figure 4.25 Pressure gradient against Water Cut at VSG= 0.29 m/s for different values of superficial velocity of liquid mixture.

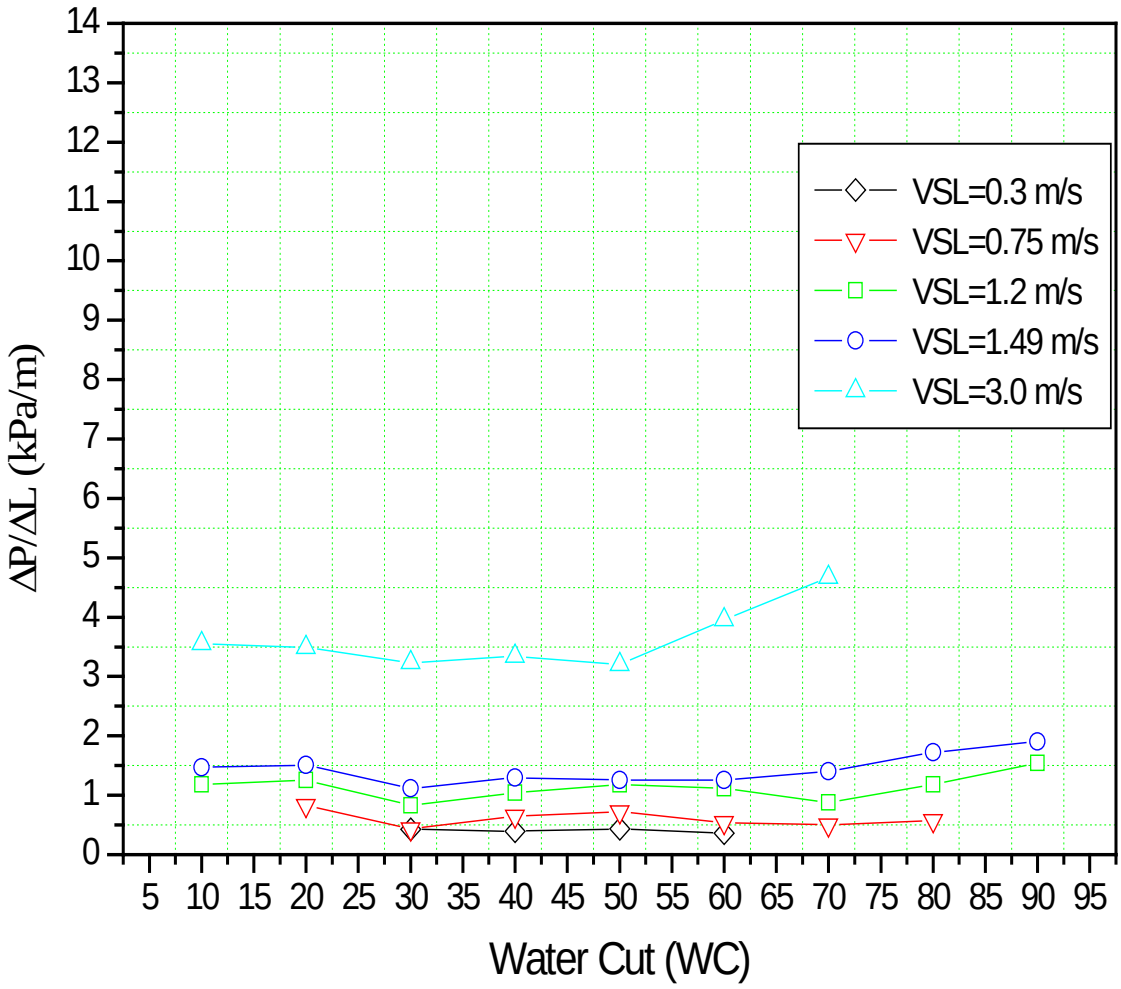

Figure 4.26 Pressure gradient against Water Cut at VSG= 0.63 m/s for different values of superficial velocity of liquid mixture.

.

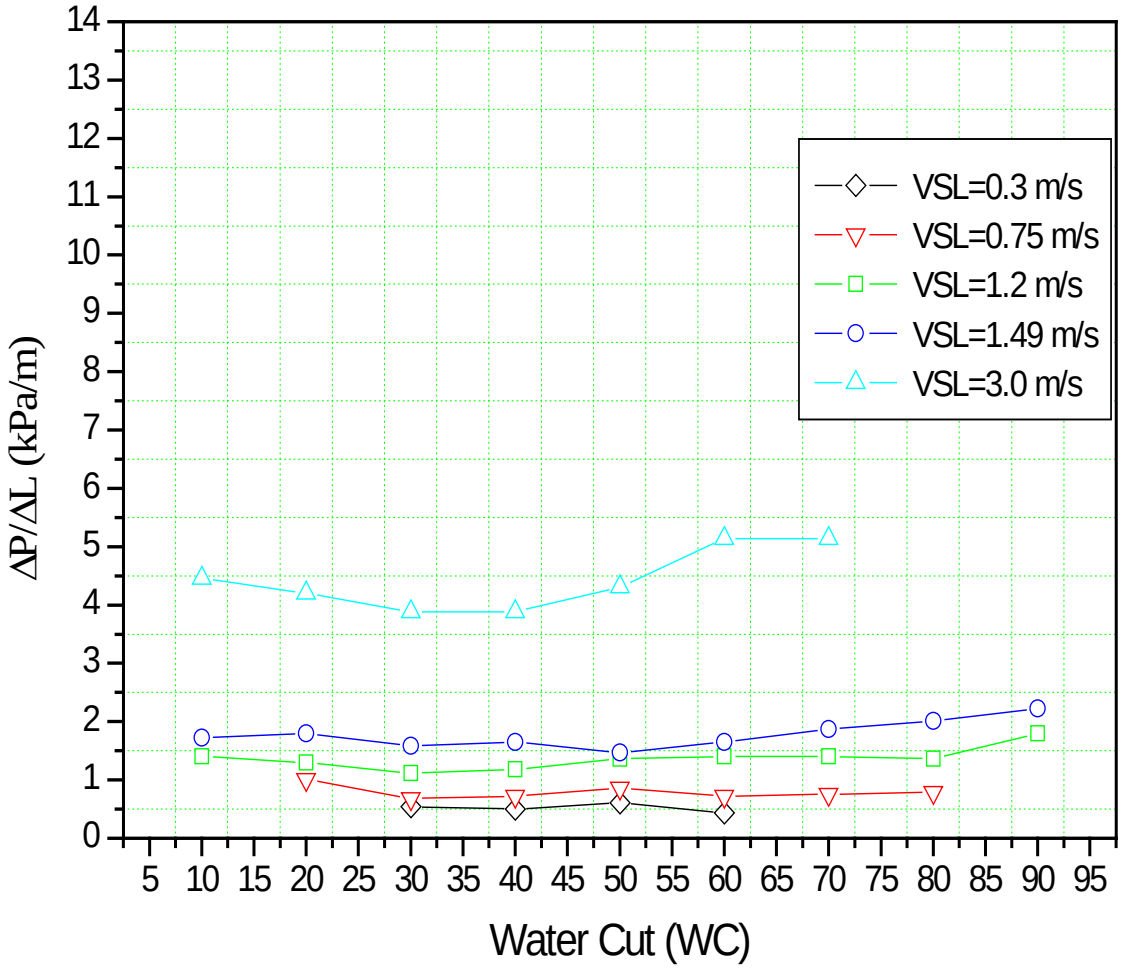

Figure 4.27 Pressure gradient against Water Cut at VSG= 1.51 m/s for different values of superficial velocity of liquid mixture.

.

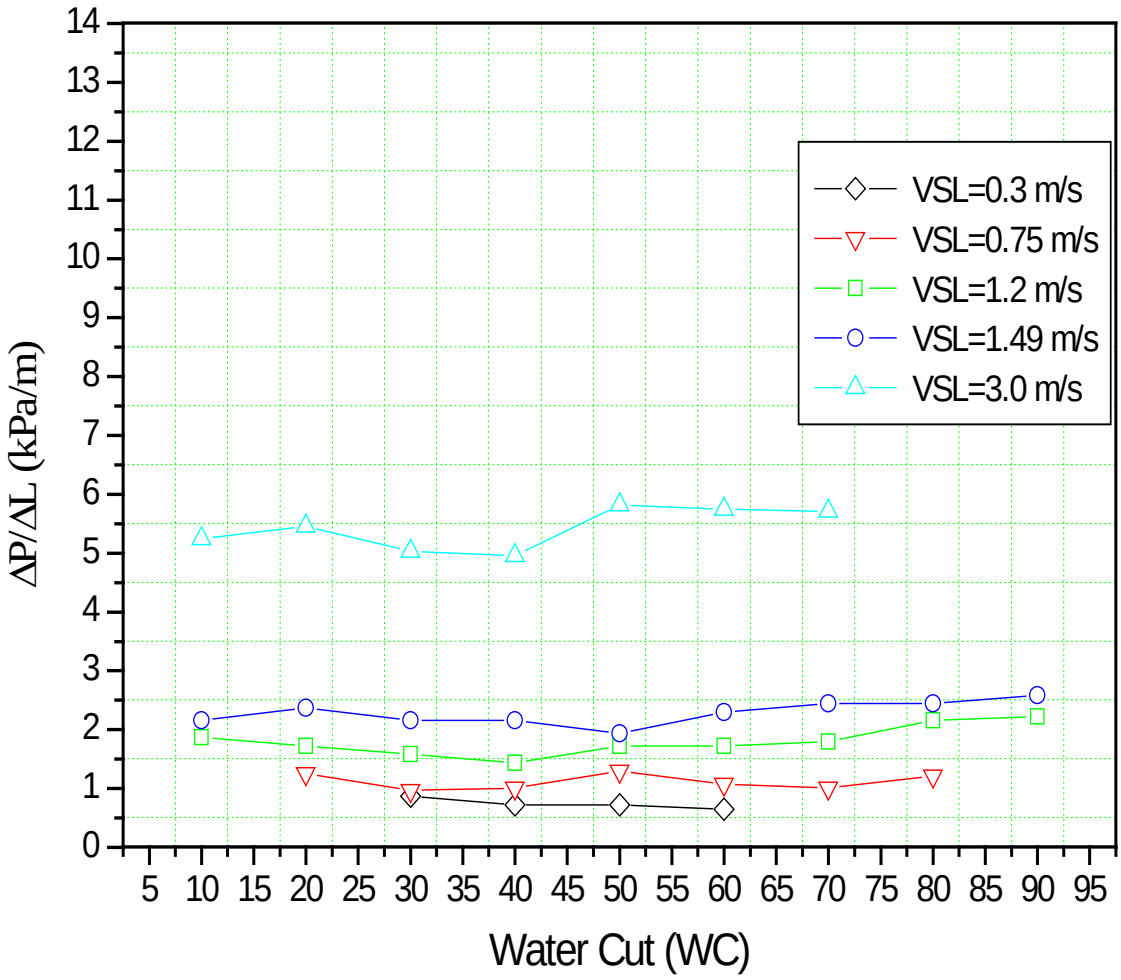

Figure 4.28 Pressure gradient against Water Cut at VSG= 3.07 m/s for different values of superficial velocity of liquid mixture.

.

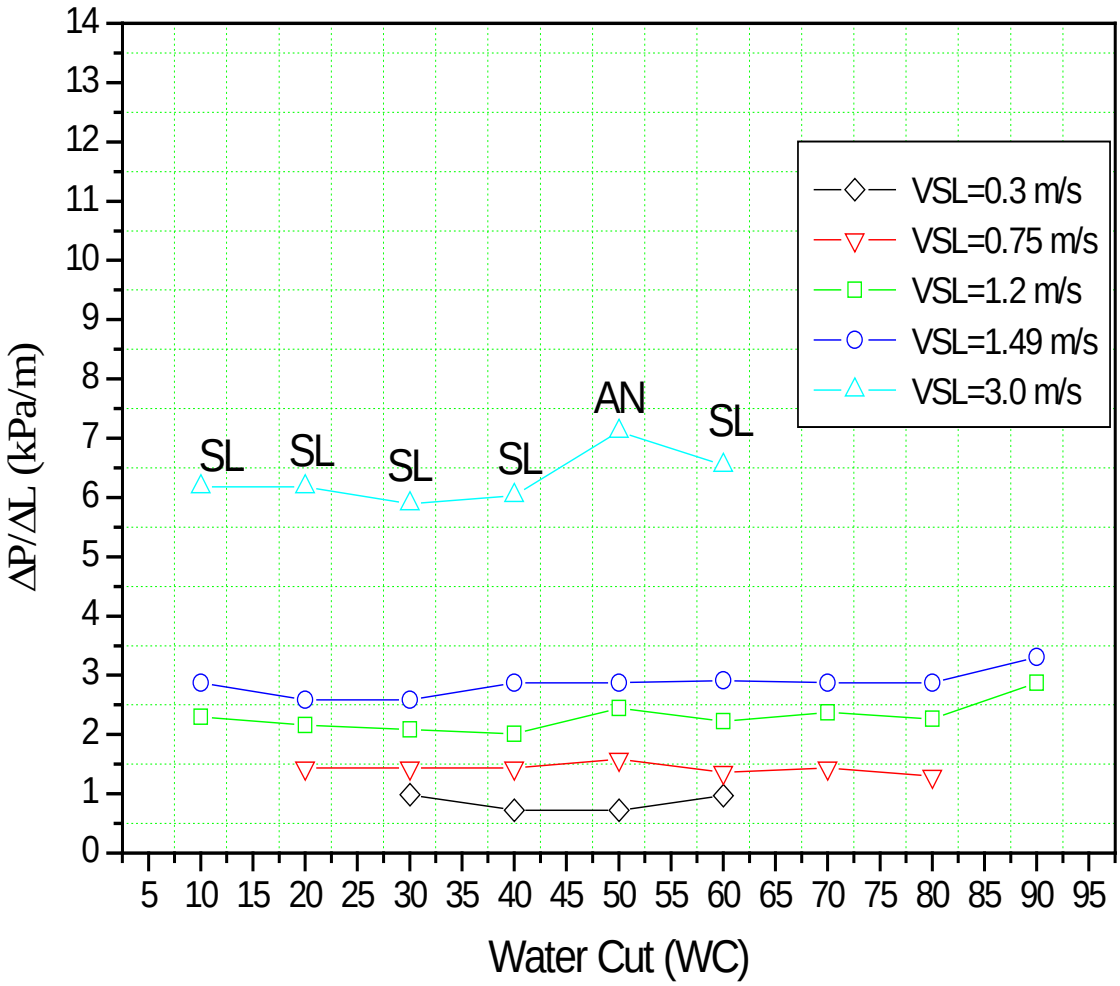

Figure 4.29 Pressure gradient against Water Cut at VSG= 4.62 m/s for different values of superficial velocity of liquid mixture.

.

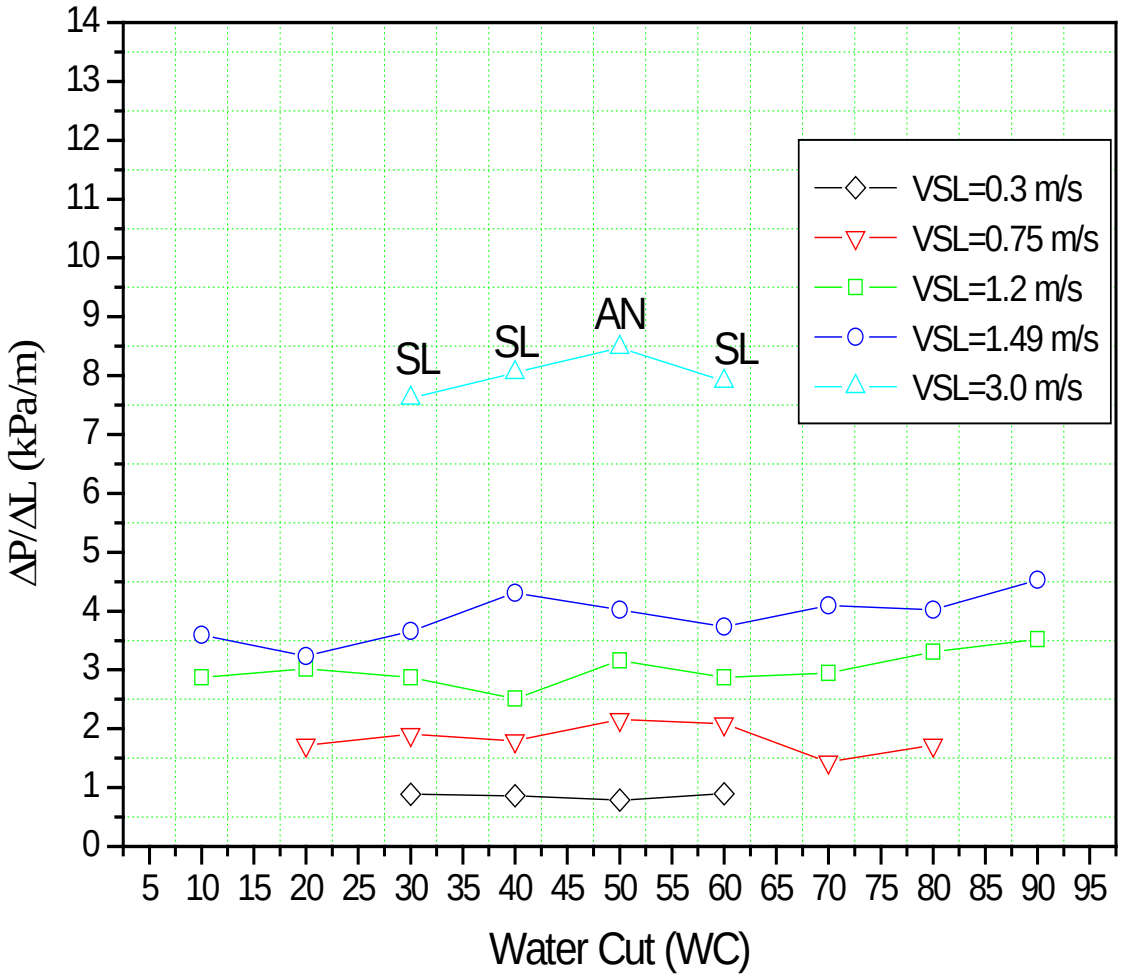

Figure 4.30 Pressure gradient against Water Cut at VSG= 7.56 m/s for different values of superficial velocity of liquid mixture.

.

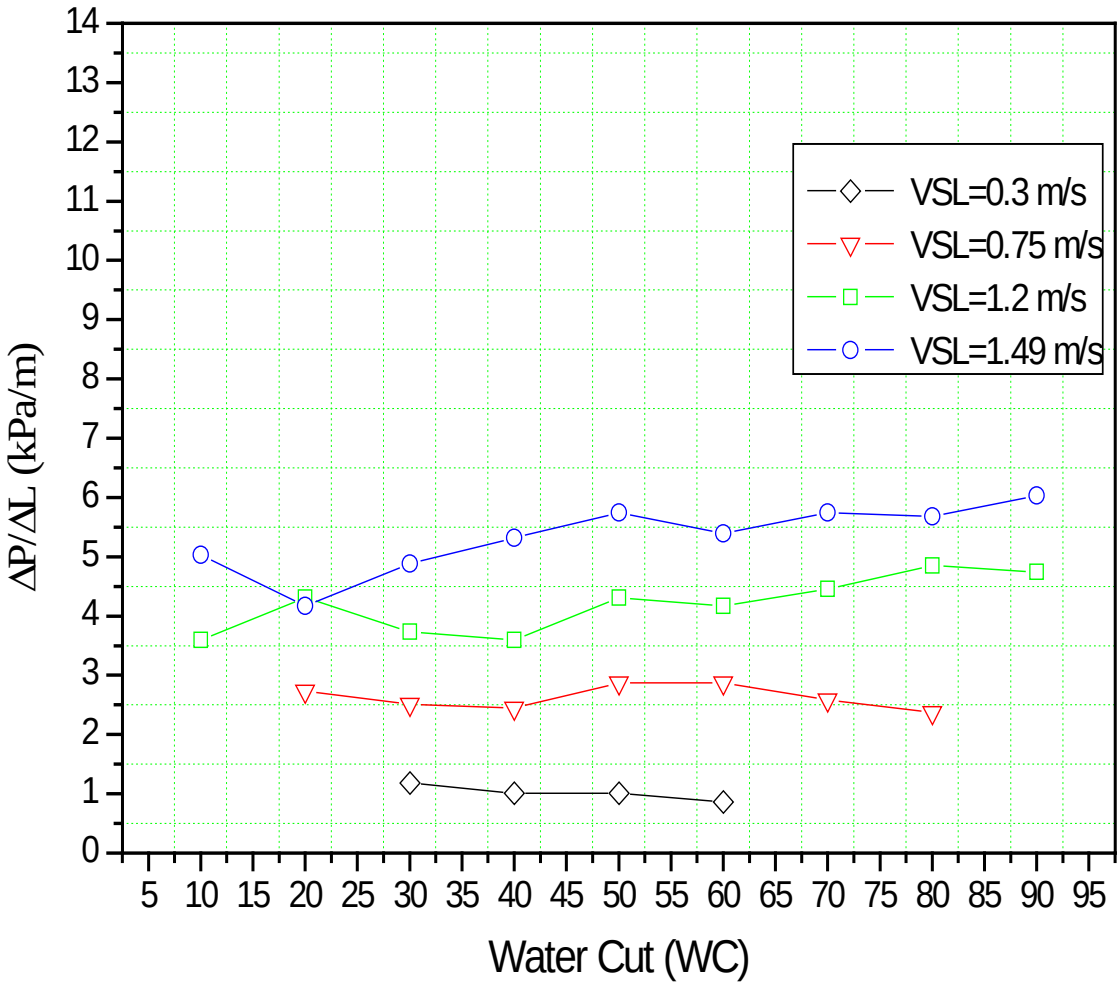

Figure 4.31 Pressure gradient against Water Cut at VSG= 12 m/s for different values of superficial velocity of liquid mixture.

.

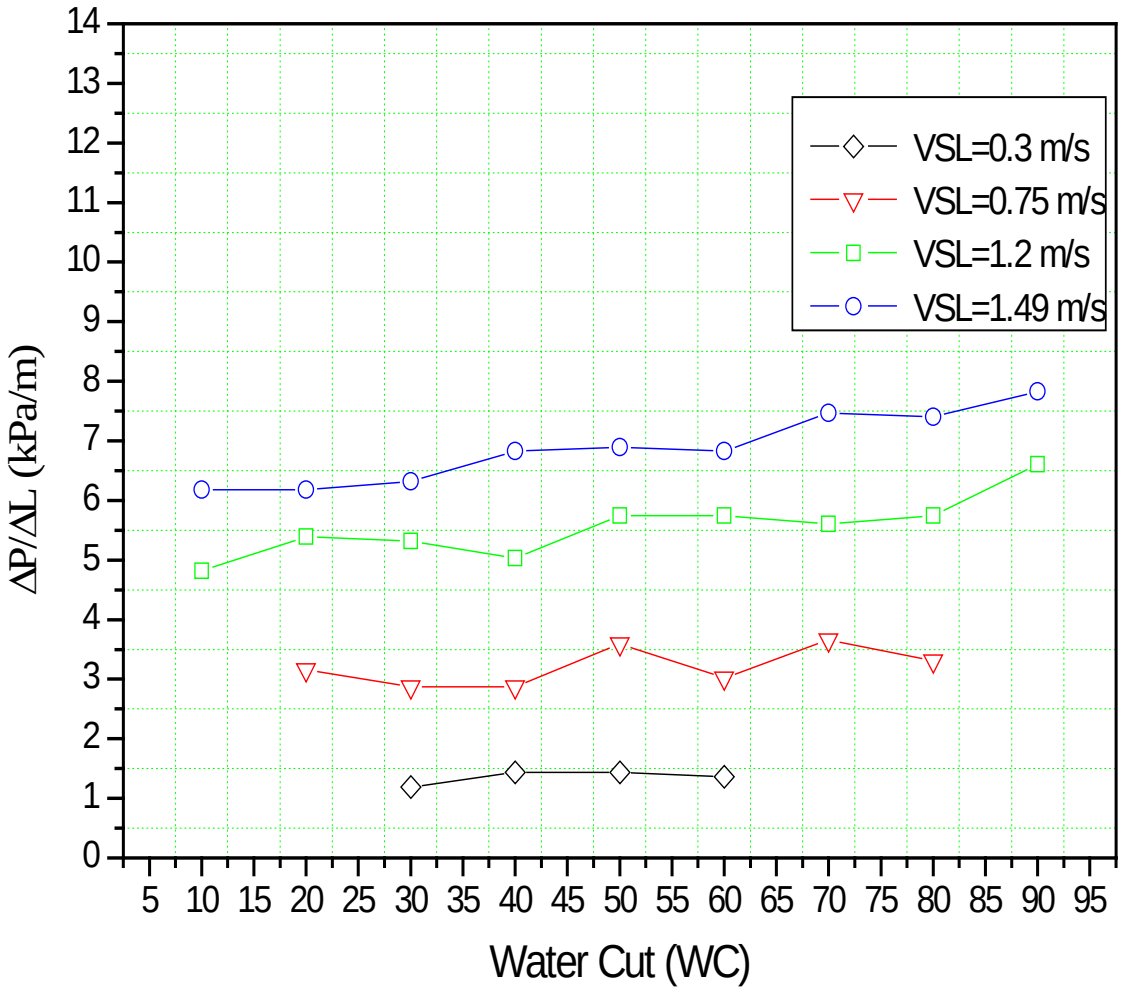

Figure 4.32 Pressure gradient against Water Cut at VSG= 16.8 m/s for different values of superficial velocity of liquid mixture.

.

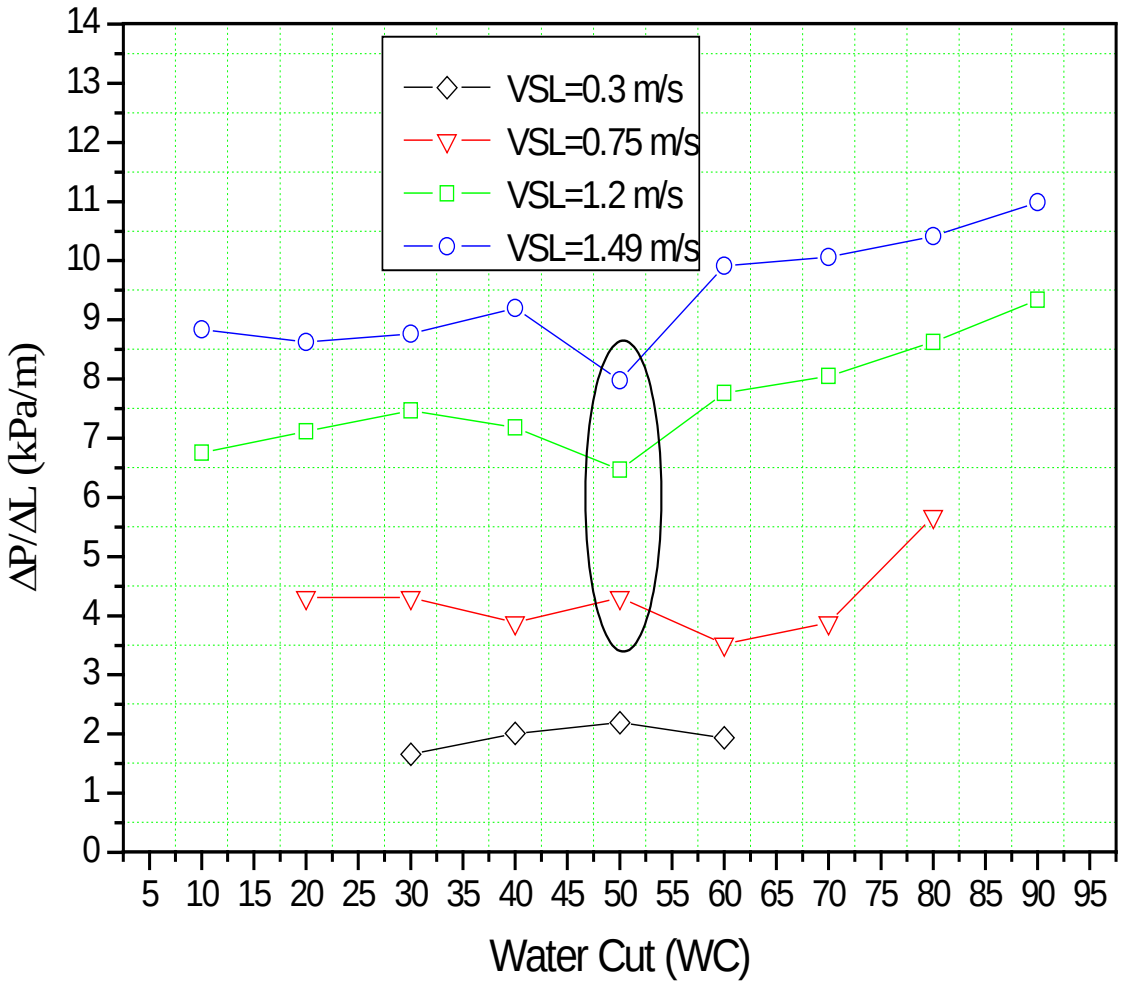

Figure 4.33 Pressure gradient against Water Cut at VSG= 30 m/s for different values of superficial velocity of liquid mixture.

.

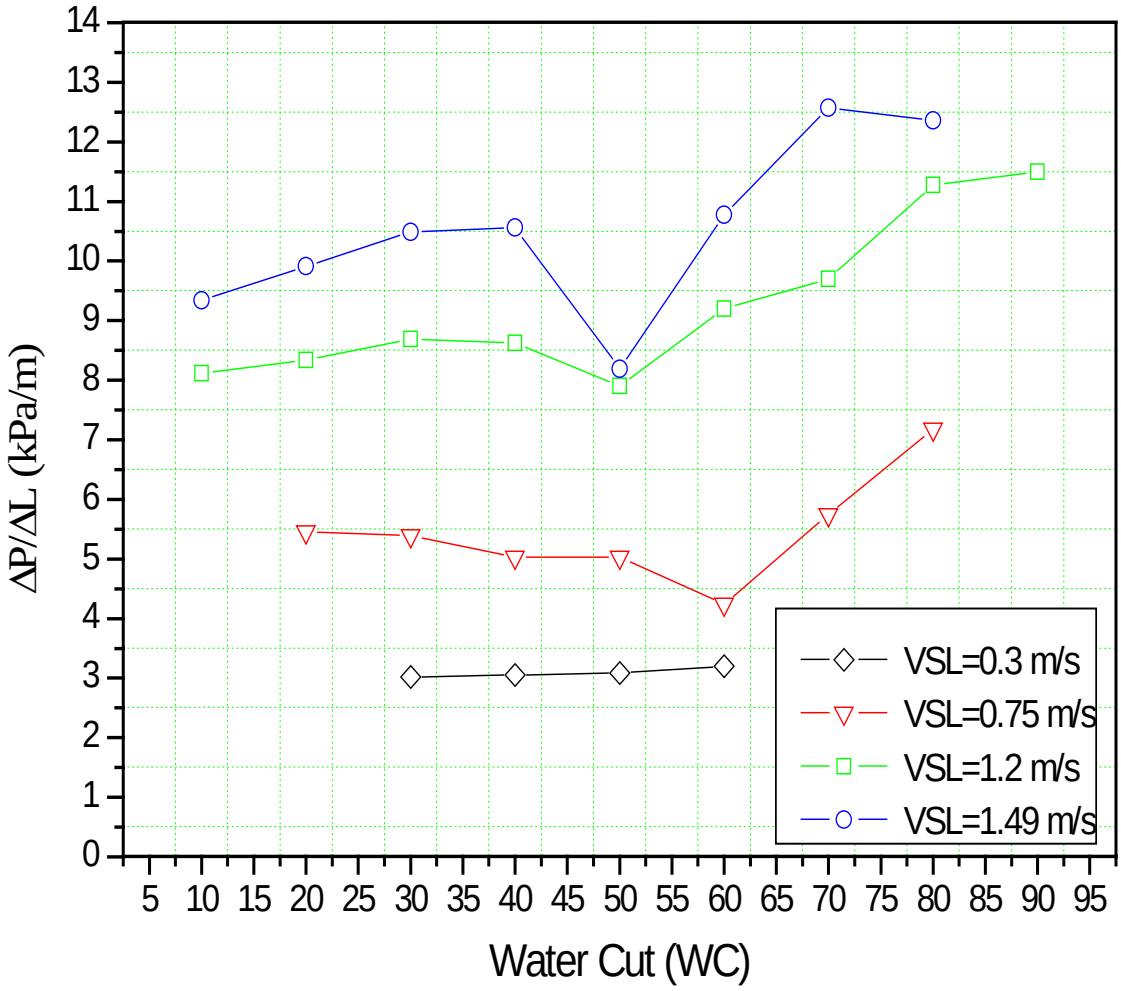

Figure 4.34 Pressure gradient against Water Cut at VSG= 44.9 m/s for different values of superficial velocity of liquid mixture.

.

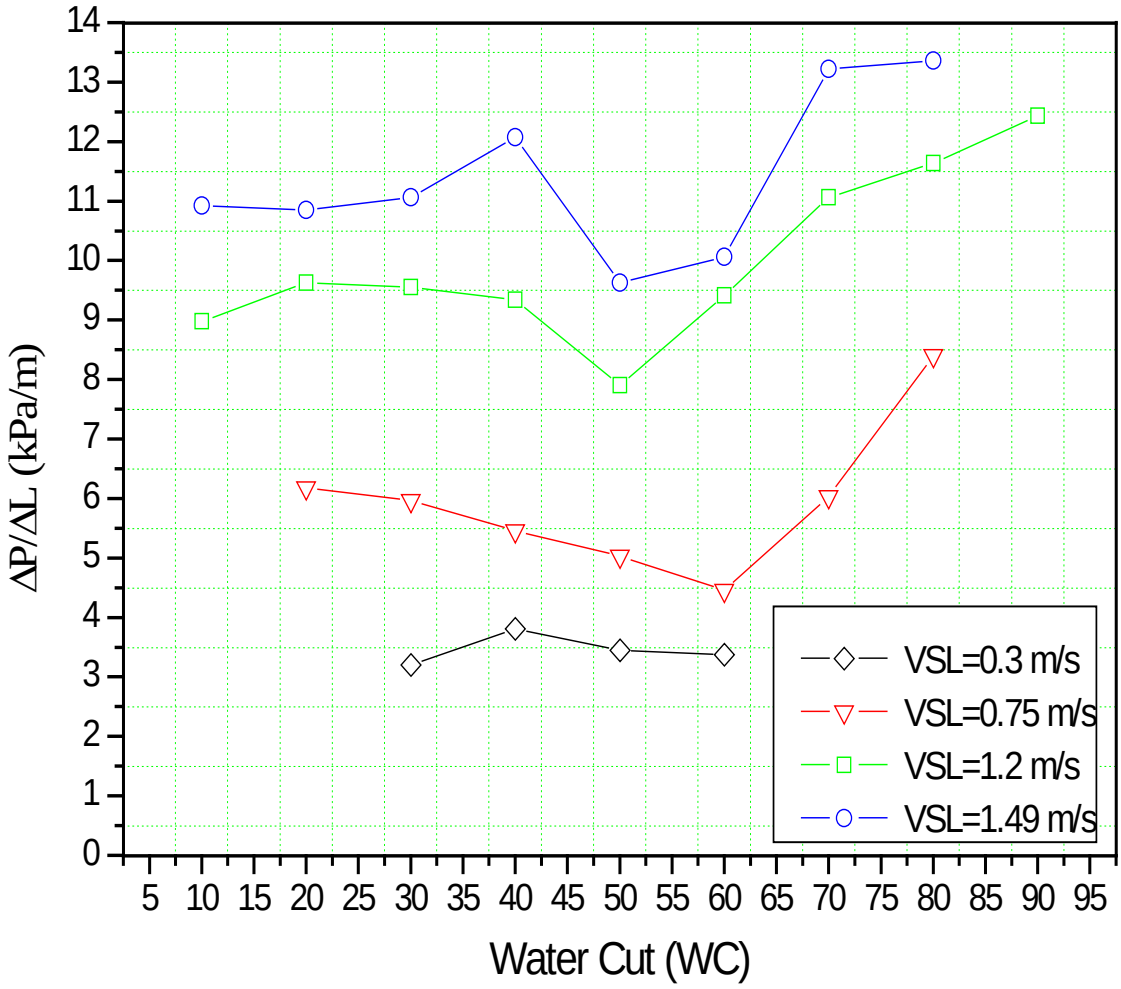

Figure 4.35 Pressure gradient against Water Cut at VSG= 52.5 m/s for different values of superficial velocity of liquid mixture.

.

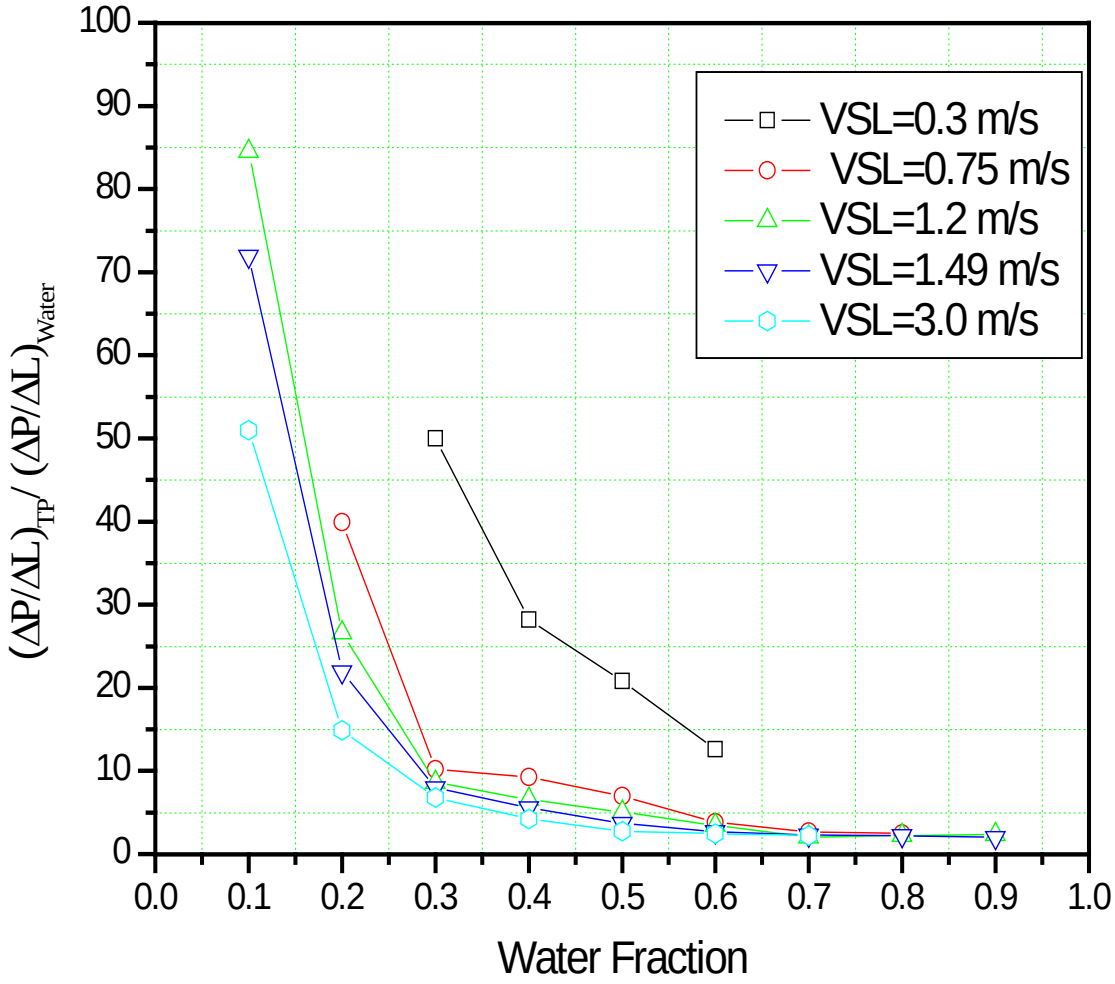

Figure 4.36 The graph of dimensionless pressure gradient against Water cut at VSG of 0.63 m/s for different VSL.

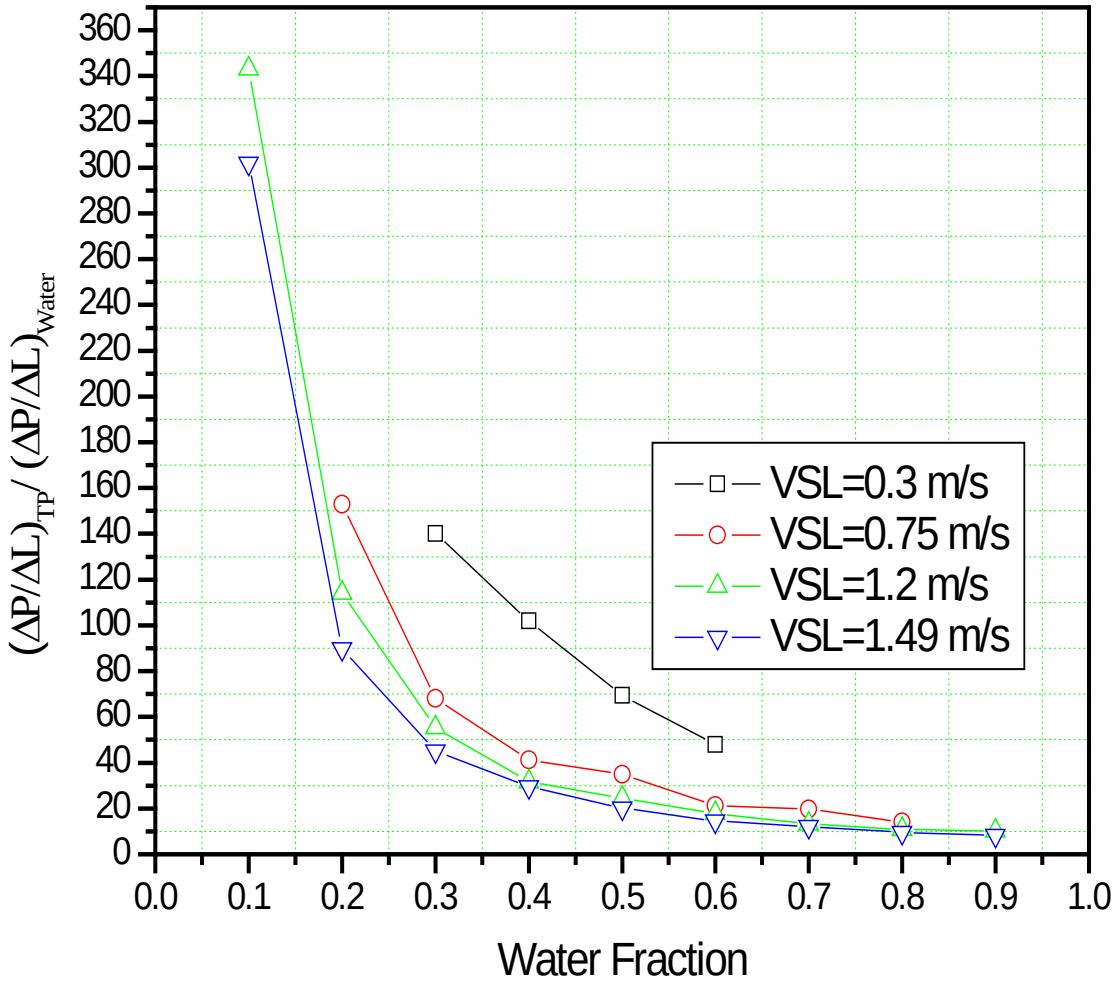

Figure 4.37 The graph of dimensionless pressure gradient against Water cut at VSG of 16.8 m/s for different VSL.

4.2.3 Effect of Liquid Mixture Reynolds Number on Pressure Gradients

The variation of the three-phase air-oil-water pressure gradient against the liquid mixture Reynolds number was observed for three different VSG of 0.63m/s, 7.56 m/s and 12.0 m/s at water cut of 30% and 40% as shown in Figure 4.38 and 4.39 respectively. The 30% and 40% water cut was chosen because it covered all the ranges of flow conditions. The pressure gradient increases as the liquid mixture Reynolds number increases with increasing VSG. The 30% and 40% water cut follow similar trend. The increase in pressure gradient was more significant at high VSG than at low VSG, this was due to the change of flow pattern. At high VSG, the flow patterns were mostly slug flow and annular flow while it was mostly stratified at low VSG.

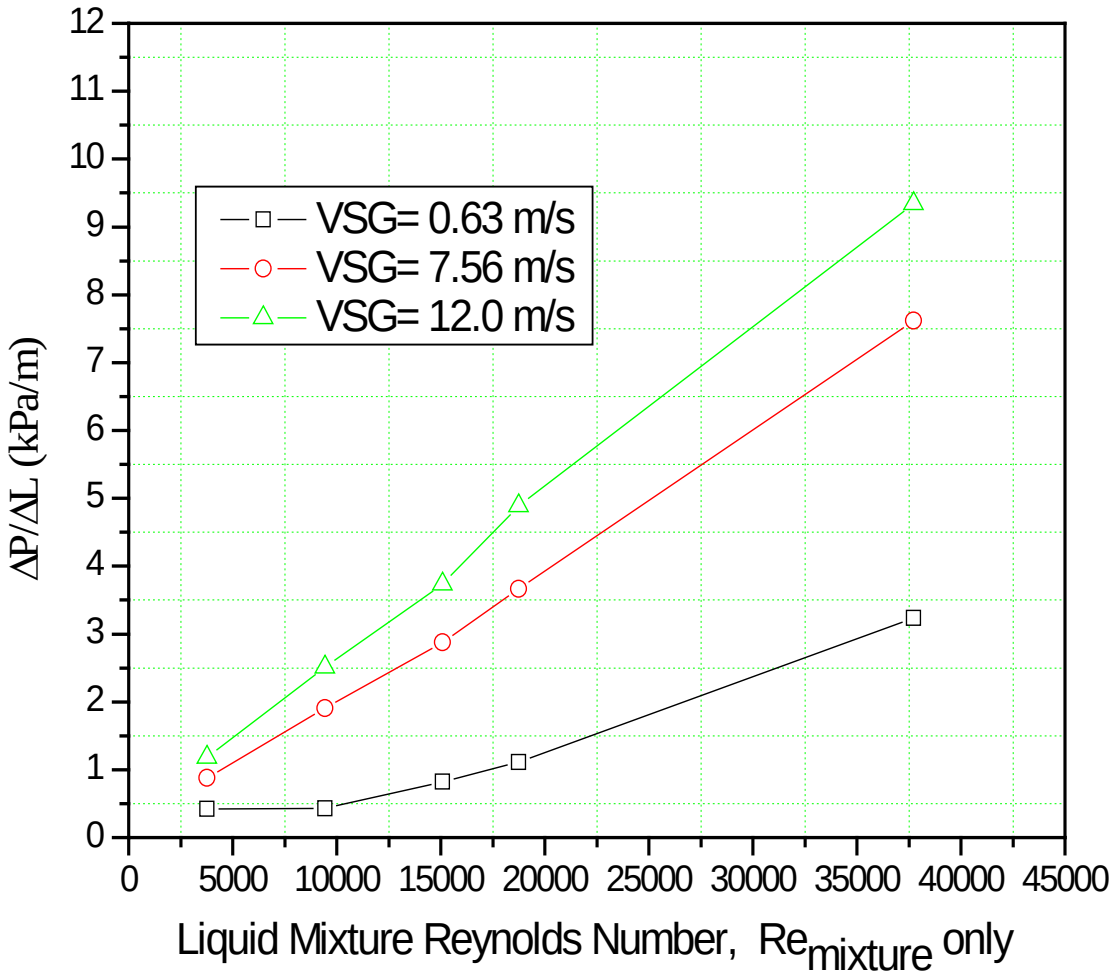

Figure 4.38 The graph of three-phase pressure gradient against liquid mixture Reynolds number only at 30% Water Cut.

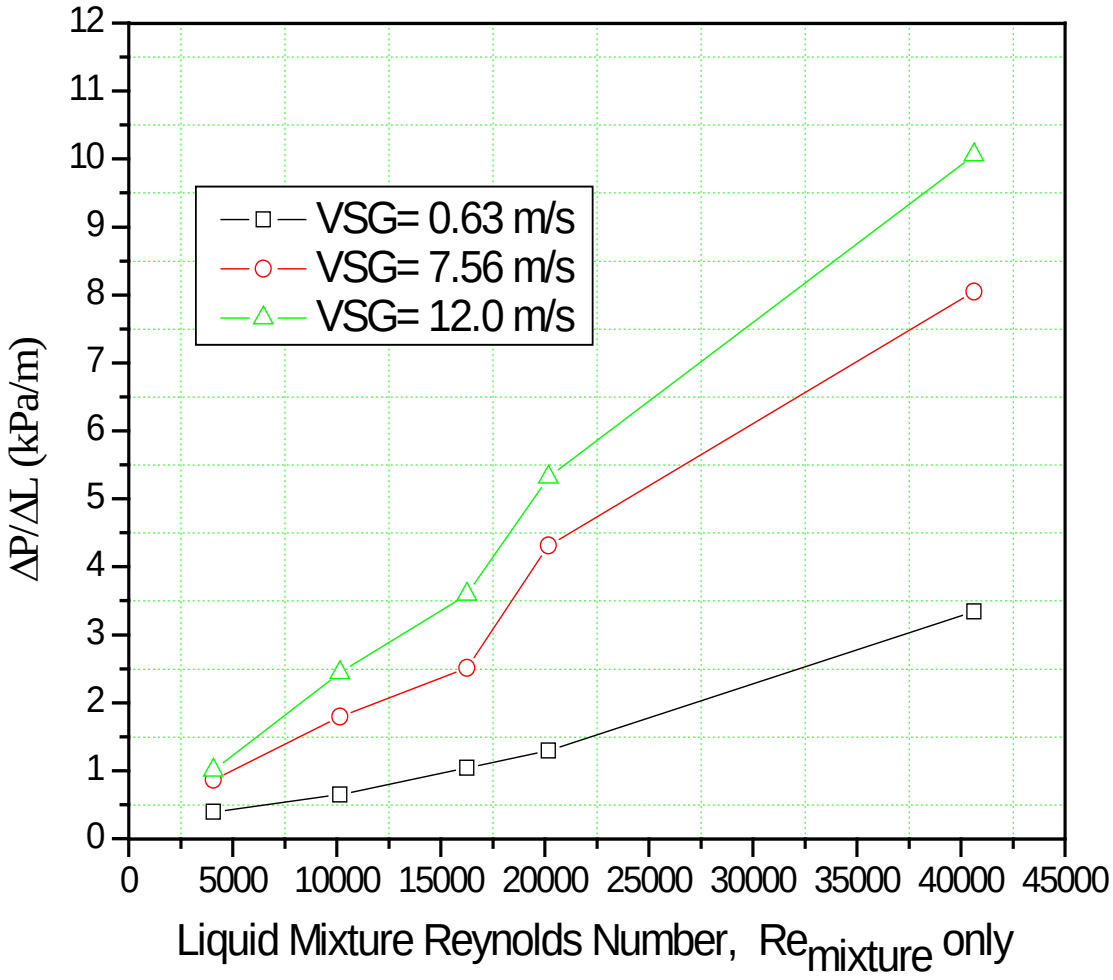

Figure 4.39 The graph of three-phase pressure gradient against liquid mixture Reynolds number only at 40% Water Cut.

4.2.4 Effect of Superficial Liquid Velocity, VSL on Pressure Gradients

For 10% water cut, at VSL of 1.2 m/s, the pressure gradient increased steadily from 1.08 kPa/m to 8.98 kPa/m as the VSG also increased from 0.29 m/s and 52.5 m/s respectively. The VSL was then increased to 1.49 m/s, the pressure gradient also increased gradually from 1.29 kPa/m to 10.92 kPa/m at 0.29 m/s and 52.5 m/s VSG respectively but when the VSL was increased to 3 m/s, the pressure gradient at high VSG could not be measured due to device instrument limitation as explained earlier and the maximum pressure gradient that could be measured was at 4.62 m/s, while the pressure gradient increased steadily from 3.37 kPa/m to 6.18 kPa/m at VSG of 0.29 m/s and 4.62 m/s respectively as shown in Table D.1 of Appendix D.

The water cut was then increased to 20%. The VSL at this water cut started from 0.75 m/s, in which the pressure gradient increased steadily from 0.718 kPa/m to 6.18 kPa/m at 0.29 m/s and 52.5 m/s VSG respectively. The VSL was then increased to 1.2 m/s, the pressure gradient also increased gradually from 1.08 kPa/m to 9.63 kPa/m at 0.29 m/s and 52.5 m/s VSG respectively while for 1.49 m/s VSL, the pressure gradient increased from 1.29 kPa/m to 10.85 kPa/m at 0.29 m/s and 52.5 m/s VSG respectively. Finally, the VSL was increased to 3 m/s and the pressure gradient was measured till it got to the maximum at VSG of 4.62 m/s. The pressure gradient increased from 3.27 kPa/m to 6.18 kPa/m at 0.29 m/s and 4.62 m/s VSG respectively as shown in Table D.2.

Furthermore, the water cut was increased to 30%. The VSL now started from 0.3 m/s, the pressure gradient increased from 0.432 kPa/m to 3.20 kPa/m at 0.29 m/s and 52.5 m/s VSG respectively. The VSL was increased to 0.75 m/s, the pressure gradient increased

steadily from 0.395 kPa/m to 5.96 kPa/m at 0.29 m/s and 52.5 m/s VSG respectively while the VSL was also increased to 1.2 m/s, the pressure gradient increased from 0.683 kPa/m to 9.56 kPa/m at 0.29 m/s and 52.5 m/s VSG respectively. For VSL of 1.49 m/s, the pressure gradient increased from 0.934 kPa/m to 11.06 kPa/m at 0.29 m/s and 52.5 m/s VSG respectively but for VSL of 3 m/s, the pressure gradient increased from 2.87 kPa/m to 9.34 kPa/m at 0.29 m/s and 12 m/s VSG respectively as that was the maximum possible pressure gradient that can be measured (see Table D.3).

For water cut of 40% and VSL of 0.3 m/s, the pressure gradient increased gradually from 0.323 kPa/m to 3.81 kPa/m at 0.29 m/s and 52.5 m/s VSG respectively but the pressure gradient was constant at 0.718 kPa/m for both 3.07 m/s and 4.62 m/s VSG. The VSL was later increased to 0.75 m/s, the pressure gradient increased steadily from 0.539 kPa/m to 5.46 kPa/m at 0.29 m/s and 52.5 m/s VSG respectively while for 1.2 m/s VSL, the pressure gradient increased from 0.898 kPa/m to 9.34 kPa/m at 0.29 m/s and 52.5 m/s VSG respectively. The VSL was then increased to 1.49 m/s and the pressure gradient increased gradually from 1.19 kPa/m to 12.07 kPa/m at 0.29 m/s and 52.5 m/s VSG respectively but when the VSL was increased to 3 m/s, the pressure gradient increased from 3.20 kPa/m at 0.29 m/s VSG till it got to the maximum pressure gradient of 10.06 kPa/m at 12 m/s VSG as shown in Table D.4.

The water cut was then increased to 50%. The VSL started from 0.3 m/s in which the pressure gradient increased from 0.395 kPa/m to 3.45 kPa/m at 0.29 m/s and 52.5 m/s VSG respectively but it was constant at VSG of 3.07 m/s and 4.62 m/s to be 0.718 kPa/m while for VSL of 0.75 m/s, the pressure gradient started from 0.718 kPa/m at 0.29 m/s VSG and remained constant till 0.63 m/s VSG before it started to increase gradually till it

got to 5.03 kPa/m at 52.5 m/s VSG. For 1.2 m/s VSL, the pressure gradient increased from 1.1 kPa/m to 7.9 kPa/m at 0.29 m/s and 52.5 m/s VSG respectively while for 1.49 m/s VSL, it increased steadily from 1.15 kPa/m to 9.63 kPa/m at 0.29 m/s and 52.5 m/s VSG respectively but for 3 m/s VSL, the pressure gradient increased from 3.05 kPa/m at 0.29 m/s till it got to its maximum pressure gradient of 13.43 kPa/m at 30 m/s VSG (see Table D.5).

For water cut of 60%, the VSL also started from 0.3 m/s in which the pressure gradient increased gradually from 0.287 kPa/m at 0.29 m/s VSG and it reached maximum pressure gradient (phase inversion) 0.970 kPa/m at 4.62 m/s VSG and then decreased to 0.898 kPa/m at 7.56 m/s VSG, it then decreased again to 0.862 kPa/m at 12 m/s VSG before it started to increase gradually to 3.38 kPa/m at 52.5 m/s VSG. For VSL of 0.75 m/s, the pressure gradient increased steadily from 0.431 kPa/m to 4.45 kPa/m at 0.29 m/s and 52.5 m/s VSG respectively while for 1.2 m/s VSL, it increased gradually from 0.934 kPa/m to 9.41 kPa/m at 0.29 m/s and 52.5 m/s VSG respectively. For 1.49 m/s VSL, the pressure gradient increased steadily from 1.1 kPa/m at 0.29 m/s till it got to its maximum peak pressure gradient of 10.78 kPa/m at 44.9 m/s VSG before it decreased to 10.06 Pa/m at 52.5 m/s VSG but for 3 m/s VSL, the pressure gradient increased gradually from 3.23 kPa/m at 0.29 m/s till it reached its maximum pressure gradient of 7.9 kPa/m at 7.56 m/s VSG as shown in Table D.6.

The water cut was increased to 70%. The VSL started from 0.75 m/s in which the pressure gradient increased from 0.431 kPa/m to 6.03 kPa/m at 0.29 m/s and 52.5 m/s VSG respectively but the pressure gradient was constant at VSG of 4.62 m/s and 7.56 m/s to be 1.44 kPa/m while for VSL of 1.2 m/s, the pressure gradient increased steadily from

0.790 kPa/m to 11.06 kPa/m at 0.29 m/s and 52.5 m/s VSG respectively. For 1.49 m/s VSL, the pressure gradient increased from 1.15 kPa/m to 13.22 kPa/m at 0.29 m/s and 52.5 m/s VSG respectively but for 3 m/s VSL, the pressure gradient increased from 4.13 kPa/m to 5.71 kPa/m at 0.29 m/s and 3.07 m/s VSG respectively as that was the maximum possible pressure gradient that can be measured at that VSG as seen in Table D.7.

The water cut was then increased to 80%. For VSL at 0.75 m/s, the pressure gradient increased steadily from 0.474 kPa/m to 8.41 kPa/m at 0.29 m/s and 52.5 m/s VSG respectively while for 1.2 m/s VSL, the pressure gradient increased from 0.970 kPa/m to 11.64 kPa/m at 0.29 m/s and 52.5 m/s VSG respectively. The VSL was then increased to 1.49 m/s, in which the pressure gradient increased steadily from 1.4 kPa/m to 13.36 kPa/m at 0.29 m/s and 52.5 m/s VSG respectively but pressure gradient at 3 m/s could not be measured due to device instrument limitation, the VSL was then increased to 2.24 m/s and the pressure gradient was measured accordingly and the values increased gradually from 2.87 kPa/m to 8.48 kPa/m at 0.29 m/s and 12 m/s VSG respectively as that was the maximum possible pressure gradient that can be measured at that VSG as shown in Table D.8.

The water cut was increased to 90%. The VSL at this water cut started from 1.2 m/s, the pressure gradient increased from 1.26 kPa/m to 12.43 kPa/m at 0.29 m/s and 52.5 m/s VSG respectively while for 1.49 m/s VSL, the pressure gradient increased gradually from 1.76 kPa/m to 10.99 kPa/m at 0.29 m/s and 30 m/s VSG respectively since this was the maximum possible pressure gradient that can be measured at that VSG. The pressure gradient at 3 m/s VSL could not be measured due to device instrument limitation,

therefore, the VSL was increased to 2.24 m/s and the pressure gradient was also measured and the values increased gradually from 2.3 kPa/m to 8.12 kPa/m at 0.29 m/s and 12 m/s VSG respectively as that was the maximum possible pressure gradient that can be measured at that particular VSL and VSG as shown in Table D.9.

It was discovered that, for a particular water cut, as the VSL increases, the pressure gradient also increases. Also, in most cases, as the VSG for a particular VSL increases, the pressure gradient also increases. The graph was plotted in Figure 4.40 to show the relationship.

The pressure gradient from the experimental data was compared with the unified model [21]. It was discovered that, at low VSG of 0.29 m/s and 0.63 m/s, the results were in good agreement with maximum error of 30% for all VSL. The comparison is as shown in Figure 4.41 and Table 4.2.

Table 4.2 Comparison of the Experimental results with the Unified Model

VSO	**VSW**	**VSG**	$FP_{Unif\ Mod}$	FP_{Expt}	**Experimental Pressure gradient**	**Unified Model Pressure gradient**	**% Absolute Error**
0.96	0.24	0.29	INT	ST	1080	833	22.84
1.192	0.289	0.29	D-B	D-B	1290	1319	2.22
2.4	0.6	0.29	D-B	D-B	3270	4174	27.63
0.3	0.45	0.63	INT	INT(SL)	540	493	8.62
0.48	0.72	0.63	INT	INT(EB)	1110	1075	3.20
0.598	0.892	0.63	INT	INT(EB)	1260	1436	14.00
1.2	1.8	0.63	D-B	D-B	3950	4588	16.14
0.96	0.24	0.63	INT	INT(EB)	1260	1201	4.76
1.192	0.289	0.63	INT	INT(EB)	1510	1789	18.48
2.4	0.6	0.63	D-B	D-B	3480	4606	32.35
0.12	0.18	7.56	INT	INT (SL)	900	1127	25.24

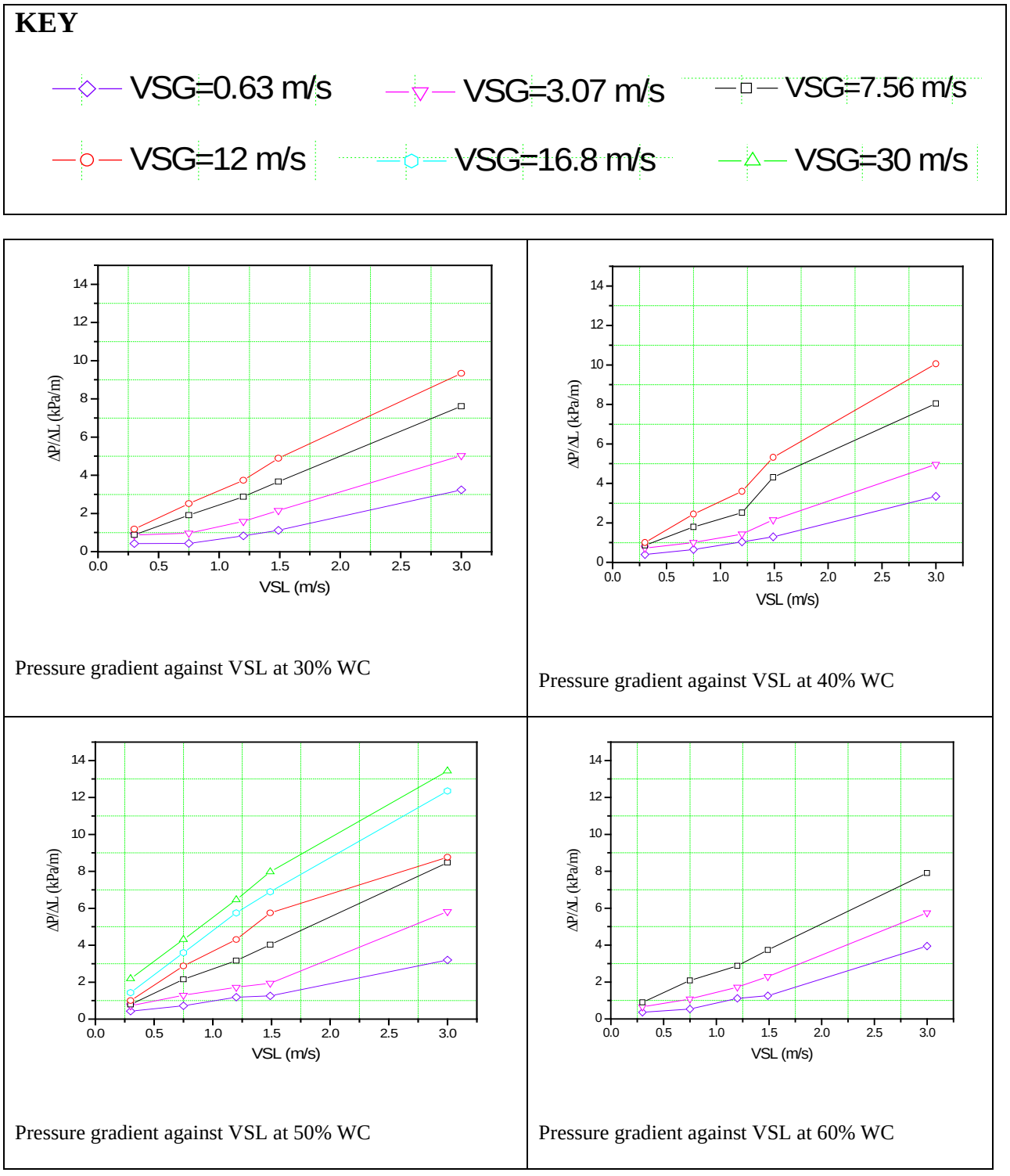

Figure 4.40 Effect of VSL on pressure gradients for VSG of 0.63m/s to 30m/s at different Water Cuts.

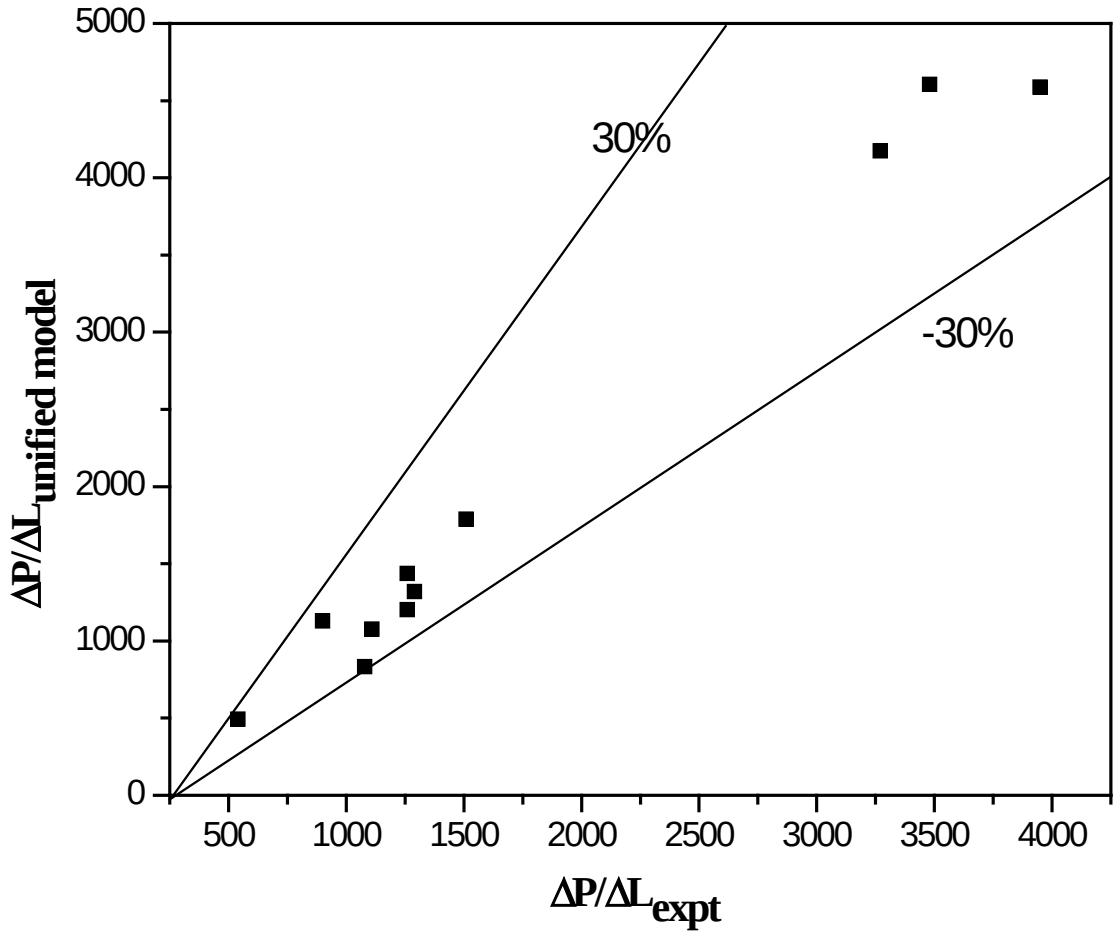

Figure 4.41 Comparison of the experimental results with the Unified Model of Zhang and Sarica [21].

CHAPTER 5

CONCLUSIONS AND RECOMMENDATIONS

A multiphase flow loop was constructed at the basement of Research Institute in King Fahd University of Petroleum and Minerals (KFUPM) to investigate flow patterns and pressure gradient of air-oil-water in a horizontal acrylic test section with inner diameter of 0.0225 m.

The effects of superficial gas velocities, water cuts, liquid mixture Reynold's number and superficial liquid velocities on pressure gradient were studied. The experiments were performed for 10% to 90% water cut in step of 10%.

This chapter was divided into two sections. Section 5.1 presented the main conclusions of the work described in this thesis. Recommendations for future work were given in section 5.2.

5.1 Conclusions

Based on experimental findings, the following conclusions can be made:

5.1.1 Single Phase Water Flow

The single phase water friction factor was measured and compared with Blasius and Zigrang & Sylvester friction factor. It gave good agreement and the roughness of the pipe was determined to be $1 \times 10^{-6}\ m$ which showed that, the pipe is smooth.

5.1.2 Air –Oil –Water Flow Pattern

1. Six flow patterns have been observed visually for a (0.2 m/s – 3.0 m/s) range of superficial liquid velocities with (0.1 – 0.9) input water cut and superficial gas velocities range (0.2 m/s – 35.14 m/s) for co-current air-oil-water and results show a strong dependence of flow patterns on water fraction, gas velocities and liquid velocities. These flow patterns are: stratified (smooth and wavy), elongated bubble, slug, dispersed bubble and annular flow patterns.
2. The water cuts have significant effects on the flow pattern. The flow patterns from 10% to 40% follow a similar trend while that of 50% and 60% also have similar pattern but quite different from that of 80% and 90% flow patterns.
3. Dispersed bubble flow pattern was not observed in 80% and 90% water cuts unlike in other water cuts.
4. There is no generalized flow pattern map for air-oil-water flow in pipelines since the flow pattern in the system depends on the physical properties of the fluids and the wetting properties of the wall surface.
5. High pressure gradient has been observed at annular flow pattern than in any other flow pattern.
6. The flow pattern was compared with unified model and it gave a good results.

5.1.3 Pressure Gradient

The experimental results were compared with that of Unified Model and it gave a good agreement at low VSG of 0.63 m/s for all VSL but it was poorly

predicted at high VSG for all levels of VSL. The following conclusions were deduced:

1. The pressure gradient increases with increasing gas flow rates.
2. The increase in superficial gas velocities led to transition of flow pattern in which the pressure gradient is highest for annular flow and lowest for stratified and dispersed bubble flow pattern.
3. For a particular superficial gas velocity, as the superficial liquid velocity increases, the pressure gradient also increases.
4. For a particular water cut, the pressure gradient increases as the superficial liquid velocity increases.
5. Also, in most cases, as the superficial gas velocity for a particular superficial liquid velocity increases, the pressure gradient also increases.
6. The pressure gradient first increases and then decreases with increasing water cut.
7. The effect of increasing water cut usually lead to phase inversion.
8. For a particular water cut, as the superficial liquid velocity increases, the pressure gradient also increases.
9. The entire dimensionless pressure gradient for each VSL approaches 1.0 as the water cut increases towards 1.0.
10. The three-phase air-oil-water reduces to the single phase pressure gradient as the water cut tends to 1.0

11. The pressure gradient increases as the liquid mixture Reynold's number increases with increasing VSG.
12. The increase in pressure gradient was more significant at high VSG than at low VSG due to changes in flow pattern.

5.2 Recommendations

The following recommendations are made based on the results of this thesis in order to improve the quality of the data and to extend the scope of the area of research:

1. The following modifications should be made to the flow loop:

    a. Flow meters that can cover both bigger and smaller scales should be used in order to have wider range of oil and water velocities.
    b. Pumps with higher capacity should be used in order to have wider range of liquid velocities.
    c. A data acquisition system should be connected to pressure transducers and also to camera so as to collect the results/data.
    d. A high speed video camera should be used to capture the flow pattern images.
    e. A temperature sensor should be mounted on the settling tank of the liquid mixture in order to accurately observe the temperature of the mixture.

f. A braided rubber hose should be mounted on the pipe before getting to the mixture pipe in order to dampen pressure fluctuations before the phases enter the test section.

2. The effects of the following should be carried out on the pressure drop and flow pattern:
    a. Varying pipe diameters
    b. Roughness and wettability of the test section.
    c. Varying angles of inclination of the pipe.
    d. Oil with higher viscosity
    e. Different refrigerants can also be used.

References

[1] Brown, K. E., 1977, *The Technology of Artificial Lift Methods*, PennWell Publishing Co., Tulsa, OK., Chap1.

[2] Hashizume, K. and Ogawa, N., 1987, "Flow pattern, void fraction and pressure drop of refrigerant two-phase flow in a horizontal pipe. III: Comparison of the analysis with existing pressure drop data on air/water and stam/ water systems," International Journal of Multiphase Flow, **13**, pp. 261-267.

[3] Sobocinski, D. P., 1955, "Horizontal Co-current Flow of Water, Gas-Oil and Air" Master's Thesis, University of Oklahoma, OK.

[4] Malinowsky, M. S., 1975, "An Experimental Study of Oil-Water and Air-Oil-Water Flowing Mixtures in Horizontal Pipes," M.S. Thesis, The University of Tulsa, OK.

[5] Beggs, D. H. and Brill, J. P., 1973, "A study of two-phase flow in inclined pipes," Journal of Petroleum technology, **25**, pp. 607-617.

[6] Duckler, A.E., Wicks M. and Cleveland R.G., 1964, "Frictional Pressure Drop in Two-Phase Flow: a Comparison of existing Correlations For pressure Loss and Holdup", AIChE Journal, **10** (1), pp.38-43.

[7] Laflin, G. C. and Oglesby, K. D., 1976, "An Experimental Study on the Effects of Flow Rate, Water Fraction and Gas-Liquid Ratio on Air-Oil-Water Flow in Horizontal Pipes," B.S. Thesis, The University of Tulsa, OK.

[8] Mandhane, J. M., Gregory, G. A and Aziz, K., 1974, "A Flow Pattern Map for Gas-Liquid Flow In Horizontal Pipes", International Journal of Multiphase Flow, **1** (4), pp.537- 553.

[9] Stapelberg, H., 1991, "The Slug Flow of Oil, Water and Air in Horizontal Tubes," PhD Dissertation, University of Hannover, Hannover.

[10] Acikgoz, M. F., Franca and Lahey Jr., R., 1992, "An Experimental Study of Three-Phase FlowRegimes", International Journal of Multiphase Flow, **18** (3), pp.327-336.

[11] Hall, A. R. W., 1992, "Multiphase Flow of Oil, Water and Gas in Horizontal Pipes," Ph.D. Thesis, Imperial College of Science, Technology and Medicine, University of London, London.

[12] Lahey, R.T., Acikgoz M.F and Franca F., 1992, "Global Volumetric Phase Fractions in Horizontal Three Phase Flows", AIChE Journal, **38**, pp.1049-1058.

[13] Donnelly, G.F., Spedding P.L and McBride W.J., 1995, "*Prediction of Two and Three Phase Flow in the Horizontal Configuration*", Offshore Technology Conference, Houston, Texas, pp.449-457.

[14] Malhotra Ajay, 1995, "Study of Two and Three-Phase Flows in Large Diameter Horizontal Pipelines", M.S Thesis, Ohio University, Ohio.

[15] Taitel, Y., Barnea, D. and Brill, J. P., 1995, "Stratified Three Phase Flow in Pipes", International Journal of Multiphase Flow, **21** (1), pp. 53-60.

[16] Chen, X. and Guo, L., 1999, “Flow patterns and pressure drop in oil-air-water three-phase flow through helically coiled tubes”, International Journal of Multiphase Flow, **25**, pp. 1053-1072.

[17] Baddie, S., Lawrence, C.J. and Hewitt, G.F., 2001, “Axial Viewing Studies of Horizontal Gas-Liquid Flows with Low-Liquid Loading”, International Journal of Multiphase Flow, **27**, pp. 1259-1269.

[18] Oddie, G., Shi, H., Durlofsky, L.J., Aziz, K., Pfeffer, B. and Holmes, J.A., 2003, “Experimental Study of Two and Three-Phase Flows in Large Diameter Inclined Pipes”, International Journal of Multiphase Flow, **29**, pp. 527-558.

[19] Petalas, N. and Aziz, K., 2000, “A Mechanistic Model for Multiphase Flow in Pipes,” Journal of Canadian Petroleum Technology, **39** (6), pp.43-55.

[20] Spedding, P.L., Donnelly, G.F. and Cole, J.S., 2005, “Three-Phase Oil-Water-Gas Horizontal Co-current flow I. Experimental and Regime Map”, Chemical Engineering Research and design Journal, **83**(A4), pp.401-411.

[21] Zhang, H.Q. and Sarica C., 2006, “*Unified Modeling of Gas/Oil/Water-Pipe Flow-Basic Approaches and Preliminary Validation*”, SPE Annual Technical Conference, Dallas, pp.1-7.

[22] Zhang H. Q., Wang Q., Sarica C. and Brill J. P., 2003a, “Unified Model for Gas/Liquid Pipe Flow via Slug Dynamics-Part 1: Model Development”, ASME Journal of Energy Research Technology, **125** (4), pp.266-271.

[23] Khor , S.H., 1998, “Three-Phase Liquid-Liquid-Gas Stratified Flow in Pipelines”, PhD dissertation, Imperial College of Science, Technology and Medicine, University of London, London.

[24] Wegmann A., Melke J. and Von Rohr P.R., 2007, “Three-Phase Liquid-Liquid-Gas Flows in 5.6 mm and 7 mm Inner Diameter Pipes”, International Journal of Multiphase Flow, **33**, pp. 484-497.

[25] Wang, S., Zhang H.Q., Sarica C. and Pereyra E., 2012, “*Experimental Study of High-Viscosity Oil/Water/Gas Three-Phase Flow in Horizontal and Upward Vertical Pipes*,” Offshore Technology Conference, Houston, Texas, pp.449-457.

[26] Constant-Machado, H., Lecleric, J.P., Avilan, E., Landaeta, G., Anorga, N. and Capote, O., 2005, “Flow Modeling of a battery of industrial crude oil/gas separators using 113 min tracer experiments”, Chem. Eng. Process, **44**, pp.760-765.

[27] Jepson, W. P., 2000, “*NSFI/UCRC Corrosion in Multiphase Systems*”, NACE International Conference, Orlando, Florida.

[28] Zigrang, D.J. and Sylvester N.D., 1985, “A review of Explicit Friction Factor Equation”, Transactions of ASME, Journal of Energy Resources Technology, **107**, pp.280-283.

[29] Thomas, M.A., 2002, “G104-A2LA Guide for Estimation of Measurement Uncertainty In Testing,” from http://www.a2la.org/guidance/est_mu_testing.pdf

[30] Collier, J.G and Thome, J.R, 1996, Convective boiling and condensation, Oxford University Press, USA.

[31] Arirachakaran, S., Oglesby, K., Shoham, O. and Brill J., 1989, "*An Analysis of Oil/Water Flow in Horizontal Pipes*", SPE Production Operating Symposium, Oklahoma, pp.155-167.

[32] Pal, R., 1996, "Viscoelastic properties of polymer-thickened oil-in-water emulsions," Chemical Engineering Science Journal, **51**, pp. 3299- 3305.

Vitae

Name: Okunrinjeje Lukman Tunde

Date of Birth: 28th of October, 1984.

Nationality: Nigerian.

Had Bachelor's degree in Mechanical Engineering from the Prestigious Obafemi Awolowo University, Ile-Ife, Nigeria in 2008.

Email address: okunrinjejelut@gmail.com

Present Address: 25th street by Rabigh, Thouqbah, Khobar Saudi Arabia.

Permanent Address: 52 Ibadan road, Ijebu-ode, Ogun state, Nigeria.

Telephone number(s) : +2348057337076, +966502865503, +966595899574

Completed Msc in Mechanical Engineering at KFUPM on December 2012.

APPENDIX A

Sample calculation for friction factor

For case of Zigrang & Sylvester friction factor:

Pipe roughness (ε) = 1×10^{-6} m

Internal diameter of pipe (D) = 0.0225 m

Reynolds number at 0.95 m/s water velocity = 23,555

Applying the Zigrang & Sylvester Correlation ,

$$\frac{1}{\sqrt{f}} = -2log\left[\frac{\varepsilon/D}{3.7} - \frac{5.02}{Re}log\left[\left(\frac{\varepsilon/D}{3.7}\right) + \frac{13}{Re}\right]\right]$$

$$\frac{1}{\sqrt{f}} = -2\log\left[\frac{(1 * 10^{-6})/0.0225}{3.7} - \frac{5.02}{23555}log\left[\frac{(1 * 10^{-6})/0.0225}{3.7} + \frac{13}{23555}\right]\right]$$

$$\frac{1}{\sqrt{f}} = -2log(1.201 \times 10^{-5} - 2.1312 \times 10^{-4}\log(1.201 \times 10^{-5} + 5.519 \times 10^{-4}))$$

$$\frac{1}{\sqrt{f}} = 6.3044$$

$$f = 0.0252$$

The same value of f in the first row of the table of single phase water friction factor shown below under the 1×10^{-6} m.

For Blasius correlation,

$f = 0.316Re^{-0.25}$

$f = 0.316 \times (23555)^{-0.25}$

$f = 0.316 \times 0.0807$

$f = 0.0255$

The Blasius friction factor is very similar to that of Zigrang & Sylvester friuction factor.

Using the entrance length correlation,

$Le = 4.4 \times D \times Re^{\frac{1}{6}}$

$Le = 4.4 \times 0.0225 \times (23555)^{\frac{1}{6}}$

$Le = 0.53\ m.$

Since the first pressure tap was placed at 1.87 m from the inlet which is greater than 0.53 m, then a fully developed flow can be achieved easily.

Single Phase water friction factors

Water flowrate (gpm)	**Water velocity (m/s)**	**Reynolds Number**	**Measured friction factor**	**Blasius friction factor**	**Zigrang & Sylvester friction factor**		
					$k = 1 \times 10^{-4} m$	$k = 1 \times 10^{-5} m$	$k = 1 \times 10^{-6} m$
6	0.95	23555	0.0269	0.0255	0.0331	0.0260	0.0252
7	1.11	27481	0.0218	0.0245	0.0326	0.0252	0.0243
9	1.43	35333	0.0239	0.0230	0.0320	0.0240	0.0229
10	1.59	39259	0.0207	0.0224	0.0317	0.0235	0.0224
12	1.91	47110	0.0217	0.0214	0.0314	0.0227	0.0215
15	2.38	58888	0.0207	0.0203	0.0310	0.0219	0.0205
18	2.86	70666	0.0196	0.0194	0.0307	0.0212	0.0197

The variation of Temperature with Safrasol D80 Viscosity

Temperature (℃)	**Viscosity (Pa.s)**
10	0.00202
12	0.00197
14	0.00191
16	0.00189
18	0.00185
20	0.00177
22.5	0.00173
23.5	0.00168
24	0.00165
26	0.00158
28	0.00152
31.1	0.00147
33.1	0.00142
35.56	0.00137
41.1	0.00132

APPENDIX B

Sample calculation for uncertainty analysis

Type A uncertainty for the pressure drop = 0.025

Type B uncertainty for the pressure drop = 0.0713

The combined uncertainty, $U_y = \sqrt{(0.025)^2 + (0.0713)^2}$

U_y = 0.0756

The expanded uncertainty, U for the pressure drop = kU_y

At 95 % confidence level, k=2

Therefore,

U= 2*0.0756

U=0.15%.

APPENDIX C

Matrix range for the pressure gradient of three-phase flow at 30% water cut

$V_{SL}\ (m/s)$	$V_{SO}\ (m/s)$	$V_{SW}\ (m/s)$	$V_{SG}\ (m/s)$
0.3	0.21	0.09	0.29
0.3	0.21	0.09	0.63
0.3	0.21	0.09	1.51
0.3	0.21	0.09	3.07
0.3	0.21	0.09	4.62
0.3	0.21	0.09	7.56
0.3	0.21	0.09	12
0.3	0.21	0.09	16.8
0.3	0.21	0.09	30
0.3	0.21	0.09	44.9
0.3	0.21	0.09	52.5

$V_{SL}\ (m/s)$	$V_{SO}\ (m/s)$	$V_{SW}\ (m/s)$	$V_{SG}\ (m/s)$
0.75	0.525	0.225	0.29
0.75	0.525	0.225	0.63
0.75	0.525	0.225	1.51
0.75	0.525	0.225	3.07
0.75	0.525	0.225	4.62
0.75	0.525	0.225	7.56

0.75	0.525	0.225	12
0.75	0.525	0.225	16.8
0.75	0.525	0.225	30
0.75	0.525	0.225	44.9
0.75	0.525	0.225	52.5

$V_{SL}\ (m/s)$	$V_{SO}\ (m/s)$	$V_{SW}\ (m/s)$	$V_{SG}\ (m/s)$
1.2	0.84	0.36	0.29
1.2	0.84	0.36	0.63
1.2	0.84	0.36	1.51
1.2	0.84	0.36	3.07
1.2	0.84	0.36	4.62
1.2	0.84	0.36	7.56
1.2	0.84	0.36	12
1.2	0.84	0.36	16.8
1.2	0.84	0.36	30
1.2	0.84	0.36	44.9
1.2	0.84	0.36	52.5

$V_{SL}\ (m/s)$	$V_{SO}\ (m/s)$	$V_{SW}\ (m/s)$	$V_{SG}\ (m/s)$
1.49	1.04	0.45	0.29
1.49	1.04	0.45	0.63
1.49	1.04	0.45	1.51
1.49	1.04	0.45	3.07
1.49	1.04	0.45	4.62

1.49	1.04	0.45	7.56
1.49	1.04	0.45	12
1.49	1.04	0.45	16.8
1.49	1.04	0.45	30
1.49	1.04	0.45	44.9
1.49	1.04	0.45	52.5

$V_{SL}\ (m/s)$	$V_{SO}\ (m/s)$	$V_{SW}\ \ (m/s)$	$V_{SG}\ (m/s)$
3.0	2.1	0.90	0.29
3.0	2.1	0.90	0.63
3.0	2.1	0.90	1.51
3.0	2.1	0.90	3.07
3.0	2.1	0.90	4.62
3.0	2.1	0.90	7.56
3.0	2.1	0.90	12

APPENDIX D

The table for the effect of VSL on pressure gradient at different water cut is presented in this appendix. The table ranges from D.1 to D.9.

Table D.1: The effect of VSL on pressure gradient at 10% Water cut

$\Delta P/\Delta L\ (kPa/m)$

VSL	VSG= 0.29	0.63	1.51	3.07	4.62	7.56	12	16.8	30	44.9	52.5
1.2	1.08	1.19	1.40	1.87	2.30	2.87	3.59	4.81	6.75	8.12	8.98
1.49	1.29	1.47	1.72	2.16	2.87	3.59	5.03	6.18	8.84	9.34	10.92
3.0	3.38	3.56	4.45	5.24	6.18	–	–	–	–	–	–

Table D.2: The effect of VSL on pressure gradient at 20% Water cut

$\Delta P/\Delta L\ (kPa/m)$

VSL	VSG=0.29	0.63	1.51	3.07	4.62	7.56	12	16.8	30	44.9	52.5
0.75	0.72	0.83	1.01	1.26	1.44	1.72	2.73	3.16	4.31	5.46	6.18
1.2	1.08	1.26	1.29	1.72	2.16	3.02	4.31	5.39	7.11	8.33	9.63
1.49	1.29	1.51	1.80	2.37	2.59	3.23	4.17	6.18	8.62	9.91	10.85
3.0	3.27	3.48	4.20	5.46	6.18	–	–	–	–	–	–

Table D.3: The effect of VSL on pressure gradient at 30% Water cut

$$\Delta P/\Delta L\ (kPa/m)$$

VSL	VSG= 0.29	0.63	1.51	3.07	4.62	7.56	12	16.8	30	44.9	52.5
0.3	0.43	0.42	0.54	0.87	0.98	0.88	1.18	1.19	1.66	3.02	3.20
0.75	0.40	0.43	0.68	0.97	1.44	1.90	2.51	2.87	4.31	5.39	5.96
1.2	0.68	0.83	1.11	1.58	2.08	2.87	3.74	5.32	7.47	8.69	9.56
1.49	0.93	1.11	1.58	2.16	2.59	3.66	4.89	6.32	8.76	10.49	11.06
3.0	2.87	3.23	3.88	5.03	5.89	7.62	9.34	–	–	–	–

Table D.4: The effect of VSL on pressure gradient at 40% Water cut

$$\Delta P/\Delta L\ (kPa/m)$$

VSL	VSG= 0.29	0.63	1.51	3.07	4.62	7.56	12	16.8	30	44.9	52.5
0.3	0.32	0.40	0.50	0.72	0.72	0.86	1.01	1.44	2.01	3.05	3.81
0.75	0.54	0.65	0.72	1.01	1.44	1.80	2.44	2.87	3.88	5.03	5.46
1.2	0.90	1.04	1.19	1.44	2.01	2.51	3.59	5.03	7.18	8.62	9.34
1.49	1.19	1.29	1.65	2.16	2.87	4.31	5.32	6.83	9.20	10.56	12.07
3.0	3.20	3.34	3.88	4.96	6.03	8.05	10.06	–	–	–	–

Table D.5: The effect of VSL on pressure gradient at 50% Water cut

$$\Delta P/\Delta L\ (kPa/m)$$

VSL	VSG= 0.29	0.63	1.51	3.07	4.62	7.56	12	16.8	30	44.9	52.5
0.3	0.40	0.43	0.61	0.72	0.72	0.79	1.01	1.44	2.19	3.09	3.45
0.75	0.72	0.72	0.86	1.29	1.58	2.16	2.87	3.59	4.31	5.09	5.03
1.2	1.11	1.19	1.37	1.72	2.44	3.16	4.31	5.75	6.47	7.90	7.90
1.49	1.15	1.26	1.47	1.94	2.87	4.02	5.75	6.90	7.97	8.19	9.63
3.0	3.05	3.20	4.31	5.82	7.11	8.48	8.76	12.36	13.43	–	–

Table D.6: The effect of VSL on pressure gradient at 60% Water cut

$$\Delta P/\Delta L\ (kPa/m)$$

VSL	VSG= 0.29	0.63	1.51	3.07	4.62	7.56	12	16.8	30	44.9	52.5
0.3	0.29	0.36	0.43	0.65	0.97	0.90	0.86	1.37	1.94	3.20	3.38
0.75	0.43	0.54	0.72	1.08	1.37	2.08	2.87	3.02	3.52	4.24	4.45
1.2	0.93	1.11	1.40	1.72	2.23	2.87	4.17	5.75	7.76	9.20	9.41
1.49	1.11	1.26	1.65	2.30	2.91	3.74	5.39	6.83	9.91	10.78	10.06
3.0	3.23	3.95	5.14	5.75	6.54	7.90	–	–	–	–	–

Table D.7: The effect of VSL on pressure gradient at 70% Water cut

$$\Delta P/\Delta L\ (kPa/m)$$

VSL	VSG= 0.29	0.63	1.51	3.07	4.62	7.56	12	16.8	30	44.9	52.5
0.75	0.43	0.50	0.75	1.01	1.44	1.44	2.59	3.66	3.88	5.75	6.03
1.2	0.79	0.88	1.40	1.80	2.37	2.95	4.45	5.60	8.05	9.70	11.06
1.49	1.15	1.40	1.87	2.44	2.87	4.10	5.75	7.47	10.06	12.57	13.22
3.0	4.13	4.67	5.14	5.71	–	–	–	–	–	–	–

Table D.8: The effect of VSL on pressure gradient at 80% Water cut

$$\Delta P/\Delta L\ (kPa/m)$$

VSL	VSG= 0.29	0.63	1.51	3.07	4.62	7.56	12	16.8	30	44.9	52.5
0.75	0.47	0.57	0.79	1.21	1.29	1.72	2.37	3.30	5.68	7.18	8.41
1.2	0.97	1.19	1.37	2.16	2.26	3.30	4.85	5.75	8.62	11.28	11.64
1.49	1.40	1.72	2.01	2.44	2.87	4.02	5.68	7.40	10.42	12.36	13.36
2.24	2.87	3.23	3.45	4.10	5.03	6.39	8.48	–	–	–	–

Table D.9: The effect of VSL on pressure gradient at 90% Water cut

$$\Delta P/\Delta L\ (kPa/m)$$

VSL	VSG= 0.29	0.63	1.51	3.07	4.62	7.56	12	16.8	30	44.9	52.5
1.2	1.26	1.54	1.80	2.23	2.87	3.52	4.74	6.61	9.34	11.50	12.43
1.49	1.76	1.90	2.23	2.59	3.30	4.53	6.03	7.83	10.99	–	–
2.24	2.30	2.95	3.38	4.20	5.10	6.47	8.12	–	–	–	–